

KLINIK UND POLIKLINIK FÜR ALLGEMEIN-,VISZERAL-,THORAX-,GEFÄß-UND TRANSPLANTATIONS-
CHIRURGIE/ MOLEKULARE ONKOLOGIE UND IMMUNTHERAPIE

DIREKTOR: Prof. Dr. Clemens Schafmayer

BETREUER: PD Dr. rer. nat. Michael Linnebacher

ERSTELLUNG IDEALER VORAUSSETZUNGEN FÜR GRUNDLEGENDE SOWIE TRANSLATIONALE *IN VIVO* FORSCHUNG

KUMULATIVE DISSERTATION

ZUR

ERLANGUNG DES AKADEMISCHEN GRADES

DOKTOR DER MEDIZINWISSENSCHAFTEN (DR. RER. HUM.)

DER

UNIVERSITÄTSMEDIZIN ROSTOCK

GUTACHTER: PD Dr. rer. nat. Michael Linnebacher, Universitätsmedizin Rostock

GUTACHTER: Prof. Dr. med. Friedrich Prall, Universitätsmedizin Rostock

GUTACHTER: Prof. Dr. rer. nat. Manfred Jücker, Universitätsklinikum Hamburg Eppendorf

VORGELEGT VON

Stephanie Matschos | GEB. AM 15.06.1987 IN Eschweiler

Rostock | (Einreichung Januar 2023, Verteidigung November 2023)

https://doi.org/10.18453/rosdok_id00004654

In der vorliegenden kumulativen Dissertation, fasse ich die Methoden und Ergebnisse kurz zusammen. Alle Ergebnisse sowie zusätzliche Informationen sind in den nachfolgend aufgelisteten Publikationen zu finden, welche die Basis meiner Dissertation darstellen:

F. Bürtin, S. Matschos, F. Prall, C. S. Mullins, M. Krohn, and M. Linnebacher, "Creation and maintenance of a living biobank-how we do it," *J. Vis. Exp.*, vol. 2021, no. 170, p. 62065, Apr. 2021.

S. Matschos *et al.*, "The HROC-Xenobank—A high quality assured PDX biobank of >100 individual colorectal cancer models," *Cancers (Basel)*, vol. 13, no. 23, Dec. 2021.

C. Maletzki *et al.*, "NSG mice as hosts for oncological precision medicine," *Lab. Investig.*, vol. 2, 2019.

INHALTSVERZEICHNIS

I.	Einleitung	1
1.1	KOLOREKTALES KARZINOM	1
1.2	BIOBANKEN	2
1.3	PDX MODELLE	3
II.	Fragestellung	4
III.	Methoden	5
3.1	BIOBANK	5
3.2	PDX GENERIERUNG	7
3.3	HISTOLOGIE	8
3.4	QUALITÄTSKONTROLLE VIA SHORT TANDEM REPEAT (STR) ANALYSE	8
3.5	MOLEKULARE ANALYSE	9
3.6	NEXT GENERATION SEQUENCING (NGS) ANALYSE	10
3.7	<i>IN VIVO</i> VERSUCHE - DOSISFINDUNGSSTUDIE	10
3.8	STATISTISCHE ANALYSEN	11
IV.	Ergebnisse	12
4.1	PATIENTEN, KLINISCHE SOWIE MOLEKULARE DATEN	12
4.2	PDX MODELLE	13
4.2.1	IDENTITÄTSPRÜFUNG	14
4.2.2	HISTOLOGIE	15
4.3	MUTATIONSANALYSE	17
4.4	<i>IN VIVO</i> VERSUCHE - DOSISFINDUNGSSTUDIE	18
V.	Diskussion	22
VI.	Zusammenfassung	26
VII.	Literaturverzeichnis	27
VIII.	Abkürzungsverzeichnis	31
IX.	Thesen	32
X.	Danksagung	33

XI.	Lebenslauf	34
XII.	Appendix	37

ABBILDUNGSVERZEICHNIS

ABBILDUNG 1: ARBEITSABLAUF UND ORGANISATION DER BIOBANK	5
ABBILDUNG 2: ARBEITSABLAUF UND ORGANISATION DER HROC-XENOBANK	6
ABBILDUNG 3: ZEITPLAN FÜR DAS BEHANDLUNGSPROTOKOLL DER DOSISFINDUNGSSTUDIE	11
ABBILDUNG 4: VERGLEICH VON PRIMÄRTUMOR UND PDX TUMOR	15
ABBILDUNG 5: UNSUPERVISED CLUSTER ANALYSIS	17
ABBILDUNG 6: (A) = HEAT MAP (B) = MUTATIONSHÄUFIGKEIT	18
ABBILDUNG 7: GEWICHTSKURVE UND ÜBERLEBENSANALYSE	20
ABBILDUNG 8: TUMORWACHSTUMSKURVE	21

TABELLENVERZEICHNIS

TABELLE 1: SEQUENZEN DER STR PRIMER	9
TABELLE 2: VERTEILUNG MOLEKULARE SUBTYPEN	13
TABELLE 3: BEHANDLUNGSBEDINGTE/UNERWARTETE TODE DER DOSISOPTIMIERUNGSSTUDIE..	19

I. EINLEITUNG

1.1 KOLOREKTALES KARZINOM

Das Fortschreiten vom kolorektalen Adenom zum Karzinom (CRC) wird durch drei Hauptwege verursacht: Mikrosatelliteninstabilität, chromosomale Instabilität und dem CpG-Insel-Methylator-Phänotyp [1]. Die Mehrheit der sporadischen kolorektalen Karzinome (~85 %) weist eine chromosomale Instabilität (CIN) mit Veränderungen der Chromosomenzahl und -struktur auf, während die verbleibenden sporadischen Fälle (~15 %) Mikrosatelliteninstabilitäten (MSI) aufweisen [1]. Zu den häufigsten erblich bedingten CRC zählt das hereditäre nicht-polypöse kolorektale Karzinom (HNPPC oder Lynch-Syndrom) (1-3 %) [1]. Das Lynch-Syndrom ist ebenfalls durch MSI gekennzeichnet und entsteht infolge eines defekten DNA-Mismatch-Reparatursystems [1].

Aufgrund der molekularen Heterogenität des CRC erfolgt eine Klassifizierung in die folgenden molekularen Subtypen: chromosomal instabil (CIN), sporadisch Mikrosatelliten instabil (spMSI), CpG-Insel-Methylator-Phänotyp (CIMP, unterteilt in high-level (CIMP-H) und low-level (CIMP-L)), sowie das Lynch Syndrom (LS) [2]. Diese repräsentieren die häufigsten CRC-Subtypen [3]. Das Tumor-UICC-Staging in der allgemeinen deutschen Darmkrebs-Population beträgt 19,5 % (Stadium I), 29 % (Stadium II), 30 % (Stadium III) und 21,5 % (Stadium IV) [4]. Die Daten des deutschen Krebsregisters ZfKD (Zentrum für Krebsregisterdaten) zeigen, dass das Durchschnittsalter der männlichen Patienten zwischen 67,6 und 68,3 Jahren und bei den weiblichen Patienten zwischen 70,6 und 71,0 Jahren liegt [5].

In der S3-Leitlinie „Kolorektales Karzinom (AWMF-Registernummer: 021/007OL)“ sind entsprechend dem UICC Stadium sowie weiteren Faktoren wie dem MSI Status, Komorbiditäten, Alter etc. die jeweils empfohlenen Therapien des CRC dargestellt [6]. Exemplarisch sind nachfolgend einige dieser generellen Empfehlungen aufgeführt. Für die adjuvante Chemotherapie des Kolonkarzinoms im Stadium III soll eine Oxaliplatin-haltige Therapie (Oxaliplatin in Kombination mit 5-FU/Folinsäure) eingesetzt werden, allerdings nicht bei Patienten über 70 Jahren [6]. Bei Kontraindikationen gegen Oxaliplatin-haltige Regime sowie in Stadium II soll eine Monotherapie mit Fluoropyrimidinen durchgeführt werden, wobei orale Fluoropyrimidine den infusionalen Schemata vorgezogen werden [6]. Bolusregime sollen wegen der höheren Toxizität nicht mehr verwendet werden [6]. Darüber hinaus sollte bei nachgewiesener Mikrosatelliteninstabilität (MSI-H) keine adjuvante Chemotherapie im Stadium II erfolgen.[6]

Trotz früher Diagnosemöglichkeiten und verbesserter Behandlung ist das CRC immer noch eine der häufigsten krebsbedingten Todesursachen weltweit [7]. Insbesondere die Tatsache,

dass einige Patienten jedoch selbst auf zielgerichtete Therapien nicht ansprechen, unterstreicht die Notwendigkeit weiterer patientenbasierter Modelle, um die Entwicklung personalisierter Behandlungen zu fördern [7], [8].

1.2 BIOBANKEN

Biobanken lagern biologische Proben ein, unter Berücksichtigung ethischer Aspekte und den gesetzlichen Rechten jeder Person, die Biomaterialien für die Forschung zur Verfügung stellt [9]. Das Konzept von Biobanken ist es biologische und klinische Daten von menschlichen Probanden zu erhalten und zu sammeln [9].

In der Literatur werden verschiedene Klassifizierungen angeboten, generell kann jedoch eine allgemeinere Unterscheidung zwischen bevölkerungsbezogenen und krankheitsorientierten Biobanken getroffen werden [9]. Die erste konzentriert sich auf die Untersuchung der möglichen zukünftigen Entwicklung von häufigen und komplexen Krankheiten, während die zweite auf spezifische Krankheiten, vor allem Krebs, ausgerichtet ist [9].

Beispielsweise wurde in der Biobank-Studie publiziert von Heervä *et al.* das Überleben von Patienten mit kolorektalen Erkrankungen analysiert, die in einem Universitätskrankenhaus über einen Zeitraum von 12 Jahren diagnostiziert und behandelt wurden, um Faktoren zu bewerten, die zum Überleben beitragen [10]. Wohingegen Peila *et al.* den Zusammenhang zwischen Testosteron, Östradiol und Sexualhormon-bindendem Globulin (SHBG) und dem Risiko für Darmkrebs ($n = 3247$) bei 206508 Männern und 219106 Frauen, die in der UK Biobank erfasst sind, untersuchten [11].

Indem verschiedene Fachleute mit unterschiedlichem Fachwissen zusammen arbeiten, können komplexe Forschungsstrategien im Gesundheitswesen entwickelt werden [9]. Neben kleineren Biobanken von beispielsweise Universitätsklinken und den zugehörigen Forschungslaboren, gibt es auch große Infrastrukturnetze, wie z. B. die Pan-European Biobanking and Biomolecular Resources Research Infrastructure (BBMRI) [9].

Die Aufarbeitung sowie die Lagerung der Biomaterialien sind dabei stets von entscheidender Bedeutung für die Qualität der Proben [9], [12]. Normalerweise verbleibt chirurgisch reseziertes Gewebe bei Raumtemperatur bevor es stabilisiert wird. Die Zeit, die vor der Stabilisierung vergeht, wird als warme Ischämie bezeichnet und ist eine entscheidende Variable, die die Degradation vor der Fixierung beeinflusst. Das Gewebe sollte daher, sofern möglich, bei einer kalten Temperatur auf Eis oder im Kühlschrank bei 4 °C unmittelbar nach der Operation aufbewahrt werden, da zelluläre Veränderungen begrenzt und der Abbau verzögert wird. Der Zeitraum, in dem das Gewebe nach der Resektion aber vor der Formalinfixierung oder dem Einfrieren auf Eis oder bei 4 °C aufbewahrt wird, ist die kalte Ischämiezeit [9], [12].

In der Vergangenheit wurden alle Arten von Proben bei -20 °C aufbewahrt, sowohl für die kurz- als auch für die langfristige Lagerung. Heute liegen die Standardtemperaturen für die Lagerung von Geweben und Zellen zwischen -80 °C und -150 °C. Tiefsttemperaturen bewahren die Integrität von Proteinen, DNA, RNA und zellulären Bestandteilen. Eine Temperatur von -80 °C ist heute der Standard für die Konservierung von menschlichen Geweben, allerdings wird Flüssigstickstoff empfohlen, insbesondere die Dampfphase (-150 °C) gegenüber der Flüssigphase (-196 °C) wegen des Risikos einer Kontamination durch schwebende Gewebefragmente [9], [12].

1.3 PDX MODELLE

Das derzeit beste Modell, das die Eigenschaften des ursprünglichen Tumors widerspiegelt, ist das PDX Modell (patient-derived xenograft), da es die biologischen Merkmale des ursprünglichen Tumors, einschließlich Mikroarchitektur, Pathomorphologie und genetische Veränderungen erhält [8], [13]. Tentler *et al.* haben festgestellt, dass CRC-PDX Tumoren die intratumorale klonale Heterogenität, die chromosomale Instabilität sowie die Histologie des primären Patiententumors für bis zu 14 Passagen beibehalten [8], [14].

Aufgrund der starken Heterogenität der Tumoren von beispielsweise Speiseröhrenkrebs und Bauchspeicheldrüsenkrebs ist eine Gewebekbank mit einer ausreichenden Anzahl von Proben erforderlich, um die Vielfalt der Tumorarten abzudecken [15]. Damhofer *et al.* haben zur Untersuchung dieser Tumorarten eine Biobank in ihrem Institut errichtet, um ausreichend Tumorgewebe nach Tumorresektion oder bei inoperablen Tumoren perioperativ durch zusätzliche Biopsien zu sammeln, umso ein Panel von 29 PDXs von Speiseröhren- und Bauchspeicheldrüsenkrebs zu erstellen [15]. Die Untersuchungen haben weiterhin gezeigt, dass diese PDXs mehrere der (immuno-) histologischen und biochemischen Merkmale der ursprünglichen Tumoren widerspiegeln [15].

Die verwendeten Mäuse müssen immungeschwächt sein, um eine Transplantatabstoßung zu verhindern [16]. Bevorzugter Mausstamm für ein effizientes Engraftment von primären humanen Tumoren sind NSG Mäuse, da sie eine vollständige Null-Mutation im Gen aufweisen, das die Interleukin-2-Rezeptor-Gamma-Kette kodiert, was zu einem Mangel an multiplen Zytokin-Signalen führt, wodurch viele Bereiche der angeborenen Immunität, einschließlich der Differenzierung der natürlichen Killerzellen, gestört werden [16].

II. FRAGESTELLUNG

In dieser Arbeit wird analysiert, warum eine wissenschaftlich geführte PDX Biobank nötig ist und welche Möglichkeiten sich daraus für die Forschung ergeben.

Die Möglichkeit einer genauen Vorhersage des individuellen klinischen Behandlungserfolg, insbesondere für die späte präklinische Prüfung neuer Therapeutika, zeigt den klaren Bedarf an mehr wissenschaftlich geführten PDX Biobanken, die eine große Anzahl individueller Tumoren enthalten [8], [13], [17], [18]. Die große Sammlung von Patientenmaterial in der HROC-Biobank, die sowohl Tumor- als auch normales Epithelgewebe enthält, dient als ideale Ausgangsplattform, um eine große Anzahl individueller PDX Modelle zu erstellen.

Dies führte zu einer qualitätsgesicherten PDX Biobank mit mehr als 100 individuellen CRC-Fällen, die alle spezifischen molekularen Subtypen des CRC abdeckt [19]. Somit stellt diese PDX Biobank eine ideale Plattform dar, um neue Wirkstoffe für die adjuvante Therapie zu untersuchen. Dies bietet die Möglichkeit gezielt spezifische molekulare Subtypen oder Veränderungen, in Kombination mit Untersuchungen zu unterschiedlichen molekularen Signalwegen in den Tumorzellen im Vergleich zum normalen Epithelgewebe, zu bestimmen [19]. Ein solcher Ansatz wurde kürzlich von Medico und Kollegen beschrieben. Hier haben die Autoren tumorspezifische Veränderungen identifiziert, die aus klinisch verwertbaren Kinase-Targets bestehen, für die es bereits zugelassene Medikamente gibt [20]. Omics-Daten sowohl aus dem PDX Modell als auch dem ursprünglichen Patiententumor können einerseits den Eintritt neuer Medikamente in die Klinik beschleunigen und andererseits würden solche gepaarten Datensätze die Identifizierung und Validierung von prädiktiven Biomarkern erleichtern [8].

Schließlich ist das PDX Gewebe, wie von uns und anderen Gruppen beschrieben, eine ideale Quelle für die Etablierung sekundärer Zelllinien [21], [22] als auch für die Generierungsversuche von Organoiden aus Patienten (PDO) [22], [23]. Dadurch kann die Gesamterfolgsrate erheblich gesteigert werden, von 10-13 % für primäre, aus Patientenmaterial gewonnene Zelllinien [21], [24] auf etwa 30 % für sekundäre, d. h. von PDX-abgeleiteten Zelllinien [21]. Die Vision ist eine integrierte Biobank-Sammlung, bestehend aus umfassend charakterisiertem primärem Patientenmaterial, 2D-Zelllinien, PDX und PDO. Die Nutzung dieser soll Forschungsstrategien unterstützen, von eher grundlegenden mechanistischen Ansätzen bis hin zur translationalen Arzneimittelentwicklung und zu Tests im Endstadium präklinischer Studien. Der Aufbau und die langfristige Pflege von Plattformen wie der integrierten HROC-Biobank sind von entscheidender Bedeutung um die Gesamtzahl der an onkologischen *in vivo*-Studien beteiligten Tiere zu minimieren [19].

III. METHODEN

3.1 BIOBANK

Die HROC-Biobank bestehend aus dem primären Tumorgewebe, Normalgewebe, Serum, isolierten Lymphozyten aus peripherem Blut (PBL), Patienten-abgeleiteten Xenografts (PDX), sowie primären und sekundären Zelllinien, unterliegt strengen Richtlinien und erfordert sowohl eine sorgfältige Vorbereitung als auch eine gut abgestimmte Infrastruktur [25].

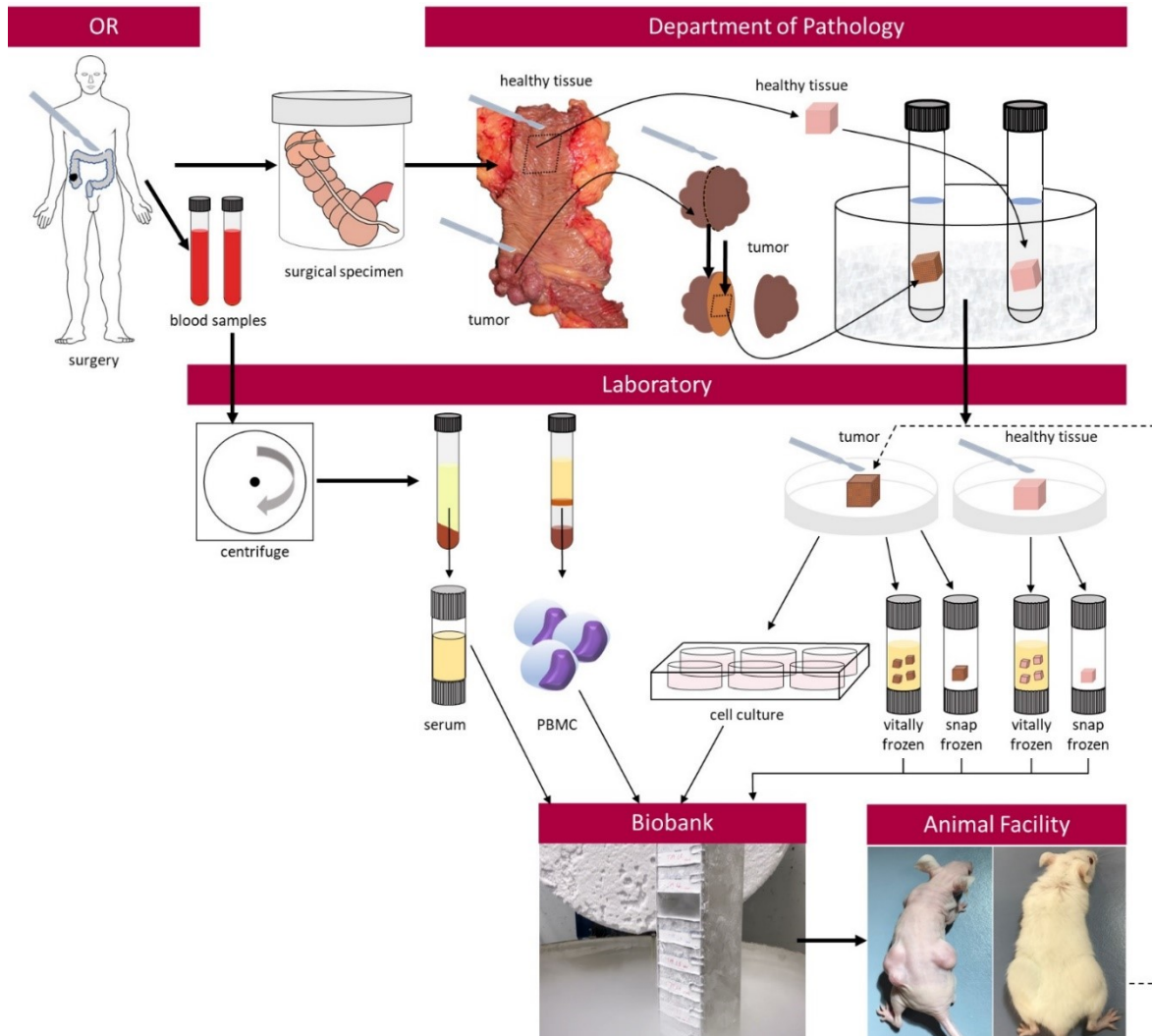


Abbildung 1: Arbeitsablauf und Organisation der Biobank [25], beginnend bei der Probensammlung in der Klinik und der weiteren Aufarbeitung dieser Proben im Labor.

Resezierte Darmgewebe oder Metastasen werden unmittelbar nach der Resektion in die Pathologie gebracht. Nach dem Ermessen des behandelnden Pathologen werden kleine Tumorstücke und Normalgewebe entnommen, sofern dies der Befunderstellung nicht schadet und der Patient seine Einwilligung erteilt hat. Die weiteren Prozesse finden im Labor unter

sterilen Bedingungen statt. Nekrotische Teile des Tumors werden verworfen und das verbleibende Tumorgewebe wird in kleine, identische Würfel geschnitten und zur späteren Verwendung vital kryokonserviert. Außerdem wird ein kleiner Teil des Tumors mechanisch zerkleinert und für die Etablierung von primären Zellkulturen verwendet. Darüber hinaus werden Blutproben, die dem Patienten prä- und postoperativ entnommen wurden, zur Gewinnung von Serum und PBLs aufbereitet. Die Aufarbeitung dieser Proben ist detailliert beschrieben von Bürtin *et al.* [25].

Um die Patientendaten zu anonymisieren, wurde jedem Fall ein Alias zugewiesen, der sich wie folgt zusammensetzt: HRO für Hansestadt Rostock, C für Kolonkarzinom und einer fortlaufenden Nummer. Metastasen wurden mit der Kennung Met als Abkürzung für Metastase versehen. Diese wurde direkt nach der HROC-Nummer angefügt. Im Falle mehrerer Tumoren wurde eine zusätzliche Tumornummer aufgenommen [19], [25].

Da die Patientenproben limitiert sind und die Etablierungsrate primärer Zellkulturen immer noch relativ gering ist, ermöglichen PDX nicht nur die Erhaltung und Erweiterung der Biobank, sondern auch die Generierung von sekundären Tumorzelllinien.

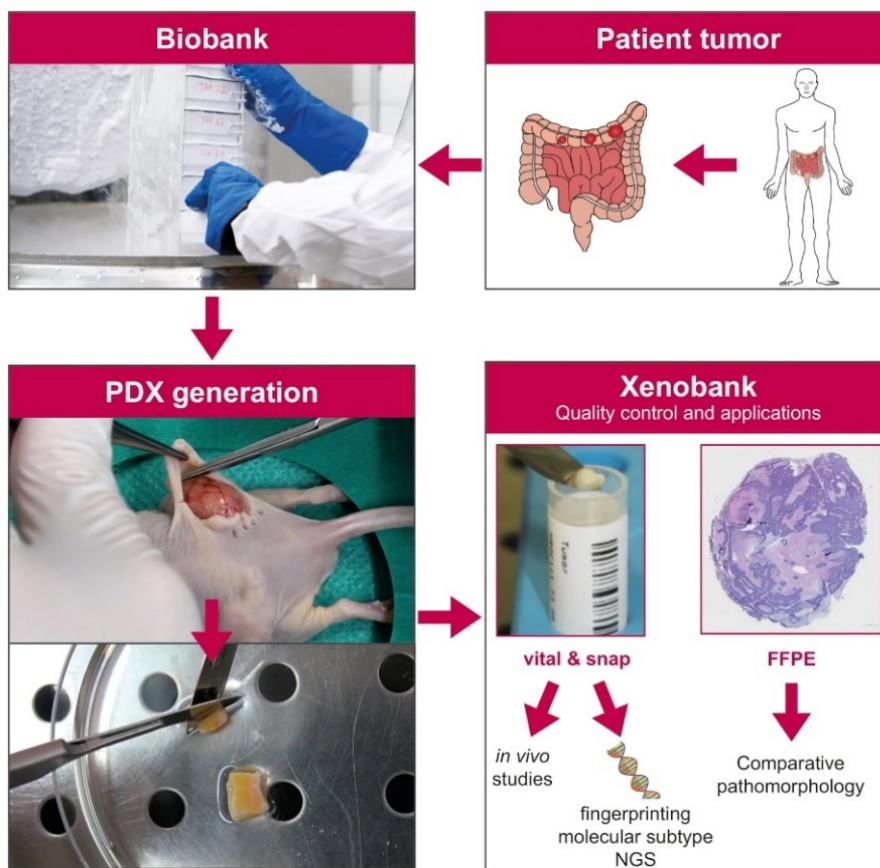


Abbildung 2: Arbeitsablauf und Organisation der HROC-Xenobank Die gesammelten und vital kryokonservierten Patiententumorgewebe werden für das PDX Engraftment verwendet und die entstehenden PDX Tumoren werden für spätere Verwendungen asserviert.

Für das PDX Engraftment werden die kryokonservierten Tumorstücke aufgetaut und subkutan in die Flanken von immundefizienten Mäusen implantiert. Die ausgewachsenen PDX werden entweder anschließend für weitere Xenotransplantationen verwendet oder können für eine spätere Verwendungen erneut kryokonserviert werden. Zusätzlich werden snap frozen Aliquots für anschließende molekulare Analysen erzeugt und ein repräsentativer Querschnitt des PDX Tumor eingebettet, um vergleichende histologische Analysen durchführen zu können [19], [25].

3.2 PDX GENERIERUNG

Die PDX Tumortransplantation erfolgte gemäß den Richtlinien des örtlichen Ausschusses für Tiernutzung und -pflege, dem Landesamt für Landwirtschaft, Lebensmittelsicherheit und Fischerei, Mecklenburg-Vorpommern mit den Genehmigungsnummern: LALLF M-V/TSD/7221.3-1.1-071/10; 7221.3-1-015/14; 7221.3-1-005/17; 7221.3-2-020/17 und 7221.3-1-007/19 [19], [25], [26].

Die verwendeten Mäusestämme wurden in der Zentralen Versuchstierhaltung des Rudolf-Zenker-Institut für Experimentelle Chirurgie der Universitätsklinik Rostock gezüchtet und unter spezifizierten, pathogenfreien Bedingungen gehalten und einem 12-Stunden-Licht-/12-Stunden-Dunkel-Zyklus ausgesetzt. Die Mäuse erhielten Standard Pellet Futter und Wasser *ad libitum* [19], [25], [26].

Vitale Tumoraliquots der Patiententumoren aus der HROC-Biobank wurden den Tieren unter Narkose (Ketamin/Xlazin, 90/6 mg) subkutan in die linke und rechte Flanke implantiert [19], [25]. Bei den Therapiemäusen erfolgte ausschließlich die Implantation in die rechte Flanke [26]. Aufgrund der Transplantationsrate von bis zu 80 % ist der bevorzugte Mausstamm für diese erste Passage NOD.Cg-Prkdc^{scid} Il2rg^{tm1Wjl}/SzJ (NSG). Die weitere Passage kann entweder mit NSG oder mit NMRI-*Foxn1*^{nu} durchgeführt werden. Die PDX Tumoren wurden mit anonymisierten Patienteninformationen, wie unter 3.1 beschrieben benannt, gefolgt von der Abkürzung Tx, die für die Passage des PDX Tumors steht, gefolgt von der Abkürzung Mx, die für die fortlaufende Nummerierung der Mäuse steht [19], [25].

Alle Tumortransplantationen wurden an 6-12 Wochen alten Mäusen, sowohl männlich als auch weiblich, mit einem Gewicht von 18-30 g durchgeführt. Vor der Xenotransplantation wurden vier vitale Tumoraliquots (3x3x3 mm) in 100 µl Matrigel (Corning, Kaiserslautern, Deutschland) für >10 min bei 4 °C inkubiert. Nach einer 30-tägigen Antibiotikabehandlung (Trinkwasser mit Cotrimoxazol: Dosierung 8 mg Trimethoprim und 40 mg Sulfamethoxazol pro kg Körpergewicht) wurde das Tumorstadium wöchentlich überwacht, bis sich der Tumor etabliert hatte und auf einen maximalen Durchmesser von 14,2 mm angewachsen war. Wenn das maximale

Tumorzvolumen von 1500 mm³ erreicht war oder die Mäuse einen schlechten Gesundheitszustand aufzeigten, wurden die Tumoren explantiert [19], [25].

Die Zeit des Tumorwachstums bis zur Explantation wurde als Tumor-Entnahmezeit definiert [19].

Nach der Explantation der PDX Tumoren wurden die Tumoren in Tissue Storage Lösung (Miltenyi, Bergisch-Gladbach, Deutschland) bis zur weiteren Verarbeitung gelagert. Snap frozen Aliquots wurden so schnell wie möglich durch sofortiges Eintauchen der Tumorstücke in flüssigen Stickstoff asserviert, um eine hohe Qualität, insbesondere der RNA-Moleküle, zu gewährleisten [19], [25]. Vitale Aliquots wurden hergestellt, indem vier Tumorstücke von 3x3x3 mm in 1,5 mL Einfriermedium (fötales Rinderserum Serum mit 10 % DMSO) überführt und in CoolCell® LX-Gefrierbehältern (CryoShop, München, Deutschland) mit 1 °C pro Minute auf -80 °C eingefroren [19], [25], [27].

Während der Bearbeitung der PDX Tumoren wurde der Grad der Nekrose beurteilt und dokumentiert, was eine Einteilung in nicht nekrotisch, kaum nekrotisch, intermediär nekrotisch und stark nekrotisch ermöglicht [19].

Die Fälle die in die HROC-Xenobank eingeschlossen wurden, verfügen über folgende qualitätsgesicherte Proben: n = 30 vitale PDX Gewebesicherungen (bestehend aus vier kleinen Würfeln mit einer Seitenlänge von etwa 3 mm, um insgesamt mindestens 120 Implantationen zu ermöglichen), sowie mindestens n = 5 snap frozen Aliquots Proben, die sich ideal für molekulare Analysen eignen. Es ist bemerkenswert, dass die Backups aller 125 Fälle in weniger als 10 Durchgängen und in der Regel in weniger als 5 Durchgängen erstellt wurden. Damit wurde eine größtmögliche Nähe zum Ursprungsgewebe gewährleistet. Darüber hinaus wurde für alle Fälle der HROC-Xenobank ein Teil eines PDX Tumors eingebettet [19].

3.3 HISTOLOGIE

Für jedes PDX Modell der HROC-Xenobank wurde ein repräsentativer Querschnitt oder die Hälfte eines subkutanen PDX Tumors unmittelbar nach der Explantation in Formalin fixiert und mittels Routineverfahren in Paraffin eingebettet [19]. H&E-gefärbte Schnitte (4-5 µm) wurden in lichtmikroskopischen Untersuchungen analysiert, um die morphologischen Merkmale jedes einzelnen PDX Modells zu beurteilen [28]. Ein Vergleich mit dem jeweiligen Originaltumor des Patienten wurde von einem zertifizierten Pathologen (FP) durchgeführt [19].

3.4 QUALITÄTSKONTROLLE VIA SHORT TANDEM REPEAT (STR) ANALYSE

Die fluoreszenzmarkierten, PCR-amplifizierten DNA-Fragmente von D5S818, D7S820, D16S539, D13S317, vWA, TPOX, THO1, CSF1PO und Amelogenin wurden zusammen mit

dem Standard GeneScan™ LIZ500 (Applied Biosystems® Thermo Fisher Scientific, Waltham, MA, USA) in die Kapillare für die elektrophoretische Größentrennung mit ABI-Geräten injiziert. Die entsprechend ihrer Größe aufgetrennten PCR-Fragmente wurden durch Messung ihrer Fluoreszenzintensität bei verschiedenen Emissionswellenlängen gemessen und als FSA aufgezeichnet, nachdem sie durch die Kapillare von der Kathode zur Anode gewandert sind, wobei kleinere Fragmente schneller wandern als größere Fragmente [29]. Die Anwendung von Primerpaaren, die mit drei verschiedenen Fluoreszenzfarbstoffen FAM (blau), HEX (grün) und TAMRA (rot) gelabelt sind, ermöglicht die Bestimmung der Fragmentgrößen aller genannten Marker (die Primer sind im Einzelnen in Tabelle 1 aufgeführt) in einer einzigen Analyse [19].

Tabelle 1: Sequenzen der STR Primer [19].

Primer	Sequence
D5S818 for	5'-HEX-GGT GAT TTT CCT CTT TGG TAT CC-3'
D5S818 rev	5'-AGC CAC AGT TTA CAA CAT TTG TAT CT-3'
D7S820 for	5'-HEX-ATG TTG GTC AGG CTG ACT ATG-3'
D7S820 rev	5'-GAT TCC ACA TTT ATC CTC ATT GAC-3'
D16S539 for	5'-HEX-GGG GGT CTA AGA GCT TGT AAA AAG-3'
D16S539 rev	5'-GTT TGT GTG TGC ATC TGT AAG CAT GTA TC-3'
D13S317 for	5'-HEX-ATT ACA GAA GTC TGG GAT GTG GAG GA-3'
D13S317 rev	5'-GGC AGC CCA AAA AGA CAG A-3'
vWA for	5'-6-FAM-GCC CTA GTG GAT GAT AAG AAT AAT CAG TAT GTG-3'
vWA rev	5'-GGA CAG ATG ATA AAT ACA TAG GAT GGA TGG-3'
TPOX for	5'-6-FAM-ACT GGC ACA GAA CAG GCA CTT AGG-3'
TPOX rev	5'-GGA GGA ACT GGG AAC CAC ACA GGT TA-3'
THO1 for	5'-6-FAM-ATT CAA AGG GTA TCT GGG CTC TGG-3'
THO1 rev	5'-GTG GGC TGA AAA GCT CCC GAT TAT-3'
CSF1PO for	5'-6-FAM-AAC CTG AGT CTG CCA AGG ACT AGC-3'
CSF1PO rev	5'-TTC CAC ACA CCA CTG GCC ATC TTC-3'
Amelogenin for	5'-ACC TCA TCC TGG GCA CCC TGG TT-3'
Amelogenin rev	5'-TAMRA-AGG CTT GAG GCC AAC CAT CAG-3'

3.5 MOLEKULARE ANALYSE

Die Mikrosatelliteninstabilität (MSI) und der Methylierungsstatus der CpG-Inseln [2], [30], [31] wurde für alle in diese Studie einbezogenen Fälle bestimmt. Die Klassifizierung war MSI-H, wenn zwei oder mehr Mikrosatellitenmarker entweder des Bethesda-Panels oder des "six mononucleotide" Panel, bestehend aus BAT25, BAT26, CAT25, NR21, NR24 und NR27, Bandenverschiebungen zeigten [2], [21]. Die Klassifizierung hinsichtlich des CpG-Insel-Methylator-Phänotyp (CIMP) wurde wie folgt vorgenommen: Wurde die Analyse nach Ogino *et al.* durchgeführt, wurde der Subtyp in CIMP-H, non MSI, unterteilt, wenn 4 Loci und in CIMP-L, non MSI, wenn 1-3 CIMP-Loci von 5 analysierten Loci methyliert waren [2], [30]. Bei der Analyse nach Weisenberger *et al.* definierten 3 methylierte CIMP-Loci von 5 untersuchten Loci CIMP-H, non MSI. Eine weitere Unterscheidung in CIMP-L, non MSI fand nicht statt [19], [31].

3.6 NEXT GENERATION SEQUENCING (NGS) ANALYSE

Insgesamt wurden 121 Datensätze analysiert die entweder von der Firma Centogene (Rostock, Deutschland) erstellt oder aus einem früheren Datensatz, bestehend aus Whole Exom Sequencing (WES) Analysen, extrahiert wurden [32]. WES Analysen erfolgten von 20 PDX Fällen und 12 Primärtumoren. Die übrigen Analysen wurden mit einem Solid Tumor Panel von Centogene durchgeführt, das aus 105 vollständig sequenzierten Genen besteht, sowie aus Mutations-Hotspots von weiteren 146 Genen [19]. Bei der Auswertung der NGS-Daten wurden ausschließlich Mutationen berücksichtigt, die pathogen oder wahrscheinlich pathogen sind sowie Mutationen mit unklarer Bedeutung. Ausgeschlossen waren alle gutartigen Mutationen und Mutationen, die als Risikofaktor eingestuft wurden oder solche die die „drug response“ beeinflussen. Außerdem wurden nur die Mutationen aus den Rohdaten berücksichtigt, die die folgenden Qualitätskriterien, darunter der Filter "Pass", codierendes Synonym, eine Qualität von 30 und eine Allelhäufigkeit (variant allele frequency) von mindestens 15 erfüllten [19].

3.7 IN VIVO VERSUCHE - DOSISFINDUNGSSTUDIE

Die Implantation des PDX Tumors erfolgte, wie unter 3.2 beschrieben, in NSG Mäusen. Für die Dosisfindungsstudie wurden die Mäuse nach der Tumoretablierung in die folgenden Therapiegruppen mit jeweils zwei Tieren pro Gruppe randomisiert (Abbildung 3): (1) 5-FU-Bolus (80 mg/kg Körpergewicht, intraperitoneal (i.p.), wöchentlich, insgesamt dreimal); (2) 5-FU niedrig dosiert (30 mg/kg Körpergewicht, i.p. täglich, insgesamt fünfmal); (3) 5-FU/Leucovorin (LV) in niedriger Dosierung (20/10 mg/kg Körpergewicht, dreimal wöchentlich i.p., insgesamt neunmal); (4) 5-FU/LV niedrig dosiert (10/20 mg/kg Körpergewicht, i.p. fünfmal wöchentlich, insgesamt zehnmal); (5) Capecitabin-Bolus (800 mg/kg Körpergewicht, peroral (p.o.), zweimal wöchentlich, insgesamt sechsmal); und (6) Capecitabin in niedriger Dosierung (350 mg/kg Körpergewicht, p.o., fünfmal wöchentlich, insgesamt 15-mal) [26].

Alle Mäuse erhielten während der Experimente täglich zubereitetes eingeweichtes Futter. Tumorwachstum und Körpergewicht wurden dreimal wöchentlich bestimmt, um eine behandlungsbedingte Toxizität zu überwachen. Die Entnahme der Tumoren erfolgte nach Abschluss der Therapie oder wenn die Mäuse einen schlechten Gesundheitszustand aufzeigten (Gewichtsverlust >20 % gegenüber dem Beginn der Therapie), wenn die Mäuse ein sozio-physiologisches Verhalten zeigten sowie wenn die Tumorgroße >1000 mm³ erreichte [26].

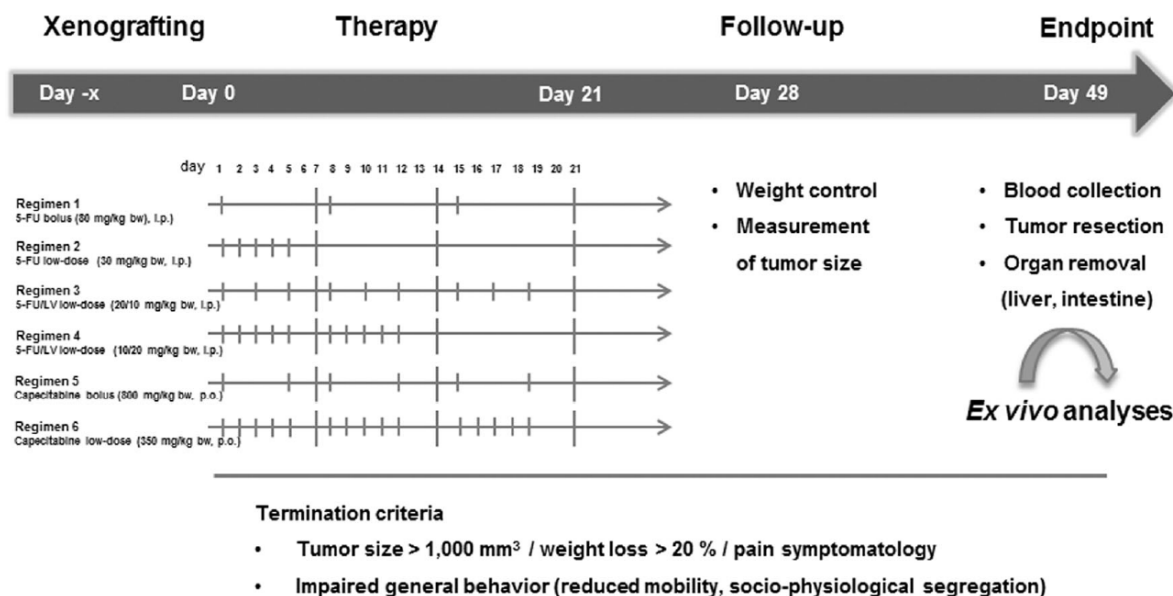


Abbildung 3: Zeitplan für das Behandlungsprotokoll der Dosisfindungsstudie NSG Mäusen wurden individuelle PDX Tumorgewebe implantiert. Nachdem sich der Tumor etabliert hatte (~6 mm), wurden die Mäuse in sechs Behandlungsarme aufgeteilt (die Injektionsintervalle sind durch kurze vertikale Linien gekennzeichnet, lange vertikale Linien geben Wochen an). Jede Gruppe bestand aus zwei Mäusen. Die Nachbeobachtung erfolgte durch wöchentliche Gewichtskontrollen und die Überwachung des Tumorwachstums. Der experimentelle Endpunkt wurde definiert durch übermäßiges Tumorwachstum (>1000 mm³) oder beeinträchtigtes allgemeines Verhalten der Mäuse [26].

Sowohl Blutproben als auch Tumorgewebe, Leber, Niere, Dünn- und Dickdarm wurden für weitere Untersuchungen entnommen [26].

3.8 STATISTISCHE ANALYSEN

Die statistischen Analysen wurden entweder mit dem Statistikprogramm GraphPad PRISM Version 5.2 und 8 oder IBM SPSS Statistics durchgeführt.

Heatmap- und Mutationshäufigkeitsanalysen wurden in PRISM Version 8 durchgeführt [19]. Die Ergebnisse der Dosisfindungsstudie wurden in PRISM Version 5.2 ausgewertet [26]. Nach Bestätigung der Normalitätsannahme (D'Agostino & Pearson omnibus normality test) wurden die Daten mittels one-way Anova (Bonferroni's Multiple Comparison Test) analysiert. Das Kriterium für die Signifikanz wurde auf $p < 0,05$ festgelegt [26].

In SPSS wurde eine nichtparametrische bivariate Korrelationsanalyse nach Kendall-Tau und Spearman's Rangkorrelationskoeffizient und Fisher's exact test durchgeführt [19]. Die Clusteranalyse wurde mit Origin Pro 2017G durchgeführt (Parameter: Clustermethode = Furthest Neighbor; Distanztyp = Euclidean) [19].

IV. ERGEBNISSE

4.1 PATIENTEN, KLINISCHE SOWIE MOLEKULARE DATEN

Zum Zeitpunkt der Veröffentlichung der HROC-Xenobank waren von insgesamt 261 CRC-Patienten aus der HROC-Biobank 167 individuelle PDX Modelle erstellt (64,0 %) [19]. Für die HROC-Xenobank wurden 125 dieser Fälle detailliert analysiert, da die nachfolgenden Kriterien erfüllt wurden: (I) anhaltendes Wachstum in immundefizienten Mäusen und (II) Lagerung PDX Gewebe in ausreichender Menge und (III) PDX Gewebe in angemessener Qualität [19].

Im Mai 2020 erfolgte eine Aktualisierung der bereits zuvor beschriebenen [21] verfügbaren Patienteninformationen wie weiteren Behandlungen, Wiederauftreten der Krankheit, progressionsfreies und Gesamtüberleben etc. Diese Daten sind in der Publikation von Matschos *et al.* [19] in der Supplementären Tabelle S1 aufgeführt. Die Tumorproben der Patienten bestehen aus 100 primären Adenokarzinomen, einem neuroendokrinen Tumor, und fünfundzwanzig Proben metastatischen Ursprungs. Die Metastasen traten größtenteils in der Leber (80,0 %) auf, zusätzlich auch in der Bauchdecke, dem Gehirn, der Lunge und dem Bauchfell sowie multiviszeral (jeweils n = 1) [19].

Die Geschlechterverteilung der 125 eingeschlossenen Patientenfälle war 56,8 % männlich und 43,2 % weiblich. Das Durchschnittsalter betrug 69,7 Jahre (zwischen 30 und 98 Jahren). Die UICC-Stadien der Tumoren betragen 11 % im Stadium I, 29 % im Stadium II, 27 % im Stadium III und 33 % im Stadium IV. Die T-Stadien waren 30 % T4, 59 % T3, 10 % T2 und 1 % T1; M-Stadien 1 % M2 und 32 % M1; bei 67 % wurden keine Metastasen festgestellt (M0). Das Tumorgrading (G) betrug 2 % G1, 55 % G2 und 43 % G3 [19].

Da die integrierten Biobankaktivitäten im Jahr 2006 begannen und ein laufender Prozess sind, decken die einbezogenen Fälle den Zeitraum von 2006 bis 2019 ab. Daher war es nicht möglich, die 5-Jahres-Überlebensrate für alle Patienten zu berechnen. Dementsprechend war die Festlegung eines Grenzwerts für die Berechnung der Überlebenszeit notwendig [19].

Zum Stichtag Mai 2020 waren 54 Patienten noch am Leben, 71 Patienten waren verstorben. Drei Patienten starben perioperativ, innerhalb von 30 Tagen nach der Operation (entsprechend der Clavien-Dindo-Klassifikation). Bei den übrigen 68 verstorbenen Patienten betrug das progressionsfreie Überleben durchschnittlich 13,0 Monate (von 0 bis 119) und das Gesamtüberleben betrug 32,6 Monate (zwischen 1 und 133) [19].

Die individuelle Tumorgeschichte und das Therapieschema jedes Patienten wurden, falls zutreffend, detailliert aufgeführt, inklusive Art und Dauer der Therapie sowie den angewendeten Chemotherapeutika (Publikation von Matschos *et al.*, Supplementäre Tabelle S1) [19]. Da die meisten unserer internen Therapiestudien mit verschiedenen Wirkstoffen im Vergleich

zur Standardtherapie laufen oder demnächst veröffentlicht werden, sind die Therapeutika, die im Vergleich zur Standardtherapie eine Verringerung des PDX Tumorwachstums zeigten, ausschließlich in der Supplementären Tabelle S1 (Publikation von Matschos *et al.*) [19] aufgelistet. Da eine ideale CRC-PDX Sammlung die molekulare Heterogenität der klinischen Fälle annähernd abbilden sollte, wurden die Fälle der HROC-Xenobank entsprechend der unter 1.1 beschriebene molekularen Subtypen klassifiziert (Tabelle 2).

Tabelle 2: Verteilung molekulare Subtypen [19].

Molecular Subclass Determination (n = 125):		
CIN	65	52 %
spMSI-H	29	23.2 %
CIMP-H, non MSI	10	8 %
CIMP-L, non MSI	10	8 %
Lynch syndrome	10	8 %
Neuroendocrine tumor	1	0.8 %

Die Verteilung der molekularen Subtypen entspricht weitgehend der allgemeinen klinischen Verteilung [3]. Nur spMSI-H und LS sind überrepräsentiert, was höchstwahrscheinlich auf die hohen Anwachsraten dieser molekularen Subtypen zurückzuführen ist [33].

4.2 PDX MODELLE

Die HROC-Xenobank enthält acht Fälle von Primärtumor- und Metastasengewebe desselben Patienten, nämlich: HROC72 und HROC72Met1; HROC147 und HROC147Met1; HROC277, HROC277Met1 (synchron), und HROC277Met2 (metachron); HROC278 und HROC278Met1; HROC300 und HROC300Met1; HROC348 und HROC348Met1; HROC362 und HROC362Met1 sowie HROC405 und HROC405Met1. Zusätzlich sind drei Fälle eingeschlossen, die zwei Metastasen ein und desselben Patienten enthalten: HROC103Met1 und Met2, HROC230Met1 und Met2, sowie HROC313Met1 und Met2. Außerdem sind zwei Fälle von verschiedenen Primärtumoren desselben Patienten enthalten: HROC252Tu1, Tu2 und Tu3, sowie HROC386Tu1 und Tu2 [19].

Die durchschnittliche Entnahmezeit betrug für alle einbezogenen PDX Modelle bezogen auf alle Passagen 105 Tage (Spanne 38 bis 287). Es wurden keine signifikanten Unterschiede festgestellt bezüglich der Entnahmezeit beim Vergleich der ersten Passage mit 120 Tagen (Spanne 36 bis 329) im Vergleich zu 106 Tagen (Spanne 35 bis 324) für die zuletzt durchgeführten Passagen der einbezogenen PDX Modelle [19].

Mäuse, deren schlechter Gesundheitszustand zu einer vorzeitigen Explantation des Tumors führte, wurden von der Berechnung der Entnahmezeit ausgeschlossen. Diese Fälle sind in der Supplementären Tabelle S1 (Publikation von Matschos *et al.*) [19] mit >x Tagen angegeben.

Die Entnahmezeiten zwischen der ersten und der letzten Passage jedes einzelnen Patientenfalls wurden verglichen und die verlängerte oder verringerte Dauer ist in den Spalten AG und AH der Supplementären Tabelle S1 (Publikation von Matschos *et al.*) [19] durch Pfeile gekennzeichnet. Ein Trend zu einer kürzeren Entnahmezeit für die letzten Passage wurde in der Mehrzahl der Fälle beobachtet: 70/125 (56 %). Eine Korrelation mit dem molekularem Subtyp oder Merkmalen des PDX zeigten sich nicht.

Außerdem war ein direkter Vergleich zwischen der Verwendung von frischem und vital gefrorenem Gewebe für dieselbe Passage in 28 Fällen möglich (Supplementäre Tabelle S2, Publikation von Matschos *et al.* [19]). In 23 dieser Fällen (82,1 %) wurde eine kürzere Zeit bis zur Entnahme beobachtet, wenn die PDX Gewebe frisch passagiert wurden (ungepaarter t-Test $p = 0,0003$).

Eine Korrelationsanalyse ergab neben den erwarteten positiven Korrelationen des UICC-Stadium mit dem progressionsfreien Überleben sowie dem Gesamtüberleben der Patienten, Korrelationen zwischen den PDX Modellmerkmalen und den Eigenschaften des Patiententumors (Supplementäre Tabelle S3, Publikation von Matschos *et al.*[19]).

Es korrelierten der molekulare Subtyp mit dem Zeitpunkt der Entnahme von PDX Tumoren (Korrelation $p < 0,001$, exakter Fischertest $p = 0,008$), die Anzahl der Mäuse, die zur Erzeugung ausreichender Backups erforderlich war, mit dem molekularen Subtyp (Korrelation $p = 0,002$, exakter Fischertest $p = 0,048$) sowie die Lokalisation des Tumors mit der Dauer bis zur Entnahme (Korrelation $p = 0,002$, exakter Fischertest $p = 0,047$). Tumoren des rechten Kolons benötigten im Allgemeinen weniger als 90 Tage. Bei den anderen Lokalisationen, betrug die Dauer 90-180 Tage bis zum Auswachsen. Bezüglich des molekularen Subtyp sind MSI-H-Tumoren, sowohl sporadische als auch Lynch-assoziierte, in den meisten Fällen in weniger als 90 Tagen ausgewachsen. Die übrigen molekularen Subtypen brauchten 90-180 Tage, um die angegebene Größe zu erreichen. Die meisten PDX Fälle des spMSI-H-Typ konnten mit weniger als 3 Mäusen erzeugt werden, während die höchste Anzahl von Mäusen, häufig $> 4,5$ Mäuse, für CIMP-L-Tumoren, die nicht vom MSI-Typ sind, erforderlich waren [19].

4.2.1 IDENTITÄTSPRÜFUNG

Die genetische Identität aller etablierten PDX Modelle im Vergleich zum ursprünglichen Patientengewebe wurde durch eine STR- Analyse bestätigt, wie zuvor beschrieben [34]. Die PDX waren entweder genetisch identisch mit dem jeweiligen Patienten oder stammten von ihm ab, mit zwei Ausnahmen: Für die PDX HROC32 T3 M7 und HROC223 T2 M1 konnten mittels Fingerprint-Analyse keine auswertbaren Signale erzeugt werden. Allelische Ungleichgewichte sowie kleine Verschiebungen in der Allellänge wurden regelmäßig für PDX des MSI-Subtyps

beobachtet. Diese beiden Phänomene sind bekannt. Die Möglichkeit des Vergleichs mit verschiedenen Patientengewebe sowie primären und sekundären Zelllinien, ermöglichte eine valide Identitätsüberprüfung der MSI-Fälle [19].

4.2.2 HISTOLOGIE

H&E-gefärbte Schnitte von FFPE-Blöcken wurden verwendet, um die morphologischen Merkmale jedes einzelnen PDX Modells zu bestimmen. Darüber hinaus wurden die PDX Tumoren mit dem jeweiligen Original-Patiententumor durch einen zertifizierten Pathologen (FP) verglichen. Abbildung 4 zeigt drei ausgewählte Fälle: HROC172, HROC260 und HROC386Tu1 [19].

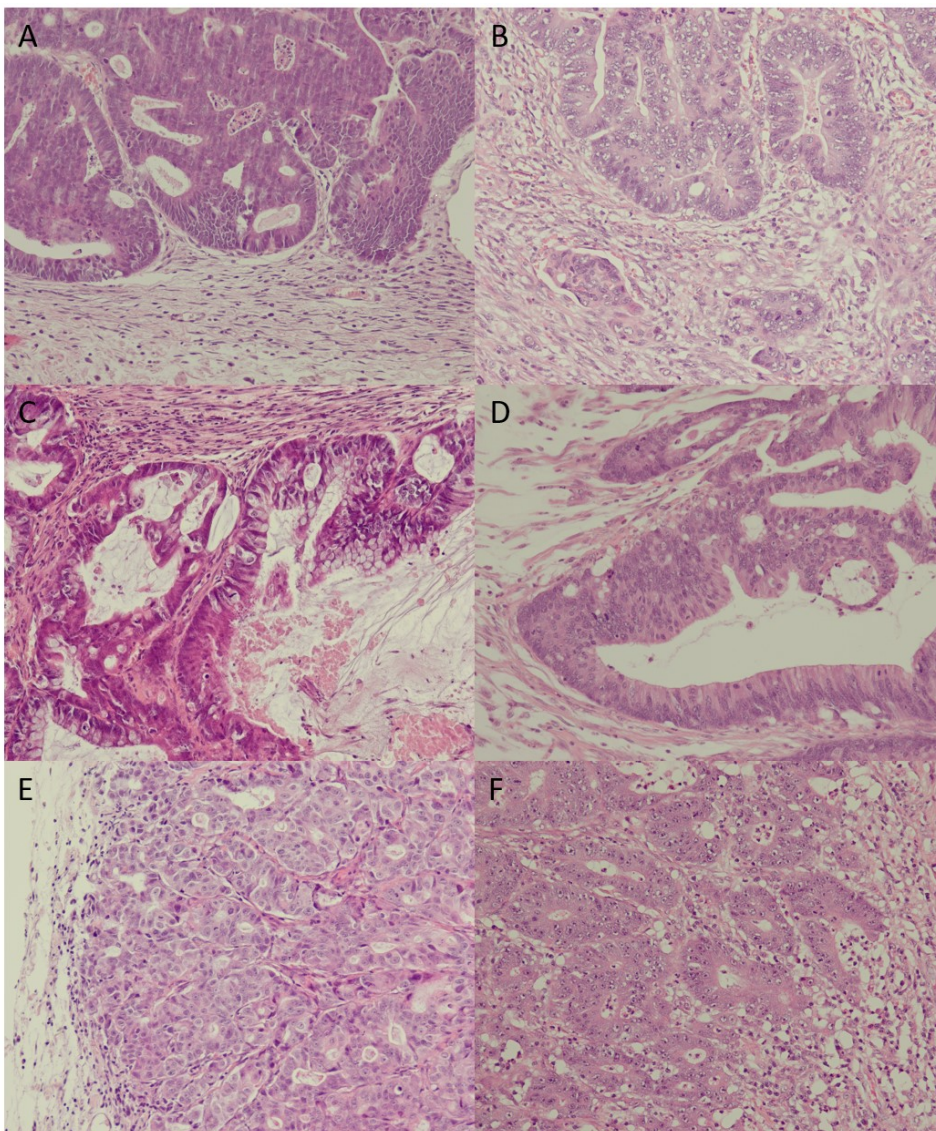


Abbildung 4: Vergleich von Primärtumor und PDX Tumor in 20-facher Vergrößerung: (A) = HROC172 Primärtumor, (B) = HROC172 T2 M2; (C) = HROC260 Primärtumor, (D) = HROC260 T2 M5; (E) = HROC386Tu1 Primärtumor, (F) = HROC386Tu1 T1 M1. Im Fall von HROC172 stimmen PDX Zytomorphologie und Architektur mit dem Primärtumor überein, Stromadesmoplasie und Tumor Budding deutlich reduziert; im Fall von HROC260 stimmen PDX Zytomorphologie und -Architektur mit dem Primärtumor überein und die villös-muzinöse Struktur wurde ebenfalls reproduziert; im Fall von PDX HROC386Tu1 wurden die Zytomorphologie und die Architektur des Primärtumors exakt reproduziert [19].

Einzelheiten zu den histologischen Untersuchungen sind in der Supplementären Tabelle S4 (Publikation von Matschos *et al.*) [19] aufgeführt. Bei 17 der 125 Fälle war ein Vergleich nicht möglich, da nicht genügend FFPE Patiententumormaterial zur Verfügung stand, für insgesamt 108 Fälle war ein direkter Vergleich möglich. Übereinstimmung von Patienten- und PDX Tumorstruktur wurde in 92 Fällen (85,2 %) festgestellt, geringfügige Unterschiede zeigten 11 Fälle (10,2 %) und deutliche Unterschiede traten in 5 Fällen (4,6 %) auf. Hier zeigte eine STR-Analyse mit gDNA, die aus Schnitten derselben FFPE-Gewebeblöcke isoliert wurde, die für die histologische Untersuchung verwendet wurden, die genetische Identität mit den jeweiligen Patientenproben bei drei der fünf Fälle (HROC251, HROC370 und HROC447). Für die Fälle HROC32 und HROC223 vermutete der Pathologe eine starke Kontamination der PDX Gewebe mit murinen oder humanen lymphatischen Zellen. Da die STR-Analyse bei diesen beiden PDX Geweben nicht erfolgreich war, wurden, wie oben erwähnt, speziesspezifische PCR-Analysen durchgeführt. Die Ergebnisse ließen den Schluss zu, dass in den PDX Geweben überwiegend murine Thymomzellen vorhanden waren. Bemerkenswert sind die Identitätstests von HROC32-PDX Gewebe nach der ersten Mauspassage, sowie von zwei PDX Zelllinien, die aus der gleichen Passage wie das FFPE-Gewebe stammen, stimmten mit den Identitäten der Patienten überein [19].

Ein Vergleich von PDX Tumoren, die aus der gleichen Passage, aber von verschiedenen Tieren stammten, lieferte exakt übereinstimmende pathomorphologische Ergebnisse für sechs Fälle mit unterschiedlichen molekularen Subtypen (HROC92, HROC111Met1, HROC131, HROC169, HROC324 und HROC430) (Supplementäre Tabelle S4, Publikation von Matschos *et al.* [19]). Dies deutet daraufhin, dass die Erhaltung der biologischen Merkmale des ursprünglichen Tumors wie Mikroarchitektur und Pathomorphologie intrinsische Merkmale des individuellen Modells sind und zu erwarten ist, dass diese über mehrere Passagen hinweg stabil erhalten bleiben, wie Tentler *et al.* bereits gezeigt haben [2].

Bei der Explantation von PDX Tumoren wurde der Grad der Nekrose bestimmt. Obwohl es sich hierbei nicht um eine sehr präzise Methode handelt, konnten die PDX Fälle in vier Kategorien eingeteilt werden: nicht, kaum, mittelgradig und stark nekrotisch (Supplementäre Tabelle S1, Spalte AJ, Publikation von Matschos *et al.* [19]). Hier zeigte sich keine signifikante Korrelation zwischen dem Grad der Nekrose und den Patientendaten. Allerdings waren die MSI-Fälle, sowohl sporadische als auch LS-Fälle, die PDX Modelle, die weniger Mäuse für eine vollständige Asservierung benötigten, und die PDX Fälle mit kürzerer Dauer bis zur Entnahme, selten hochgradig nekrotisch: Es gab nur 4/39 Fälle (10,3 %) gegenüber 27/86 Fällen (31,4 %) bei den übrigen molekularen Subtypen. Stark nekrotische PDX Tumoren behielten diese Eigenschaft auch in späteren Passagen. Die gepaarten PDX Fälle von primären und metastasierten Tumoren von denselben Patienten (n = 8) wiesen immer sehr ähnliche Nekrosekategorien auf (Supplementäre Tabelle S1, Publikation von Matschos *et al.* [19]).

Die orange hervorgehobenen Cluster enthalten hauptsächlich CIN-Fälle (70,0 und 65,7 %), während das gelb markierte Cluster fast ausschließlich aus sporadischen MSI-Tumoren besteht (88 %). Das rot markierte Cluster konnte jedoch keinem spezifischen molekularen Subtyp zugeordnet werden [19].

Außerdem wurde die Anzahl der pathogenen und wahrscheinlich pathogenen Mutationen pro Gen und Fall in einer Heatmap dargestellt (Abbildung 6A). Die Mutationshäufigkeit der einzelnen Gene ist in Abbildung 6B zu sehen. Die am häufigsten mutierten Gene in der HROC-Xenobank sind APC (50,4 %), KRAS (39,8 %), TP53 (37,2 %), BRAF (23,0 %) und PIK3CA (17,7 %) [19].

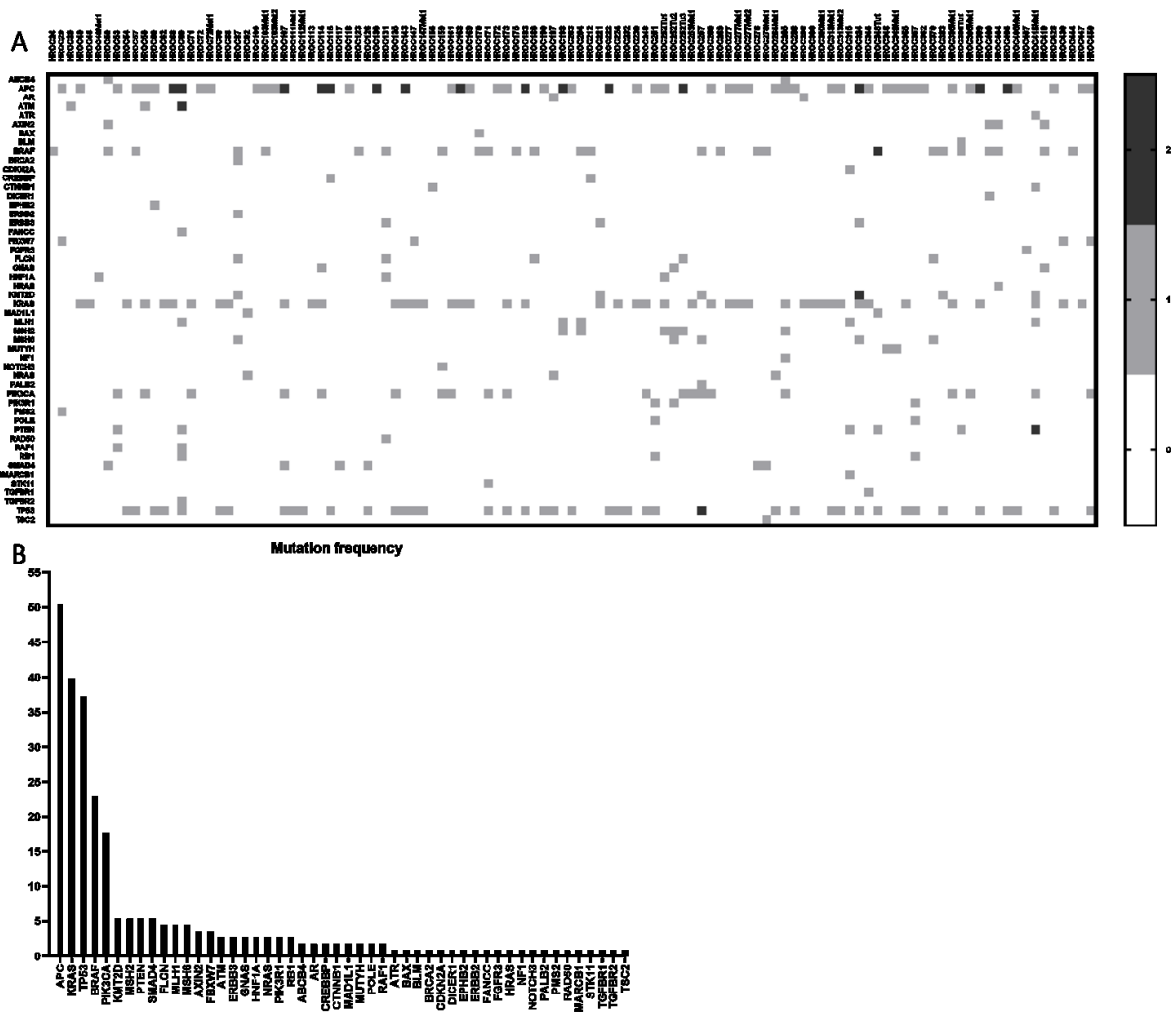


Abbildung 6: (A) = Heat Map (B) = Mutationshäufigkeit (A) veranschaulicht die Anzahl der pathogenen und wahrscheinlich pathogenen Mutationen pro Gen und Fall in einer Heatmap und die aus diesen Daten berechnete Mutationshäufigkeit für jedes Gen in % ist in (B) dargestellt [19].

4.4 IN VIVO VERSUCHE - DOSISFINDUNGSSTUDIE

NSG Mäuse mit PDX aus verschiedenen CRC-Fällen wurden zunächst mit 30 mg/kg Körpergewicht 5-FU behandelt (i.p. dreimal wöchentlich, insgesamt neunmal; n = 4 Fälle) [26]. Die

Tumoren zeigten zwar Wachstumshemmungen bis hin zur Schrumpfung, allerdings war diese Dosis toxisch für die Mäuse und in 4/4 PDX Fällen trat der unerwartete Tod ein. Eine Reduzierung der 5-FU-Dosis auf 20 mg/kg Körpergewicht, wie sie in einer anderen *in-vivo*-Studie zum Ansprechen von 5-FU auf HROC-PDX in NMRI-*Foxn1*^{nu} Mäusen (nämlich HROC24) beschrieben wurde, verhinderte die Toxizität [35]. Eine Dosisreduzierung hob jedoch die therapeutische Wirkung von 5-FU auf, mit Tumorstadiumskurven ähnlich denen der Kontrollmäuse (Daten nicht gezeigt) [26]. Aus diesem Grund war es notwendig, ein 5-FU-Schema systematisch zu bestimmen und dieses für nachfolgende Studien mit dem NSG Stamm zu optimieren. Genauer gesagt, wurde aus sechs verschiedenen 5-FU-Applikationen die am besten verträgliche Applikation mit optimaler therapeutischer Wirkung ermittelt. Mäuse mit etablierten PDX (n = 4 individuelle PDX Modelle, nämlich HROC29, HROC40, HROC46, und HROC222, n = 2 Mäuse/Gruppe) wurden, wie unter 3.7 beschrieben, in die sechs Behandlungsgruppen randomisiert [26].

Alle Behandlungsschemata gingen mit einem vorübergehenden Gewichtsverlust (Abbildung 7a), Fellkräuseln und unterschiedlichem Ausmaß an Durchfall einher. Schema 1 (5-FU-Bolusinjektion) wies eine geringe Toxizität auf, 75 % der Mäuse überlebten diese Therapie (Tabelle 3 und Abbildung 7b). Der Gewichtsverlust trat vorwiegend 3-4 Tage nach der Injektion auf, wobei sich die Mäuse danach erholten (Abbildung 7a). Schema 2 (niedrig dosiertes 5-FU) beeinträchtigte den Gesundheitszustand schwer, was zu einem massiven Gewichtsverlust der betroffenen Mäuse führte (Tag 7: -23 % gegenüber Tag 0). Infolgedessen starben die meisten Mäuse aufgrund der 5-FU-vermittelten Toxizität innerhalb von einer Woche nach der Behandlung (Tabelle 3 und Abbildung 7b). Die Gesamtüberlebensrate betrug nur 25 %. Im Gegensatz dazu, war der Allgemeinzustand der Mäuse nach der Behandlung mit 5-FU/LV (Schema 3 und 4) oder Capecitabin (Schema 5 und 6) nicht wesentlich beeinträchtigt, was sich hinsichtlich dieses Nebenwirkungsprofils als vorteilhaft erwies. Bei diesem letztgenannten Schema wurden Gewichtsveränderungen hauptsächlich zu späteren Zeitpunkten beobachtet (Tag 11-16), blieben aber bis zum Ende der Therapie (~10 % gegenüber Tag 0) (Abbildung 7a). 5-FU/LV beeinflusste das Gewichtsmuster nur geringfügig, insbesondere wenn es in niedriger Dosis verabreicht wurde (Schema 4) [26].

Tabelle 3: Behandlungsbedingte/unerwartete Tode der Dosisoptimierungsstudie [26].

Schema	Verstorben %		Durchschnittliche Todeszeit [d]
	Behandlungsbedingt	Unerwartet	
1	25	0	14
2	75	0	7
3	12,5	0	11
4	0	0	-
5	12,5	25	3
6	0	12,5	1

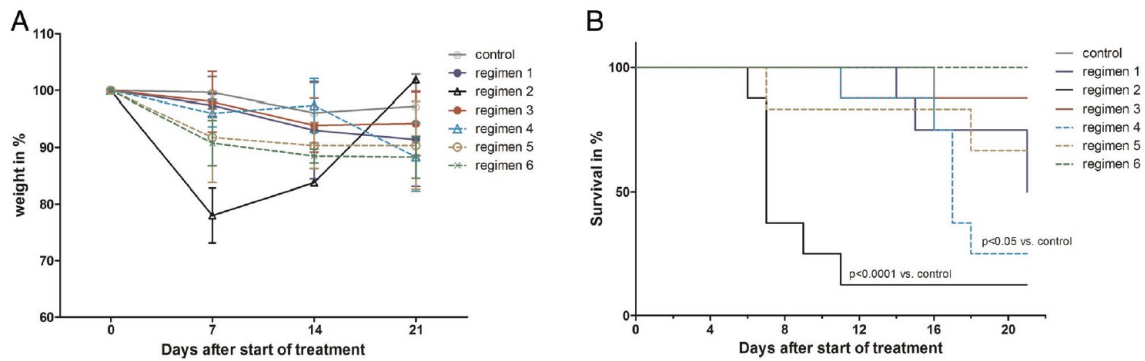


Abbildung 7: Gewichtskurve und Überlebensanalyse A: Das Körpergewicht wurde dreimal wöchentlich kontrolliert und ein Gewichtsverlust erfolgte vor allem in der frühen Phase der Behandlung, der sich in den meisten Fällen wieder erholte. Die Werte sind angegeben als % Gewicht vs. Tag $0 \pm SD$; $n = 8$ Mäuse pro Behandlung, $n = 1$ Kontrollmaus/ einzelner PDX Fall. B Die Analyse der Kaplan-Meier-Überlebenskurve zeigt Veränderungen zwischen den einzelnen Behandlungen, mit der höchsten behandlungsbedingten Toxizität in Schema 2 unabhängig vom PDX Fall. $n = 8$ Mäuse pro Schema, $n = 1$ Kontrollmaus/einzeln PDX Fall. Signifikante Unterschiede zwischen Behandlungs- und Kontrollmäusen sind wie folgt: $p < 0,05$ Schema 4 vs. Kontrolle; $p < 0,0001$ Schema 2 vs. Kontrolle. One way-ANOVA (Bonferroni's Multiple Comparison Test) [26].

Die *in vivo* Arzneimittelwirkung ist in Abbildung 8 dargestellt. Die Tumorgrößen sind standardisiert und werden in Prozent zur jeweiligen Kontrolle jedes einzelnen PDX Falls angegeben. Das Ansprechen auf die Medikamente variierte zwischen den Schemata und PDX Modellen verschiedener molekularen Subtypen [26].

Im Einzelnen verlangsamte das Schema 1 das Tumorwachstum über den gesamten Beobachtungszeitraum in 3/4 der Fälle (HROC29, HROC40 und HROC46) im Vergleich zu den jeweiligen Kontrollgruppen ($p < 0,05$ vs. HROC222; Abbildung 8). Im Fall von HROC222 wurde kein Ansprechen auf die Behandlung beobachtet. Schema 2 beeinträchtigte das Tumorwachstum in den beiden PDX Modellen HROC40 und HROC46, ging aber mit einer massiven Toxizität einher ($p < 0,05$ gegenüber HROC222; Abbildung 7b). Das Tumorwachstum aller einzelnen PDX Modelle wurde durch Schema 3 geringfügig beeinträchtigt und bei Schema 4 wurde kein Ansprechen auf die Behandlung beobachtet (Abbildung 8). Diese spezielle Behandlungsgruppe zeigte sogar eine Tendenz zu beschleunigtem Tumorwachstum (HROC40 zu Beginn, HROC222 zu späteren Zeitpunkten). Die Therapieschemata 5 und 6 verzögerten das Tumorwachstum geringfügig, mit allerdings individuellen Unterschieden [26].

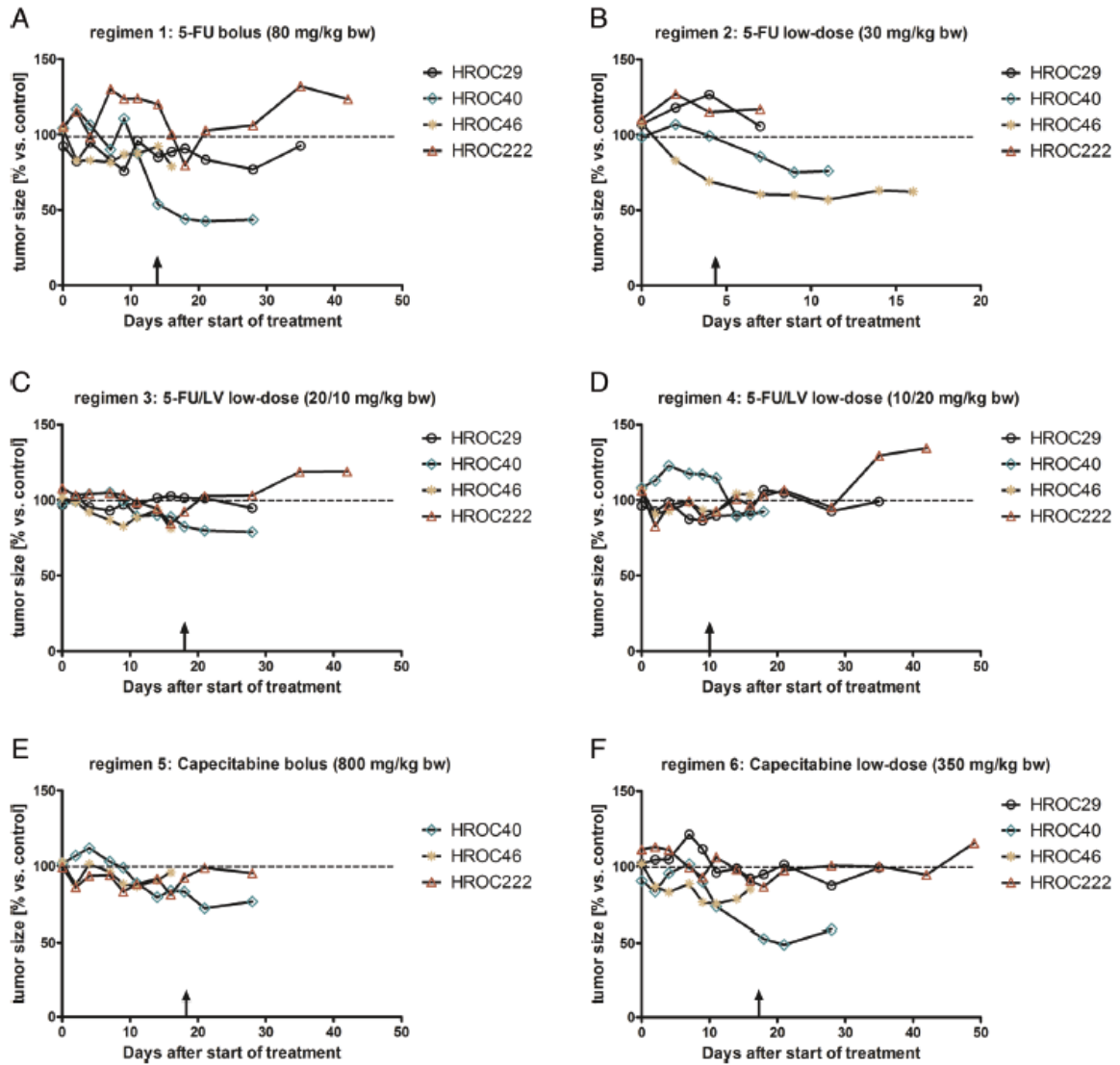


Abbildung 8: Tumorwachstumskurve NSG Mäuse mit etablierten PDX wurden wie unter 3.7 beschrieben behandelt. Die Tumorgröße wurde dreimal wöchentlich mit einer Schieblehre gemessen. Wachstumskurven für jeden PDX Fall (nämlich HROC29, HROC40, HROC46 und HROC222) sind entsprechend der sechs Behandlungsschemata dargestellt. Die Pfeile zeigen das Ende der Behandlung an. Die Werte sind als prozentuale Tumorgröße im Vergleich zur Tumorgröße der entsprechenden Kontrollmaus dargestellt (= unbehandelt, auf 100 % gesetzt); n = 8 Mäuse pro Schema, n = 1 Kontrollmaus/individueller PDX Fall. Signifikante Unterschiede zwischen den einzelnen PDX Fällen jeder Therapie sind: Schema 1: $p < 0,05$ HROC222 vs. HROC29, HROC40 und HROC46; Schema 2/3: $p < 0,05$ HROC222 vs. HROC40 und HROC46; Schema 6: $p < 0,05$ HROC222 vs. HROC40 und HROC46; $p < 0,05$ HROC29 vs. HROC40 und HROC46; One way-ANOVA (Bonferroni's Mehrfachvergleichstest) [26].

V. DISKUSSION

Ausgangsgrundlage zur Erstellung der gut charakterisierten individuellen HROC-Xenobank ist die stetig wachsende HROC-Biobank, welche neben der Einhaltung der gesetzlichen Bestimmungen zum Datenschutz, Medizinrecht und Tierschutz eine gute Infrastruktur und ein gut eingespieltes Team erfordern. Selbstverständlich ist zusätzlich zur gut organisierten Zusammenarbeit von Labor und Klinik die Einhaltung von SOPs bei der Aufarbeitung der Proben unablässig, um eine gleichbleibende Qualität des Biobanking zu garantieren [25].

Entsprechend der von Mattar *et al.* beschriebenen Anforderungen an die Erstellung einer PDX Biobank bezüglich Probencharakterisierung und –validierung sowie der genomischen Profilerstellung und vergleichenden histologischen Untersuchungen [36] wurde eine CRC-Xenobank etabliert, die 125 individuelle PDX Modelle mit einer ausreichenden Anzahl von vitalen Backups, eingefrorenen Aliquots für molekulare Analysen und FFPE-Material enthält [19].

Die vergleichende pathomorphologische Analyse und die genetische Identitätsprüfung bestätigten die große Nähe der HROC-Xenobank-Modelle zu den ursprünglichen Patiententumoren [19]. Außerdem konnte bestätigt werden, dass PDX Modelle in den meisten Fällen die biologischen Eigenschaften des Originaltumors beibehalten [8], [13], [37].

Jedes individuelle HROC-PDX Modell reproduziert die pathomorphologischen Strukturen aus dem ursprünglichen Patiententumor und darüber hinaus zeigte der Vergleich von PDX Tumoren, die von der gleichen Passage aber von verschiedenen Tieren stammten, exakt übereinstimmende pathomorphologische Ergebnisse [19]. Daraus folgt, dass die biologischen Merkmale des Originaltumors, wie Mikroarchitektur und Pathomorphologie, intrinsische Merkmale des individuellen Tumors sind und daher auch in den PDX abgeleiteten Modellen konserviert werden und höchstwahrscheinlich über mehrere Passagen hinweg stabil sind. Es wurde bereits gezeigt, dass CRC-PDX die Histologie und andere Merkmale des Primärtumors beibehalten, einschließlich intratumoraler klonaler Heterogenität und chromosomaler Instabilität, für bis zu 14 Passagen [8].

Darüber hinaus rekapitulierten die HROC-PDX Modelle präzise die Mutationsprofile der primären Patiententumoren und bestätigten damit frühere Daten [37]–[39]. Insbesondere wurden pathogene oder wahrscheinlich pathogene Mutationen, die in den Originaltumoren detektiert wurden, auch in den PDX Tumoren nachgewiesen [19]. Der aktuelle Goldstandard zum Vergleich der NGS-Daten Analyse sind die Daten des Cancer Genome Atlas Network (TCGA). Der Vergleich zu den TCGA-Ergebnissen zeigte einige Unterschiede. Das am häufigsten mutierte Gen, APC, betrug 72,5 % im TCGA Datensatz, verglichen mit einer Häufigkeit von nur 50,4 % im HROC-Xenobank Datensatz. Das PIK3CA-Gen hatte eine Häufigkeit von 27,5 % in TCGA und 17,7 % in der HROC-Xenobank. Die Häufigkeiten für eine BRAF-Mutation lagen bei 11,6 % (TCGA) und 23 % (HROC-Xenobank). Den auffälligsten Unterschied zeigte die

TP53-Mutationshäufigkeit mit 58,8 % in den TCGA Daten, während die HROC-Daten lediglich 37,2 % aufzeigten. Ähnliche Häufigkeiten wurden jedoch für KRAS beobachtet mit 40,8 % (im Vergleich zu 39,8 %) [40].

Im Vergleich zu den von Lee *et al.* veröffentlichten Mutationshäufigkeiten für APC (60 %) und KRAS (49 %) ähneln die Ergebnisse denen der HROC-Xenobank [41]. Die von Burgenske *et al.* veröffentlichte Mutationshäufigkeit für PIK3CA (15-25 %) weicht nicht von unserer Beobachtung (17,7 % in der HROC-Xenobank) ab [42].

Wenn man sich auf hypermutierte Tumoren konzentriert, erhöht sich die Mutationshäufigkeit in TCGA auf 57,5 % für BRAF. Die Überrepräsentation von hypermutierten Tumoren in der HROC-Kohorte erklärt wahrscheinlich die höhere Häufigkeit von BRAF-Mutationen in den HROC-Daten.

Darüber hinaus tragen viele der HROC-PDX Modelle eine höhere Anzahl von Mutationen mit unklarer Bedeutung, als die Originaltumoren [19], während Abdirahman *et al.* solche zusätzlichen Mutationen in ihren seriell transplantierten Tumoren nicht beobachteten [37]. Entsprechend der von Brown *et al.* aufgestellten Hypothese könnten Mutationen, die in PDX, aber nicht in ursprünglichen Tumorproben von Patienten entdeckt wurden, schwer zu detektierende, niedrigfrequente Klone in den ursprünglichen Tumoren widerspiegeln [43].

Die Daten des deutschen Krebsregisters ZfKD (Zentrum für Krebsregisterdaten) zeigen, dass 56 % der Patienten mit fortgeschrittenem Darmkrebs männlich waren. Das Durchschnittsalter der männlichen Patienten lag zwischen 67,6 und 68,3 Jahren und bei den weiblichen Patienten zwischen 70,6 und 71,0 Jahren [5]. Das Durchschnittsalter der HROC-Studienpopulation beträgt 69,7 Jahre (Spanne 30 bis 98 Jahre) und liegt damit genau innerhalb der ZfKD-Bereiche [19]. Darüber hinaus entspricht der Männeranteil in der HROC-Studienpopulation mit 56,8 % männlichen Patienten der in der ZfKD angegebenen. Das Tumor-UICC-Staging betrug in unserer Studie 11 % (Stadium I), 29 % (Stadium II), 27 % (Stadium III) und 33 % (Stadium IV), verglichen mit 19,5 % (Stadium I), 29 % (Stadium II), 30 % (Stadium III) und 21,5 % (Stadium IV) in der allgemeinen deutschen CRC-Population [4]. Somit entspricht der Anteil von Darmkrebs im Stadium II genau, und der Anteil des Stadiums III nahezu mit der allgemeinen deutschen Darmkrebs-Population überein. Allerdings ist CRC-Stadium IV deutlich überrepräsentiert und Stadium I deutlich unterrepräsentiert, verglichen mit der Normalverteilung der Darmkrebsstadien in Deutschland. Teilweise ist dies einfach auf die Tatsache zurückzuführen, dass unsere Biobank-Sammlung auf Fälle beschränkt ist, die bei der Diagnose in der Pathologie über ausreichend Tumormaterial verfügen; daher müssen Fälle mit niedrigeren Stadien häufig ausgeschlossen werden. Außerdem wurden alle Fälle an einem Universitätszentrum gesammelt, wohin in der Regel die niedergelassenen Ärzte auch mehr fortgeschrittene Stadien überweisen [19].

Die Analyse der molekularen Subtypen ergab, dass unsere HROC-Xenobank-Kohorte die üblichen CRC-Subtypen repräsentiert [3]. Allerdings sind die spMSI-H- und LS-Fälle überrepräsentiert. Dies lässt sich am besten durch die Tatsache erklären, dass MSI-Tumoren deutlich besser engrafte als MSS Tumoren. Eine solche Diskrepanz bei den Transplantationsraten in Verbindung mit dem MS-Status wurde auch berichtet für Magenkrebs mit 55,93 % vs. 23,64 %; $p < 0,0001$ [33]. Zusätzlich wuchsen diese PDX schneller aus und es waren weniger Mäuse erforderlich, um eine ausreichende Menge an Backups zu erzeugen. Unsere Gruppe beschrieb zuvor den molekularen Subtyp ($p = 0,003$), insbesondere den MS-Status ($p = 0,001$), als Parameter, der die Erfolgsrate der PDX Etablierung aus CRC-Resektionsproben beeinflussen kann [21]. Es ist auch von Bedeutung, wenn auch in geringerem Maße, dass MSI-H PDX Tumoren oft nicht stark nekrotisch waren und daher nur selten, aufgrund dieser unerwünschten Eigenschaft, aus der endgültigen Kohorte ausgeschlossen wurden.

Die Kombination der Patientenproben der HROC-Biobank, den Proben der qualitätsgesicherten HROC-Xenobank sowie den daraus abgeleiteten Modellen, ermöglichen zahlreiche grundlegende sowie translationale Analysen.

Da alle Proben ausschließlich nach Einwilligung aller Patienten und der unwiderruflichen Anonymisierung aller persönlichen oder klinischen Daten gesammelt wurden, ist die Nutzung der HROC-Xenobank-Modelle nicht eingeschränkt durch die Allgemeine Datenschutzverordnung in der EU und die Modelle sind daher auf Anfrage erhältlich.

Neben der Qualitätssicherung ist die detaillierte Charakterisierung der PDX Modelle die perfekte Grundlage für weitergehende Untersuchungen, insbesondere da die klinische Situation repräsentiert wird.

Aufgrund der starken Heterogenität der Tumoren ist eine Gewebekbank mit einer ausreichenden Anzahl von Proben erforderlich, um die Vielfalt der Tumorarten abzudecken. Verglichen mit beispielsweise der PDX Biobank die Damhofer *et al* (Panel von 29 PDXs von Speiseröhren- und Bauchspeicheldrüsenkrebs) [15] oder Rivera *et al*. (Panel von 49 CRC-PDX Modellen) [44] erstellt haben, ist die HROC-Biobank deutlich umfangreicher.

Die gesammelten Patientendaten, die Einteilung entsprechend dem molekularen Subtype, der histologischen Untersuchungen, der Qualität des Tumors, etc. bieten etliche Möglichkeiten Untersuchen oder Auswertungen entsprechend von Kategorien durchzuführen.

Dies ermöglicht die Auswahl einzelner Modelle nach gewünschten Merkmalen und ermöglicht zukünftige Untersuchungen, wie präklinische PDX Studien und detaillierte Untersuchungen der molekularen Signalwege, mit gut charakterisierten Proben, wie ebenfalls von Rivera *et al*. [44] dargelegt. Deren Studie beinhaltet neben der Charakterisierung der PDX Modelle, Untersuchungen zur Ansprechbarkeit des Tumors auf Krebsmedikamente sowie die Erstellung von *in vivo* Resistenzmodelle, zur Untersuchung von Schlüsselmerkmalen assoziiert mit der Cetuximab-induzierten Resistenz. Diese Studie unterstreicht ebenfalls die Leistungsfähigkeit und

den Wert von PDX Modellen als Plattform für die Identifizierung und Validierung von Biomarkern, Signalwegen und Resistenzmechanismen sowie für die präklinische Erprobung von individualisierten Krebstherapien [44], um klinisch relevante Verbesserungen in der Krebstherapie zu bieten.

Darüber hinaus kann bei den Ergebnissen einer Therapiestudie beispielsweise geprüft werden, ob es Zusammenhänge zwischen Therapieerfolg oder -misserfolg und den molekularen Subtypen oder anderen Faktoren gibt.

Die HROC-Xenobank hat bereits in ihrer Gründungsphase Standard *in-vivo*-Studien [45], [46], detaillierte Untersuchungen der molekularen Signalwege [47], Biomarker-Studien und grundlegendere Studien, die die Vorteile der snap-frozen Aliquots nutzten [48], unterstützt. Eine erste präklinische PDX Studie wurde intern gestartet, die die unter 4.4 beschriebene Dosisfindungsstudie voraus ging [26]. Die Dosisfindungsstudie zeigt, dass es unumgänglich ist vor einer groß angelegten Therapiestudie ausreichend Vorversuche zur richtigen Dosierung und Art sowie Dauer der Therapie anzufertigen.

Es sind Hinweise auf eine unterschiedliche Verträglichkeit einzelner Mausstämme gegenüber bestimmten Zytostatika beschrieben [49]–[51]. Die Dosisfindungsstudie wurde durchgeführt, um ein wirksames Behandlungsschema mit akzeptabler Toxizität bei NSG Mäusen zu entwickeln. Das Ansprechen auf das Medikament und die Toxizität war sehr heterogen, mit einer unerwartet geringen Verträglichkeit bei der Hälfte der angewandten Schemata.

Im Hinblick auf die Wirksamkeit der Behandlung waren die Schemata 2, 5 und 6 in der Dosisfindungsstudie tendenziell am besten. Da das Schema 2 mit schwerer Toxizität verbunden war, ist dieses Dosierungsschema für zukünftige Studien nicht empfehlenswert.

Glaser *et al.* wählten ebenfalls Dosis und Zeitplan für die zielgerichteten Therapien auf der Grundlage der veröffentlichten Literatur aus, allerdings war die maximal verträgliche Dosis von intraperitonealem Carboplatin/Paclitaxel (C/P) oder Ifosfamid/Paclitaxel (I/P) nicht genau definiert [52]. Aus diesem Grund wurde ebenfalls eine Dosisfindungsstudie durchgeführt um die maximal verträgliche Dosis anhand eines standardmäßigen "3 + 3"-Designs zu ermitteln, das üblicherweise in klinischen Studien der Phase 1 verwendet wird [53]. Dosislimitierende Toxizität (DLT) wurde definiert als eine Behandlungsdosis, die zu einem Gesundheitszustand von ≤ 6 oder einem Gewichtsverlust von mehr als 20 % des Ausgangswertes führte [52].

Diese Ergebnisse zeigen, dass stets Vorversuche zur Verträglichkeit und Wirkung der zu testenden Medikamente durchgeführt werden sollten, um unnötige Experimente zu verhindern.

VI. ZUSAMMENFASSUNG

Verglichen mit anderen privaten Biobanken stellt die HROC-Biobank eine der größten Sammlungen an PDX Modellen zur grundlegenden sowie translationalen Forschung dar. Entscheidend für eine qualitätsgesicherte Biobank ist die standardisierte Aufarbeitung und Lagerung der Proben sowie die umfassende Charakterisierung der Modelle.

Die vergleichende pathomorphologische Analyse und die genetische Identitätsprüfung bestätigten die große Nähe der HROC-Xenobank-Modelle zu den ursprünglichen Patiententumoren. Darüber hinaus rekapitulierten die Modelle präzise die Mutationsprofile der primären Patiententumoren. Das Durchschnittsalter der HROC-Studienpopulation beträgt 69,7 Jahre (Spanne 30 bis 98 Jahre) und liegt damit genau innerhalb der ZfKD-Bereiche. Verglichen mit der Normalverteilung der Darmkrebstadien in Deutschland sind Stadium II genau, Stadium III nahezu genau, jedoch CRC-Stadium IV deutlich über- und Stadium I deutlich unterrepräsentiert. Weiterhin ergab die Analyse der molekularen Subtypen, dass unsere HROC-Xenobank-Kohorte die üblichen CRC-Subtypen repräsentiert. Dies zeigt, dass die klinische Situation in den HROC-Modellen repräsentiert wird und sie somit die perfekte Grundlage für weitergehende Untersuchungen darstellen.

Die Leistungsfähigkeit und der Wert von PDX Modellen als Plattform für die Identifizierung und Validierung von Biomarkern, Signalwegen und Resistenzmechanismen sowie für die präklinische Erprobung von individualisierten Krebstherapien zeigen darüber hinaus nicht nur unsere Ergebnisse.

Bevor allerdings translationale Therapiestudien durchgeführt werden, sollte entsprechend der Ergebnisse der Dosisfindungsstudie zunächst stets die Verträglichkeit und Wirkung der zu testenden Medikamente in einem kleineren Vorversuch überprüft werden. Um entsprechend der 3R-Regel Tierversuche zu minimieren sowie Zeit- und Substanzverluste zu vermeiden.

VII. LITERATURVERZEICHNIS

- [1] H. T. Nguyen and H. Q. Duong, "The molecular characteristics of colorectal cancer: Implications for diagnosis and therapy (review)," *Oncol. Lett.*, vol. 16, no. 1, pp. 9–18, Jul. 2018.
- [2] C. Ostwald, M. Linnebacher, V. Weirich, and F. Prall, "Chromosomally and microsatellite stable colorectal carcinomas without the CpG island methylator phenotype in a molecular classification.," *Int. J. Oncol.*, vol. 35, no. 2, pp. 321–7, Aug. 2009.
- [3] W. Wang *et al.*, "Molecular subtyping of colorectal cancer: recent progress, new challenges and emerging opportunities," *Semin. Cancer Biol.*, vol. 55, p. 37, Apr. 2019.
- [4] R. Koch-Institut, "Krebs in Deutschland | 2015/2016," 2015.
- [5] K. A. Oppelt, S. Luttmann, K. Kraywinkel, and U. Haug, "Incidence of advanced colorectal cancer in Germany: comparing claims data and cancer registry data."
- [6] L. Onkologie, "S3-Leitlinie Kolorektales Karzinom publiziert bei."
- [7] B. Y. Oh *et al.*, "Correlation between tumor engraftment in patient-derived xenograft models and clinical outcomes in colorectal cancer patients," *Oncotarget*, vol. 6, no. 18, pp. 16059–16068, 2015.
- [8] J. J. Tentler *et al.*, "Patient-derived tumour xenografts as models for oncology drug development," *Nat. Rev. Clin. Oncol.*, vol. 9, no. 6, pp. 338–350, 2012.
- [9] L. Coppola *et al.*, "Biobanking in health care: evolution and future directions," *J. Transl. Med.*, vol. 17, no. 1, p. 172, May 2019.
- [10] E. Heervä *et al.*, "Trends in presentation, treatment and survival of 1777 patients with colorectal cancer over a decade: a Biobank study," *Acta Oncol.*, vol. 57, no. 6, pp. 735–742, Jun. 2018.
- [11] R. Peila, R. S. Arthur, and T. E. Rohan, "Sex hormones, SHBG and risk of colon and rectal cancer among men and women in the UK Biobank," *Cancer Epidemiol.*, vol. 69, p. 101831, Dec. 2020.
- [12] M. Shabihkhani *et al.*, "The procurement, storage, and quality assurance of frozen blood and tissue biospecimens in pathology, biorepository, and biobank settings," *Clin. Biochem.*, vol. 47, no. 0, p. 258, 2014.
- [13] M. Hidalgo *et al.*, "Europe PMC Funders Group Patient Derived Xenograft Models : An Emerging Platform for Translational Cancer Research," vol. 4, no. 9, pp. 998–1013, 2015.
- [14] M. Bleijs, M. Wetering, H. Clevers, and J. Drost, "Xenograft and organoid model systems in cancer research," *EMBO J.*, vol. 38, no. 15, Aug. 2019.
- [15] H. Damhofer *et al.*, "Establishment of patient-derived xenograft models and cell lines for malignancies of the upper gastrointestinal tract," *J. Transl. Med.*, vol. 13, no. 1, Apr.

- 2015.
- [16] J. Jung, H. S. Seol, and S. Chang, "The Generation and Application of Patient-Derived Xenograft Model for Cancer Research," *Cancer Res. Treat.*, vol. 50, no. 1, p. 1, Jan. 2018.
- [17] G. J. Yoshida, "Applications of patient-derived tumor xenograft models and tumor organoids," *J. Hematol. Oncol.*, vol. 13, no. 1, pp. 1–16, 2020.
- [18] A. Inoue, A. K. Deem, S. Kopetz, T. P. Heffernan, G. F. Draetta, and A. Carugo, "Current and future horizons of patient-derived xenograft models in colorectal cancer translational research," *Cancers*, vol. 11, no. 9. MDPI AG, 01-Sep-2019.
- [19] S. Matschos *et al.*, "The HROC-Xenobank—A high quality assured PDX biobank of >100 individual colorectal cancer models," *Cancers (Basel)*, vol. 13, no. 23, Dec. 2021.
- [20] E. Medico *et al.*, "The molecular landscape of colorectal cancer cell lines unveils clinically actionable kinase targets," *Nat. Commun.*, vol. 6, Apr. 2015.
- [21] C. S. Mullins *et al.*, "Integrated biobanking and tumor model establishment of human colorectal carcinoma provides excellent tools for preclinical research," *Cancers (Basel)*, vol. 11, no. 10, Oct. 2019.
- [22] T. Namekawa, K. Ikeda, K. Horie-Inoue, and S. Inoue, "Application of Prostate Cancer Models for Preclinical Study: Advantages and Limitations of Cell Lines, Patient-Derived Xenografts, and Three-Dimensional Culture of Patient-Derived Cells," *Cells*, vol. 8, no. 1, p. 74, Jan. 2019.
- [23] S. R. Nelson *et al.*, "Modelling of pancreatic cancer biology: transcriptomic signature for 3D PDX-derived organoids and primary cell line organoid development," *Sci. Rep.*, vol. 10, no. 1, Dec. 2020.
- [24] V. Dangles-Marie *et al.*, "Establishment of human colon cancer cell lines from fresh tumors versus xenografts: Comparison of success rate and cell line features," *Cancer Res.*, vol. 67, no. 1, pp. 398–407, 2007.
- [25] F. Bürtin, S. Matschos, F. Prall, C. S. Mullins, M. Krohn, and M. Linnebacher, "Creation and maintenance of a living biobank-how we do it," *J. Vis. Exp.*, vol. 2021, no. 170, p. 62065, Apr. 2021.
- [26] C. Maletzki *et al.*, "NSG mice as hosts for oncological precision medicine," *Lab. Investig.*, vol. 2, 2019.
- [27] M. Linnebacher *et al.*, "Cryopreservation of human colorectal carcinomas prior to xenografting," *BMC Cancer*, vol. 10, 2010.
- [28] F. Prall, C. Maletzki, M. Hühns, M. Krohn, and M. Linnebacher, "Colorectal carcinoma tumour budding and podia formation in the xenograft microenvironment," *PLoS One*, vol. 12, no. 10, pp. 1–12, 2017.
- [29] G. Covarrubias-Pazaran, L. Diaz-Garcia, B. Schlautman, W. Salazar, and J. Zalapa,
-

- “Fragman: An R package for fragment analysis,” *BMC Genet.*, vol. 17, no. 1, pp. 1–8, 2016.
- [30] S. Ogino *et al.*, “CpG island methylator phenotype (CIMP) of colorectal cancer is best characterised by quantitative DNA methylation analysis and prospective cohort studies,” *Gut*, vol. 55, no. 7, pp. 1000–1006, 2006.
- [31] D. J. Weisenberger *et al.*, “CpG island methylator phenotype underlies sporadic microsatellite instability and is tightly associated with BRAF mutation in colorectal cancer,” *Nat. Genet.*, vol. 38, no. 7, pp. 787–793, 2006.
- [32] L. Lazzari *et al.*, “Patient-derived xenografts and matched cell lines identify pharmacogenomic vulnerabilities in colorectal cancer,” *Clin. Cancer Res.*, vol. 25, no. 20, pp. 6243–6259, Oct. 2019.
- [33] S. Corso *et al.*, “A Comprehensive PDX Gastric Cancer Collection Captures Cancer Cell–Intrinsic Transcriptional MSI Traits,” *Cancer Res.*, vol. 79, no. 22, pp. 5884–5896, Nov. 2019.
- [34] C. Maletzki *et al.*, “Establishment and characterization of cell lines from chromosomal unstable colorectal cancer,” *World J. Gastroenterol.*, vol. 21, no. 1, p. 164, Jan. 2015.
- [35] S. Rohde *et al.*, “Application of in vivo imaging techniques to monitor therapeutic efficiency of PLX4720 in an experimental model of microsatellite unstable colorectal cancer,” *Oncotarget*, vol. 8, no. 41, p. 69756, 2017.
- [36] M. Mattar, C. R. McCarthy, A. R. Kulick, B. Qeriqi, S. Guzman, and E. de Stanchina, “Establishing and maintaining an extensive library of patient-derived xenograft models,” *Front. Oncol.*, vol. 8, no. FEB, Feb. 2018.
- [37] S. M. Abdirahman *et al.*, “A biobank of colorectal cancer patient-derived xenografts,” *Cancers (Basel)*, vol. 12, no. 9, pp. 1–19, Aug. 2020.
- [38] X. Y. Woo *et al.*, “Conservation of copy number profiles during engraftment and passaging of patient-derived cancer xenografts,” *Nat. Genet.*, vol. 53, no. 1, p. 86, Jan. 2021.
- [39] G. Rizzo, A. Bertotti, S. M. Leto, and S. Vetrano, “Patient-derived tumor models: a more suitable tool for pre-clinical studies in colorectal cancer.”
- [40] “cBioPortal for Cancer Genomics.” [Online]. Available: http://www.cbioportal.org/study/summary?id=coadread_tcga_pan_can_atlas_2018. [Accessed: 07-Oct-2021].
- [41] C. S. Lee *et al.*, “Enhancing the landscape of colorectal cancer using targeted deep sequencing,” *Sci. Rep.*, vol. 11, no. 1, p. 8154, Dec. 2021.
- [42] D. M. Burgenske *et al.*, “Establishment of genetically diverse patient-derived xenografts of colorectal cancer,” *Am. J. Cancer Res.*, vol. 4, no. 6, p. 824, 2014.
- [43] K. M. Brown, A. Xue, A. Mittal, J. S. Samra, R. Smith, and T. J. Hugh, “Patient-derived
-

- xenograft models of colorectal cancer in pre-clinical research: a systematic review,” *Oncotarget*, vol. 7, no. 40, p. 66212, 2016.
- [44] M. Rivera *et al.*, “Patient-derived xenograft (PDX) models of colorectal carcinoma (CRC) as a platform for chemosensitivity and biomarker analysis in personalized medicine,” *Neoplasia*, vol. 23, no. 1, p. 21, Jan. 2021.
- [45] Y. Shang *et al.*, “Pharmaceutical immunoglobulin G impairs anti-carcinoma activity of oxaliplatin in colon cancer cells,” *Br. J. Cancer*, vol. 124, no. 8, pp. 1411–1420, Apr. 2021.
- [46] D. Nörz *et al.*, “Combined targeting of AKT and mTOR synergistically inhibits formation of primary colorectal carcinoma tumouroids in Vitro: A 3D tumour model for pre-Therapeutic drug screening,” *Anticancer Res.*, vol. 41, no. 5, pp. 2257–2275, May 2021.
- [47] C. Marx *et al.*, “Mechanistic insights into p53-regulated cytotoxicity of combined entinostat and irinotecan against colorectal cancer cells,” *Mol. Oncol.*, 2021.
- [48] S. Bock, C. S. Mullins, E. Klar, P. Pérot, C. Maletzki, and M. Linnebacher, “Murine Endogenous Retroviruses Are Detectable in Patient-Derived Xenografts but Not in Patient-Individual Cell Lines of Human Colorectal Cancer.,” *Front. Microbiol.*, vol. 9, p. 789, 2018.
- [49] M. El-Salhy, L. Hilding, H. Royson, and V. Tjomsland, “Comparison between triple therapy with octreotide, galanin and serotonin vs. irinotecan or oxaliplatin in combination with 5-fluorouracil/leukovorin in human colon cancer,” *Int. J. Oncol.*, vol. 27, no. 3, pp. 687–691, Sep. 2005.
- [50] J. F. Dorsey *et al.*, “Tumor necrosis factor-related apoptosis-inducing ligand (TRAIL) and paclitaxel have cooperative in vivo effects against glioblastoma multiforme cells,” *Mol. Cancer Ther.*, vol. 8, no. 12, pp. 3285–3295, Dec. 2009.
- [51] H. J. Kang, S. H. Lee, J. E. Price, and L. S. Kim, “Curcumin Suppresses the Paclitaxel-Induced Nuclear Factor- κ B in Breast Cancer Cells and Potentiates the Growth Inhibitory Effect of Paclitaxel in a Breast Cancer Nude Mice Model,” *Breast J.*, vol. 15, no. 3, pp. 223–229, May 2009.
- [52] G. Glaser *et al.*, “Conventional Chemotherapy and Oncogenic Pathway Targeting in Ovarian Carcinosarcoma Using a Patient-Derived Tumorgraft,” *PLoS One*, vol. 10, no. 5, May 2015.
- [53] B. Storer, “Design and analysis of phase I clinical trials - PubMed.” [Online]. Available: <https://pubmed.ncbi.nlm.nih.gov/2790129/>. [Accessed: 09-Jun-2022].
-

VIII. ABKÜRZUNGSVERZEICHNIS

- BBMRI Biomolecular Resources Research Infrastructure
- C Kolonkarzinom
- CIMP CpG-Insel-Methylator-Phänotyp
- CIN chromosomale Instabilität
- CRC kolorektalen Adenom zum Karzinom
- HRO Hansestadt Rostock
- i.p. intraperitoneal
- LS Lynch Syndrom
- LV Leucovorin
- Met Metastase
- MSI Mikrosatelliteninstabilität
- NGS Next Generation Sequencing
- NSG NOD.Cg-Prkdc^{scid} Il2rg^{tm1Wjl}/SzJ
- PDO Patient-derived Organoid
- PDX Patient-derived Xenograft
- p.o. peroral
- STR Short Tandem Repeat
- spMSI sporadisch Mikrosatelliten instabil
- TCGA Cancer Genome Atlas Network
- WES Whole Exom Sequencing
- ZfKD Zentrum für Krebsregisterdaten

IX. THESEN

1. Das derzeit beste Modell, das die Eigenschaften des ursprünglichen Tumors widerspiegelt, ist das PDX Modell, da es die biologischen Merkmale des ursprünglichen Tumors, einschließlich Mikroarchitektur, Pathomorphologie und genetische Veränderungen erhält.
2. Die Tatsache, dass einige Patienten selbst auf zielgerichtete Therapien nicht ansprechen sowie die Möglichkeit einer genauen Vorhersage des individuellen klinischen Behandlungserfolg unterstreicht die Notwendigkeit weiterer patientenbasierter Modelle und zeigt den klaren Bedarf an mehr wissenschaftlich geführten PDX Biobanken, die eine große Anzahl individueller Tumoren enthalten, um die Entwicklung personalisierter Behandlungen zu fördern.
3. Aufgrund der starken Heterogenität der Tumoren ist eine Gewebekbank mit einer ausreichenden Anzahl von Proben erforderlich, um die Vielfalt der Tumorarten abzudecken
4. Dies führte zur Etablierung einer qualitätsgesicherten CRC-Xenobank, die 125 individuelle PDX Modelle mit einer ausreichenden Anzahl von vitalen Backups, eingefrorenen Aliquots für molekulare Analysen und FFPE-Material enthält.
5. Da eine ideale CRC-PDX Sammlung die molekulare Heterogenität der klinischen Fälle annähernd abbilden sollte, entspricht die Verteilung der molekularen Subtypen weitgehend der allgemeinen klinischen Verteilung.
6. Jedes individuelle HROC-PDX Modell reproduziert die pathomorphologischen Strukturen aus dem ursprünglichen Patiententumor und darüber hinaus zeigte der Vergleich von PDX Tumoren, die von der gleichen Passage aber von verschiedenen Tieren stammen, exakt übereinstimmende pathomorphologische Ergebnisse.
7. Pathogene oder wahrscheinlich pathogene Mutationen, die in den ursprünglichen Patiententumoren entdeckt wurden, wurden auch in den PDX Tumoren nachgewiesen, die HROC-PDX Modelle rekapitulierten demnach präzise die Mutationsprofile der primären Patiententumoren.
8. Die am häufigsten mutierten Gene in der HROC-Xenobank sind APC (50,4 %), KRAS (39,8 %), TP53 (37,2 %), BRAF (23,0 %) und PIK3CA (17,7 %).
9. Der Aufbau und die langfristige Pflege von Plattformen wie der integrierten HROC-Biobank sind von entscheidender Bedeutung, um die Gesamtzahl der an onkologischen *in vivo*-Studien beteiligten Tiere zu minimieren.
10. Da das Ansprechen auf die Medikamente zwischen den Therapieschemata und den PDX Modellen verschiedener molekularen Subtypen stark variierte, sollten stets Vorversuche zur Verträglichkeit und Wirkung der zu testenden Medikamente durchgeführt werden sollten, um unnötige Experimente zu verhindern.

X. DANKSAGUNG

Zuerst möchte ich mich ganz besonders bei PD Dr. Michael Linnebacher bedanken für die Möglichkeit in der Arbeitsgruppe Molekulare Onkologie und Immuntherapie gearbeitet zu haben, um meine Promotion dort machen zu können.

Dort habe ich nicht nur von meinem Betreuer PD Dr. Michael Linnebacher, sondern auch von meinen sehr geschätzten Kollegen sehr viel Unterstützung bekommen. Insbesondere möchte ich mich bedanken bei Mathias Krohn, Dr. med. Florian Bürtin, Dr. Christina Mullins, und Dr. Claudia Maletzki.

Weiterhin bedanke ich mich für die Unterstützung von den Mitarbeitern des Rudolf-Zenker-Institut, insbesondere PD Dr. Dietmar Zechner bei der Bearbeitung der Tierschutzanträge und Ilona Klamfuß und Karin Gerber bei Fragen zu Techniken bezüglich der laufenden Tierversuche.

Einen besonderen Dank an Prof. Dr. med Friedrich Prall bei der Begutachtung der histologischen Schnitte und der Auswertung dieser. Auch eine sehr große Hilfe bei der Durchführung der STR-Analysen, MSI sowie CIMP Analysen durch die Messung der Proben gilt Dr. Maja Hühns und Dr. Björn Schneider.

Vielen Dank auch an Daniel Wolter vom Labor der Klinik und Poliklinik für Mund-, Kiefer- und Plastische Gesichtschirurgie für die technische Unterstützung bei meinen H&E-gefärbten Schnitten.

Zuletzt möchte ich meinem Mann Christian Matschos danken, dass er in dieser Zeit immer für mich da war und mich so in meiner Arbeit unterstützt hat.

XI. LEBENS LAUF

STEPHANIE MATSCHOS

PERSÖNLICHE ANGABEN

Geburtsdatum/ort: 15.06.1987, Eschweiler
Geburtsname: Bock
Adresse: Herrenfeldchen 3, 52249 Eschweiler
Telefonnummer: 01779381095
Emailadresse: stephaniematschos@gmx.net



AKADEMISCHER WERDEGANG

- 01/2022 - 10/2022** Schreiben der kumulativen Dissertation
- 10/2014 - 12/2016** Master Medizinische Biotechnologie, Universität Rostock
Titel Masterarbeit: Nachweis muriner endogener Retroviren in Patienten-abgeleiteten Xenografts humaner kolorektaler Karzinome sowie in daraus etablierten Zelllinien; (Note Master: 1,6)
- 10/2011 - 07/2014** Bachelor Medizinische Biotechnologie, Universität Rostock
Titel Bachelorarbeit: Optimierung der Etablierung von Zelllinien humaner kolorektaler Karzinome; (Note Bachelor: 2,4)

BERUFLICHER WERDEGANG

- 10/2022 - Heute** Medizinproduktebeobachtung Firma Vygon (Aachen)
- 09/2020 - 12/2021** Familienphase
- 01/2017 - 08/2020** wissenschaftliche Mitarbeiterin
Universitätsmedizin Rostock, Arbeitsgruppe Molekulare Onkologie und Immuntherapie
- 01/2010 - 07/2011** Chemielaborantin
Kristallisationslabor der Firma Grünenthal GmbH

PUBLIKATIONEN

- 05/2022** Kiweler, Nicole *et al.* "The epigenetic modifier HDAC2 and the checkpoint kinase ATM determine the responses of microsatellite instable colorectal cancer cells to 5-fluorouracil." *Cell biology and toxicology*, 10.1007/s10565-022-09731-3
- 11/2021** Matschos, Stephanie *et al.* "The HROC-Xenobank-A High Quality Assured PDX Biobank of >100 Individual Colorectal Cancer Models." *Cancers* vol. 13,23 5882
- 09/2021** Wagner, Sandra *et al.* "Tumour-Derived Cell Lines and Their Potential for Therapy Prediction in Patients with Metastatic Colorectal Cancer." *Cancers* vol. 13,18 4717
- 04/2021** Bürtin, Florian, *et al.* "Creation and Maintenance of a Living Biobank-How We Do It." *Journal of Visualized Experiments*, vol. 2021, no. 170
- 02/2021** Shang, Yuru *et al.* "Pharmaceutical immunoglobulin G impairs anti-carcinoma activity of oxaliplatin in colon cancer cells." *British journal of cancer* vol. 124,8 (2021): 1411-1420
- 08/2020** Gock, Michael *et al.* "Patient-individual cancer cell lines and tissue analysis delivers no evidence of sequences from DNA viruses in colorectal cancer cells." *BMC gastroenterology* vol. 20,1 260
- 12/2019** Baur, Florentin *et al.* "Connecting Cancer Pathways to Tumor Engines: A Stratification Tool for Colorectal Cancer Combining Human In Vitro Tissue Models with Boolean In Silico Models." *Cancers* vol. 12,1 28
- 10/2019** Mullins, Christina S *et al.* "Integrated Biobanking and Tumor Model Establishment of Human Colorectal Carcinoma Provides Excellent Tools for Preclinical Research." *Cancers* vol. 11,10 1520
- 08/2019** Maletzki, Claudia, *et al.* "NSG Mice as Hosts for Oncological Precision Medicine." *Laboratory Investigation*, vol. 2, Springer US
- 04/2018** Bock, Stephanie *et al.* "Murine Endogenous Retroviruses Are Detectable in Patient-Derived Xenografts but Not in Patient-Individual Cell Lines of Human Colorectal Cancer." *Frontiers in microbiology* vol. 9 789
- 10/2016** Mullins, Christina Susanne *et al.* "Generation of Xenotransplants from Human Cancer Biopsies to Assess Anti-cancer Activities of HDACi." *Methods in molecular biology (Clifton, N.J.)* vol. 1510 (2017): 217-229

KONGRESS

- 03/2017** Kongress Deutsche Gesellschaft für Chirurgie; Referentin an der Sitzung Onkologie: Kolonkarzinom; Vortragstitel: Nachweis muriner endogener Retroviren in Patienten-abgeleiteten Xenografts humaner kolorektaler Karzinome sowie in daraus etablierten Zelllinien
- 03/2019** Kongress Deutsche Gesellschaft für Chirurgie; Referentin an der Sitzung Onkologie: Therapie; Vortragstitel: Problematik des Einsatzes von NSG Mäusen in der personalisierten Onkologie

XII. APPENDIX

Nachfolgend sind die Publikationen, die die Basis meiner Publikation darstellen angehängt:

1. F. Bürtin, S. Matschos, F. Prall, C. S. Mullins, M. Krohn, and M. Linnebacher, "Creation and maintenance of a living biobank-how we do it," *J. Vis. Exp.*, vol. 2021, no. 170, p. 62065, Apr. 2021.
2. S. Matschos *et al.*, "The HROC-Xenobank—A high quality assured PDX biobank of >100 individual colorectal cancer models," *Cancers (Basel)*, vol. 13, no. 23, Dec. 2021
3. C. Maletzki *et al.*, "NSG mice as hosts for oncological precision medicine," *Lab. Investig.*, vol. 2, 2019.

Creation and Maintenance of a Living Biobank - How We Do It

Florian Bürtin¹, Stephanie Matschos², Friedrich Prall³, Christina S. Mullins², Mathias Krohn², Michael Linnebacher²

¹ Department of General, Visceral, Vascular and Transplantation Surgery, University Medical Center Rostock, University of Rostock ² Molecular Oncology and Immunotherapy, Department of General, Visceral, Vascular and Transplantation Surgery, University Medical Center Rostock ³ Institute of Pathology, University Medical Center Rostock

Corresponding Author

Michael Linnebacher

michael.linnebacher@med.uni-rostock.de

Citation

Bürtin, F., Matschos, S., Prall, F., Mullins, C.S., Krohn, M., Linnebacher, M. Creation and Maintenance of a Living Biobank - How We Do It. *J. Vis. Exp.* (170), e62065, doi:10.3791/62065 (2021).

Date Published

April 10, 2021

DOI

10.3791/62065

URL

jove.com/video/62065

Abstract

In light of the growing knowledge about the inter-individual properties and heterogeneity of cancers, the emerging field of personalized medicine requires a platform for preclinical research. Over recent years, we have established a biobank of colorectal and pancreatic cancers comprising of primary tumor tissue, normal tissue, sera, isolated peripheral blood lymphocytes (PBL), patient-derived xenografts (PDX), as well as primary and secondary cancer cell lines. Since original tumor tissue is limited and the establishment rate of primary cancer cell lines is still relatively low, PDX allow not only the preservation and extension of the biobank but also the generation of secondary cancer cell lines. Moreover, PDX-models have been proven to be the ideal *in vivo* model for preclinical drug testing. However, biobanking requires careful preparation, strict guidelines and a well attuned infrastructure. Colectomy, duodenopancreatectomy or resected metastases specimens are collected immediately after resection and transferred to the pathology department. Respecting priority of an unbiased histopathological report, at the discretion of the attending pathologist who carries out the dissections, small tumor pieces and non-tumor tissue are harvested.

Necrotic parts are discarded and the remaining tumor tissue is cut into small, identical cubes and cryopreserved for later use. Additionally, a small portion of the tumor is minced and strained for primary cancer cell culture. Additionally, blood samples drawn from the patient pre- and postoperatively, are processed to obtain serum and PBLs. For PDX engraftment, the cryopreserved specimens are defrosted and implanted subcutaneously into the flanks of immunodeficient mice. The resulting PDX closely recapitulate the histology of the "donor" tumors and can be either used for subsequent xenografting or cryopreserved for later use. In the following work, we describe the individual steps of creation, maintenance and administration of a large

biobank of colorectal and pancreatic cancer. Moreover, we highlight the crucial details and caveats associated with biobanking.

Introduction

In recent years, the accumulated knowledge of cancers' morphologic, clinical and genetic properties led to the conception of cancer as a heterogeneous, individual disease. Consequently, mutational characterization of neoplasms, besides clinical and pathological features, has gained importance for clinical decision making and many targeted therapies were developed for various molecular alterations. For instance, the efficacy of cetuximab in colorectal cancer treatment can be predicted by the analysis of the *KRAS* and *PIK3CA* mutational status¹. Precision medicine aims for a tailored approach to provide the highest treatment response in each patient and avoid toxicity of inefficacious therapies². Biobanks contain tissue, blood and other biological materials of cancer patients, which are linked to the clinical data, and thus are an excellent tool for translational cancer research. Due to the large number of clinical samples, biobanks enable the detection of rare, but potentially druggable mutations, which provides new treatment opportunities for the individual patient³.

To cover as broad as possible an oncologic research spectrum, we did not restrain our activity on sample harvesting alone, but focused on the establishment of patient-derived cancer cell lines and xenografts (PDX). Traditional

2D cell lines remain the corner stone of *in vitro* research and are the prime choice for large scale drug screenings^{4,5}. Moreover, cell line analysis is often easier, cheaper and more readily available. Additionally, since patient-derived peripheral blood lymphocytes (PBL) are available, also tumor immunology can be studied *in vitro*⁶. However, the majority of newly developed drugs with promising preclinical effectivity in cell based *in vitro* or *in vivo* experiments, have shown disappointing results in clinical trials⁷. In contrast, preclinical studies based on PDX *in vivo* studies have reflected the clinical activity of antineoplastic agents much more faithfully⁸. Since PDX tissue closely reflects the histological and molecular properties of the donor tumor, PDX models are a good way to propagate the often very limited amounts of viable tumor tissue to maintain the integrity of a biobank and to allow the exchange of samples between research groups and institutions. Moreover, cancer cell lines derived from PDX tissue can be established significantly easier than primary cancer cell lines⁹. In recent years, our working group has established a comprehensive integrated colorectal and pancreatic cancer biobank by stepwise standardizing and optimizing the work flow for all biological samples in question (**Figure 1**).

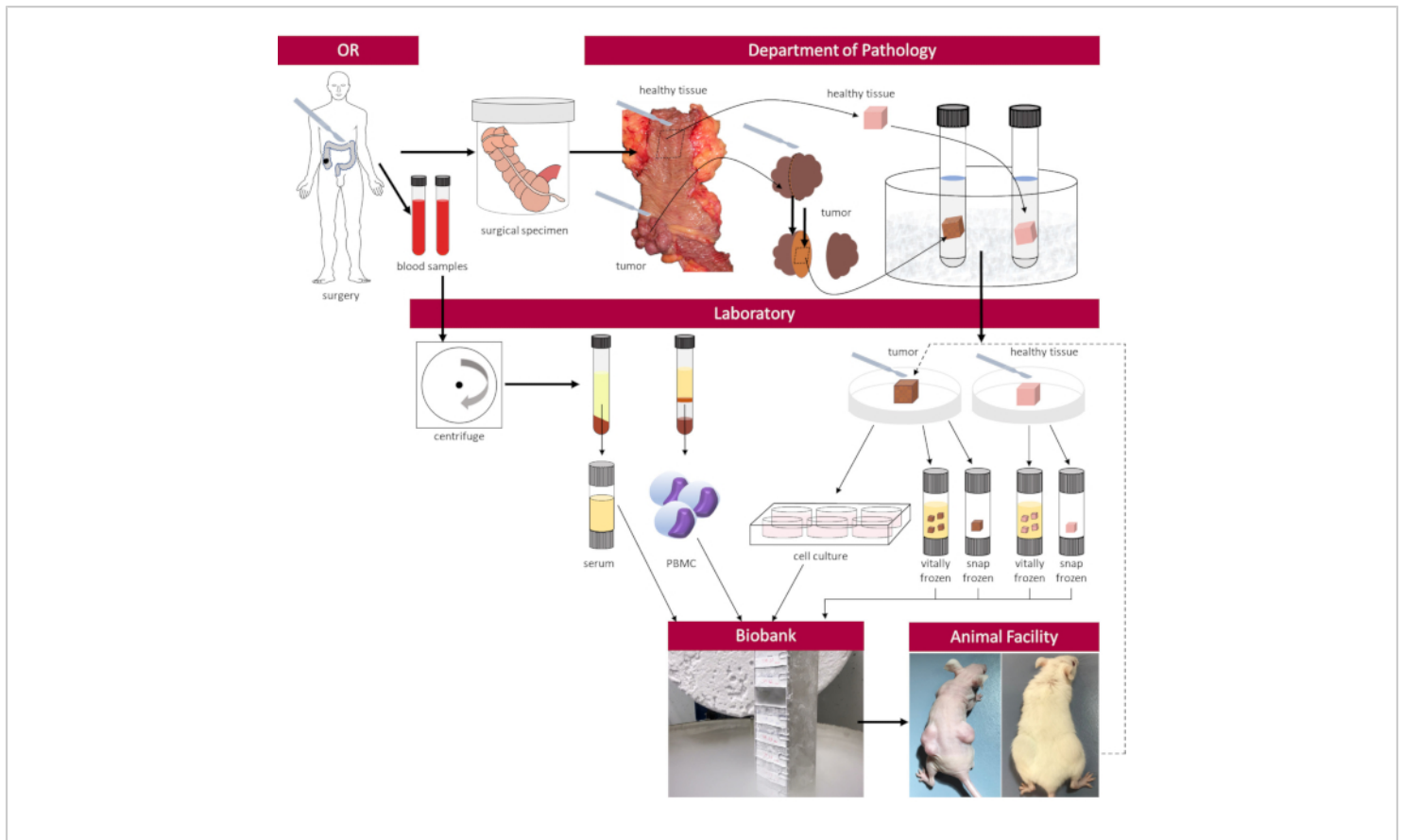


Figure 1: Workflow and organization of the biobank [Please click here to view a larger version of this figure.](#)

Protocol

The following study has been approved by the institutional review board of the University Medical Center Rostock (II HV 43/2004, A 45/2007, A 2018-0054, A 2019-0187 and A 2019-0222). Furthermore, all veterinary relevant procedures have been approved by the Landesamt für Landwirtschaft, Lebensmittelsicherheit und Fischerei Mecklenburg-Vorpommern under the registration numbers LALLF M-V/TSD/ 7221.3-2-020/17 and 7221.3-1-007/19.

1. Experimental Prerequisites

1. Meet several important framework conditions to establish and maintain a biobank.
 1. Use a clinic with a surgical department and sufficient number of oncological resections together with a well-equipped lab and sufficient academic staff. A good infrastructure and a firm liaison with a cooperating pathology department are further prerequisites.
 2. For *in vivo* research, use an animal facility with housing conditions appropriate to immunodeficient mice.

3. Obtain authorization on any research on patient-derived material from a health care ethics committee. Obtain approval on any *in vivo* research from the competent authority according to local statutory regulations.

2. Sample collection

1. The day before surgery

1. Evaluate all patients with resectable colorectal or pancreatic cancer and/or corresponding metastases for biobanking eligibility. Avoid including cases with neoadjuvant pretreatment, very small tumors, tumors of uncertain dignity or lesions which have been partly resected endoscopically before.
2. Obtain written approval of participation from the patient during the informed consent discussion about the surgical procedure. Inform timely all involved surgeons, the laboratory team as well as the pathologist.

2. Sample acquisition

1. Inform all attendants in the operation room (OR) about the tissue collection for the biobank immediately before the start of the surgical procedure.

NOTE: It is crucial that the tissue must not be fixed in formalin. If the tissue is submerged in formalin, it becomes unsuitable for integrated biobanking.

2. Draw 40 mL of heparinized blood (2 x 20 mL syringe) as well as a standard 7.5 mL serum tube immediately after anesthetic induction and transfer quickly to the lab for PBL isolation and serum processing (see step 3-4).

3. Obtain the resected specimen directly from the operating table, place it into an appropriate container and take it to the pathological department. Write down the time point of detachment from the circulation, resection and arrival at pathology.

NOTE: The suitability of the specimen for bio banking should be assessed by the cooperating pathologist who dissects a slice of tumor and non-malignant tissue. Do not excise any parts of the specimen by yourself which may compromise the subsequent pathological report.

4. Place both tissue pieces in a separate 15 to 50 mL polypropylene tube with 10 to 30 mL tissue storage solution (or DPBS) on ice. Write down the time of receipt and transfer the specimens immediately to the lab.

NOTE: The following protocol steps 3-6 must be conducted in a laminar flow cabinet under strict sterile conditions. Use all liquids at room temperature.

3. Serum processing

1. Centrifuge the 7.5 mL serum tube at 1128 x g and 4 °C for 15 min in a pre-cooled centrifuge.
2. Aliquot 1 mL serum per tube in pre-labeled cryotubes and freeze in liquid nitrogen.

4. Isolation of PBL by density gradient centrifugation

NOTE: Work parallel with each of the two 20 mL syringes.

1. Fill 20 mL of heparinized blood into a 50 mL polypropylene tube and add 15 mL of DPBS.

2. Take 15 mL of Pancoll with a serological pipette, insert the pipette carefully all the way to the bottom of the polypropylene tube and release the Pancoll very slowly to form a layer beneath the blood/DBPS column.
3. Centrifuge at 375 x g for 15 min **without** brake.
4. Aspirate and transfer the opaque interphase layer between the mid and top column of both samples into a fresh 50 mL Polypropylene tube and fill up with DPBS to 50 mL.
5. Centrifuge at 270 x g for 15 min **with** brake.
6. Aspirate and discard the supernatant, resuspend the cell pellet in 4.5 mL of freezer medium.
7. Aliquot 1.5 mL of the suspension per cryotube, close the tubes tightly and place them in a freezing container suitable for slow freezing and store at -80 °C.

5. Tissue processing

NOTE: Start with the generation of snap frozen samples of tumor and healthy tissue to maintain the integrity of nucleic acids.

1. Tumor tissue specimen
 1. Transfer the tumor specimen with several mL of tissue storage solution from the polypropylene tube to a Petri dish. Rinse with DPBS if necessary. Avoid touching the specimen and use two sterile scalpels to handle the tissue. Avoid desiccation at any time.
 2. Weigh the tumor specimen on a convenient scale in a separate dish and note the tissue weight.
 3. Evaluate size, shape and tissue quality of the tumor tissue before cutting. Aim to obtain at least one piece about the size of a pinhead for snap freezing and

four cubes of approx. 30 mm³ (edge length 3 x 3x 3 mm) each for vital cryopreservation. Generate as many 30 mm³ -cubes in quadruples as possible and generate one piece for snap freezing per 5 quadruples. Also take into account that necrotic portions must be cut off so that the cubes consist of vital tissue only.

4. Generate slices of 3 mm thickness. Cut off necrotic portions, distinguishable as gel-like or liquid mass, and cut the slices into cubes of the two desired sizes.

NOTE: Do not discard any tissue at this point.
5. Snap freezing
 1. Label cryotubes accordingly (see step 7.7).
 2. Place one small tissue piece per pre-labeled cryotube. Submerge the samples immediately into liquid nitrogen for several minutes and store at -80 °C subsequently.
6. Cryopreservation of vital tissue
 1. Label cryotubes accordingly (see step 7.7) and fill each with 1.5 mL of freezer medium. Place the freezing container beside the bench.

NOTE: Follow the next steps as quickly as possible. Since the DMSO in the freezer medium has cytotoxic properties, the time of the tissue being submerged in freezer medium without proper cooling should not exceed 2 minutes.
 2. Arrange the 30 mm³ cubes in quadruples. Shove necrotic tissue and other remains to the edge of the dish, but do not discard them.
 3. Scoop the cubes with the scalpel blade and transfer 4 cubes per cryotube. Make sure that

the tumor pieces are entirely submerged in freezer medium. Close the tubes tightly and place them in a freezing container suitable for slow freezing and store in a -80 °C freezer.

4. Transfer cryotubes into a suited storage system for long term storage at -140 °C or lower. Documentation in the laboratory inventory management system is mandatory.
2. Healthy tissue specimen: Repeat steps 5.1.1. to 5.1.6.4 for the healthy tissue specimen.

6. Primary cell culture

1. Disintegrate the remains of the tumor tissue, including the necrotic scrap, in the Petri dish with the scalpels to pieces as small as possible.
2. Place a sterile cell strainer (100 µm pore size) on top of a 50 mL polypropylene tube.
3. Use a serological pipette to add 5-10 mL of DPBS to the Petri dish, float the tissue remains and pipette up and down to generate a suspension.
4. Transfer the suspension with the pipette to the cell strainer.
5. Repeat Steps 6.3-6.4 until all tissue remains are resolved from the Petri dish.
6. Use the plunger of a 20 mL one-way syringe to squeeze the cell and tissue suspension through the cell strainer.
7. Rinse with 5-10 mL of fresh DPBS, discard the cell strainer and close the tube properly.
8. Centrifuge the suspension at 180 x g for 5-10 minutes.
9. Prepare a collagen-I precoated 6 well plate with 1.5 mL of medium per well.

10. Aspirate and discard the supernatant. Resuspend the pellet in 3 mL of DPBS or medium and add 500 µL of the suspension to each well. Place the plate into the incubator (100% humidity, 5% CO₂, 37 °C)
11. Monitor the plate daily for cell growth and contamination.

NOTE: Further cell culturing up to the point of establishment of a permanent cell line is not described here.

7. PDX Generation

1. Conduct *in vivo* experiments only by appropriately qualified persons meeting the requirements of the competent authority of your jurisdiction.
2. House immunodeficient mice under specific-pathogen-free (SPF) conditions satisfying the demands of the used mouse strain. The hygienic measures include individually ventilated cages, autoclaved food, water and nesting material as well as a safety air lock and the wearing of personal, protective equipment.
3. Autoclave all instruments beforehand and use only one set of instruments for each tumor case to avoid cross-contamination. Handle the tumor tissue as aseptic as possible. All plastic items named below should be sterile, single-use and discarded after each surgery.

NOTE: Determined by the method of freezing four tumor tissue pieces per cryotube, the PDX generation requires always two mice per sample, ideally resulting in four PDX tumors.
4. Choose the desired primary tumor for engraftment via the laboratory inventory management system and transfer the sample (vitaly preserved tumor tissue) from the main storage tank to a portable liquid nitrogen container

(Intermediate storage at $-80\text{ }^{\circ}\text{C}$ on dry ice is also convenient).

5. Put on personal protective equipment before entering the SPF-section (scrubs, clogs, apron, hair cover, surgical mask and overshoes), disinfect your hands and all equipment.
6. Matrigel soaking
 1. Remove the cryotube from the liquid nitrogen container and await thawing of the specimen.
 2. Label a 50 mL polypropylene tube and fill with 35 mL of DPBS.
 3. Tilt the cryotube up and down and transfer the content immediately to the polypropylene tube as soon as the tissue-medium-slush can be shifted. Gently rinse the tumor tissue pieces, discard the main volume from the tube in a separate vessel, close the lid and put the tube up-side-down, so that the four tissue pieces gather in the lid.
 4. Put a Petri dish on the cooling accumulator and place 100 μL of Matrigel as a single droplet into the middle. Use anatomical forceps to transfer the tumor pieces into the Matrigel. Make sure that each piece is covered completely with Matrigel. Incubate for 10 minutes at $4\text{ }^{\circ}\text{C}$.
7. Mouse anesthesia (2 mice per sample, work in parallel)
 1. Prepare a 3:1- stock of a ketamine (100 mg/mL) and xylazine (20 mg/mL) anesthetic solution. The recommended dose is 90/6 mg/kg body weight.
 2. Weigh the mouse and draw up the necessary anesthetic solution into a single use insulin syringe.
 3. Place the mouse on the grid of the cage, pull its tail gently with one hand to induce a forward movement

and simultaneously grab the neck with a pinch grip of the other hand. Lift the mouse of the grid and turn the holding hand, so that animal's back rests on your palm. Immobilize one of the hind legs with your pinky and inject the narcotics intraperitoneally. Put the mouse back to its cage and await narcotic induction.

4. Place the anesthetized mouse on the heating plate and cover the eyes with ointment to avoid corneal harm. Assess the depth of anesthesia by gently pinching the back foot of the mouse with surgical forceps.

NOTE: Absence of movement indicates deep narcosis. Any kind of movement either requires more time for reaching the desired narcotic depth or an additional dose of anesthetics.

8. Surgical procedure

1. Form a skin fold by pinching the neck of the mouse and inject the microchip subcutaneously with the applicator (See step 9 for programming details)
2. Shave the flanks of the mouse if necessary (NMRInu/nu mice do not require shaving), apply povidone-iodine with a cotton swab and use surgical drape to create a sterile field.
3. Lift the skin of the flank with surgical forceps, make a small incision of circa 4 mm and form a small subcutaneous pocket by blunt preparation with scissors.
4. Put one tumor piece into each pocket and place it at the rear end.

5. Clip the end of a 100 μ L pipette tip and aspirate the remaining Matrigel from the Petri dish and apply it equally into each skin pocket.
6. Close the wounds with simple interrupted sutures and apply spray dressing.
9. Scan the microchip and check validity of mouse- and tumor-ID.
10. Prepare a new cage with fresh bedding and nesting material, as well as a gnawing stick. Fold a "cushion" out of paper towels and lay down the mouse with elevated head under an infrared heat lamp.
11. Mix 0.25 mL of trimethoprim/sulfamethoxazole (400 mg/80 mg) with 100 mL of drinking water and administer via the drinking bottle. Consider that one mouse consumes approximately 150 mL per kg body weight daily.

NOTE: Since the subcutaneous PDX-model is not associated with postoperative pain, neither during the wound healing process, nor during tumor outgrowth, postoperative analgesia is not required. Please note that the animal welfare guidelines of your institution/authority may differ.

12. Monitoring of experimental animals
 1. Monitor the mice daily for signs of distress. This can be delegated to qualified animal caretakers.
 2. Keep up the postoperative antibiotic treatment with the aforementioned dosage for 4 weeks. Replace the antibiotic mixture twice per week.
 3. Measure the tumor size at least once per week, ideally daily, with a caliper (tumor volume = $0.52 \times \text{length} \times \text{width} \times \text{height}$ [mm^3]) and record in the database.

8. PDX harvesting and processing

1. Harvest and process the PDX tumor, when:
 - The tumor size reaches the target volume of 1.500 mm^3 .
 - The tumor bearing animal shows signs of distress and/or disease and treatment is futile.
 - The tumor becomes ulcerated or penetrates the skin of the mouse.
2. Read out the microchip to identify the correct PDX.
3. Euthanize the mouse by a legal method (depending on national guidelines) as for example CO_2 -asphyxiation or ketamine/xylazine injection followed by cervical dislocation.
4. Lift the skin with surgical forceps at the flanks and incise with Metzenbaum scissors a few millimeters distant from the tumor.
5. Detach the skin above the tumor by blunt preparation, then carefully grasp the tumor with anatomical forceps and detach the tumor from the superficial fascia of the body.
6. Rinse the tumor with DPBS, put it into a Petri dish and remove adjacent connective tissue.
7. At this point, perform one of the following:
 1. Cut 30 mm^3 cubes and create new PDX (Proceed with protocol at point 7.7.4).
 2. Cut the tumor into slices, which are then transferred to histology cassettes and preserved in 4% formaldehyde for later paraffin embedding.
 3. Preserve the tumor in a tube with tissue storage solution to add it to the biobank (Proceed with protocol at step 3.) and/or create PDX-derived cell lines (Proceed with protocol at step 4.)

9. Biobank and data management

1. Assign an internal ID to each tumor case according to

Table 1.

Laboratory location/name	cancer entity	consecutive case number	specification	consecutive number
	C=colorectal		_Met=Metastasis	
	P=pancreatic		_Tu=Tumor	
Example: HROC389_Met2 = Rostock, colorectal cancer, case 389, second metastasis				

Table 1: Definition of the sample ID.

2. Store the patient consent in electronic and paper form together with the tumor-ID.
3. Gather as much clinical data as possible and store them anonymized and separately.
4. Use a data management software (e.g., Freezerworks) or other and create an interface with a label printing software to generate temperature-resistant, self-sticking bar code labels.
5. Add a new sample by opening the data management software, define the specimen type and record the following information: tumor ID, tissue type, freezing method, date, responsible employee, passage number, mouse ID and mouse strain.
6. Assign the samples to specific positions in the storage tank.
7. Tracing and monitoring of PDX (Applies to step 7-8)
 1. Use a MS Access data base (or a similar system) on a portable, Bluetooth-enabled device (laptop or tablet) to record tumor ID, date of implantation, date

of euthanasia, mouse age and strain as well as tumor growth over time.

2. Connect the microchip reader to the device and read out the microchip prior to implantation.
3. Assign a specific ID to each mouse; we use the following scheme: (**see Table 2 below**)
4. After implantation, record the ID together with the mouse characteristics in the data base.
5. Re-read the microchip and check, if the specifications of the microchip, the data base and the cryotube label are consistent.
6. Create a label for each mouse cage accordingly.

NOTE: To create a physical back up, stick the cryotube labels with the corresponding microchip labels into a booklet and note date and mouse strain.
7. To monitor the tumor growth of the individual PDX, scan the microchip of the mouse with the reader connected to the data base device for identification and record the tumor size measured by caliper each week.

8. Plan the ideal time point of PDX harvesting by analyzing the growth curve of the tumor.

Tumor-ID	Prior storage in N ₂ (=f)	Passage (=T) number	consecutive mouse (=M) number
Example: HROP12 fT0 M1 = Rostock, pancreatic cancer, case 12, generated from frozen primary tissue, first passage, mouse 1.			

Table 2: Definition of the PDX ID.

Representative Results

In our hands, the establishment rate of primary cell cultures (**Figure 2A & B**) was 12.9% in a large series⁹. The majority of attempts to isolate expandable tumor cells from fresh surgical resected specimens failed due to a lack of outgrowth or early contamination. Cell line establishment was considered successful after 3 passages with a steady growth under

standard culture conditions (DMEM, 10% FCS, standard culture vessel) and validation of epithelial differentiation via FACS-analysis¹⁰. Cell lines derived from PDX tumors (**Figure 2C & D**) showed a higher establishment rate of 23.6% which is also due to the possibility of repetitive attempts in contrast to primary resected tumors⁹. However, some mixed cultures (**Figure 2E**) cannot be freed of fibroblastic growth or are even lost due to fibroblastic overgrowth (**Figure 2F**).

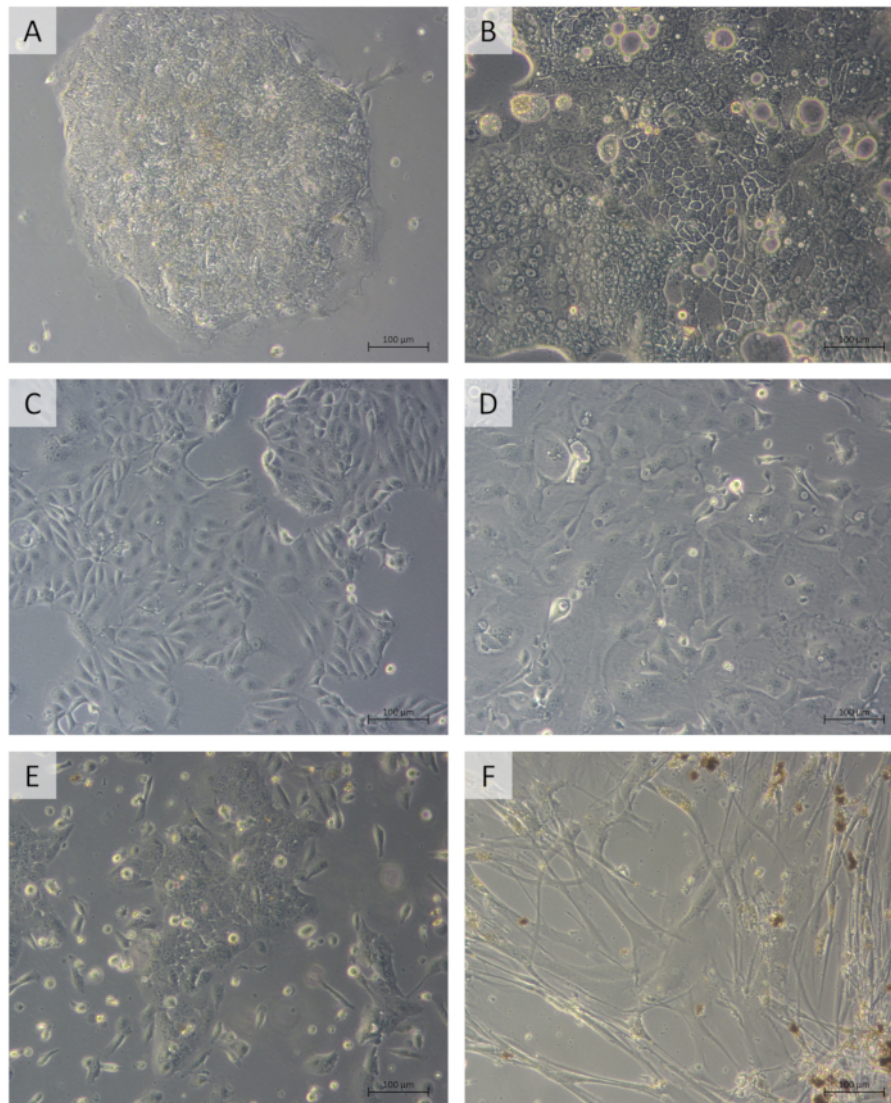


Figure 2: Cell culture. Primary cancer cell lines, derived from a metastasis of colon cancer case HROC313, passage 21 (A) and pancreatic cancer case HROP88, passage 5 (B). PDX-derived cancer cell lines of colon PDX HROC285 T0 M2 (D) and pancreatic PDX HROP10 T5 M2, passage 4 (E). Mixed culture of fibroblasts and cancer cells from pancreatic cancer HROP75, passage 8 (C) and fibroblastic overgrowth (F). [Please click here to view a larger version of this figure.](#)

Considering changes in PDX generation protocol, mouse strains used and also experimenters over several years, as well as large differences in the amount of tumor tissue available for engraftment, it is not trivial to give the overall success rate of PDX generation. In a very recent series of PDX generation experiments performed by two researchers

(S.M. and F.B.), primary outgrowth rates of 63% for colorectal PDX (an exemplary histology can be depicted from **Figure 3A**) and 48% for pancreatic PDX (**Figure 3B**) were observed. The outgrowth of murine or human lymphomas at the implantation site is relatively rare, but can mimic successful PDX outgrowth (**Figure 3C**). Apart from histopathological

examination, concordance between PDX models and their donor patients was regularly confirmed by short tandem repeat (STR) analysis (**Figure 3D**). To the present day the biobank comprises >50 primary and >50 secondary

colorectal, 3 primary and 6 secondary pancreatic cancer cell lines as well as >150 colorectal and 19 pancreatic PDX models.

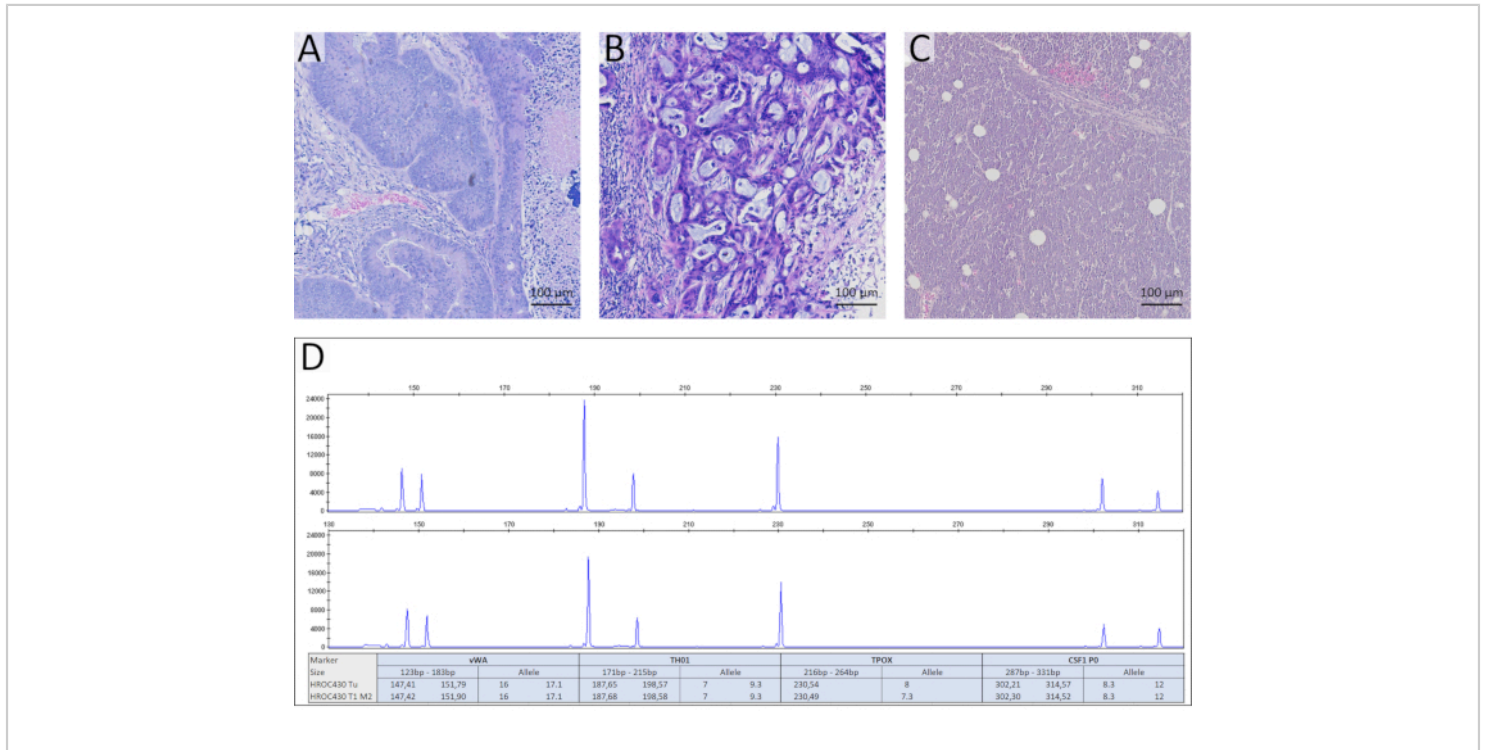


Figure 3: Representative histological comparison of colorectal (A) and pancreatic PDX (B). Human lymphoma at the implantation site mimicking PDX outgrowth (C). Genetic identity testing of a PDX model (HROC430 T1 M2) to the original patient tumor tissue (HROC430Tu) by short tandem repeat (STR) analysis. Comparison of the nine STR loci, vWA, TH01, TPOX, CSF1 PO (FAM dye) and D5S818, D13S317, D7S820, D16S539 (HEX dye) using multiplex PCR with fluorescent-labeled primers following capillary electrophoresis confirmed genetic concordance of the PDX and donor tumor (D). [Please click here to view a larger version of this figure.](#)

Discussion

The generation of a living biobank presupposes, apart from complying with the legal regulations of privacy, medical law and animal welfare, a good infrastructure and a well-coordinated team. It has proven advantageous to directly involve a part of the surgical staff in the research procedures, since they can very well assess the suitability of the individual

patient for tissue donation. Moreover, patients tend to consent with biobanking more frequently, when their written approval is obtained within the course of the surgical informed consent discussion. To save time and resources, cases that will presumably yield insufficient amounts of tumor tissue should not be selected for biobanking. When it comes to specimen acquisition, the maxim "communication is key" is a simple, but often overlooked truth. It only takes a single uninformed

theatre nurse or surgical colleague to ruin the specimen right at the outset by proceeding as usual and adding formaldehyde to the resection specimen. Therefore, it is absolutely crucial that every single member of the involved staff gets acquainted with the SOP for biobanking. Surgeons should be noticed the day before and right at the start of the procedure about scheduled tissue collection. Furthermore, cases selected for biobanking, should be highlighted in the electronic OR plan. Tissue harvesting from the surgical specimen should be performed by a pathologist. First, this will ensure that the tissue harvesting does not interfere with the final pathological report. Second, this increases the probability of receiving tissue with adequate amounts of viable cancer tissue. Especially in pancreatic cancers with a pronounced desmoplastic reaction and frequent necrotic areas, viable parts are hard to identify macroscopically for the untrained eye. As an exception to this rule, tissue blocks from large hepatic or pulmonary metastases, may at times be excised "back-table" by the surgeon, if surgical margins can be defined macroscopically. Rectal cancer resected by total mesorectal excision (TME), might not be suitable for biobanking, since tissue harvesting from the resected specimen prior to paraffin embedding might interfere with the TME quality assessment. Alternatively, tissue for biobanking can be acquired by transanal biopsy of rectal cancer.

The establishment rates for primary cell cultures derived from the original tumor are generally low. PDX-derived, secondary cell cultures can more likely be successfully established. We recommend testing of different media for each case and use of antibiotic supplements for the first passages to reduce contamination to a minimum since the harvested tissue is rarely sterile. After successful propagation, each individual cell line should be confirmed as a cancer cell line by FACS analysis and regularly tested for mycoplasma contamination.

To exclude cross-contamination, regular STR analysis is advisable. It should be noted, that the establishment protocol for primary and secondary cell lines is constantly subjected to optimization. Details concerning the composition and success rates of the single media are clearly beyond the scope of this work and will be published separately.

For PDX engraftment, tumor tissue can be either implanted directly after resection or cryopreserved in fetal calve serum with 10% DMSO or similar freezing media for delayed implantation. Implantation immediately upon tumor tissue harvesting puts a strain on logistics and laboratory staff, and xenografting results after cryopreservation are not inferior at all¹⁰. Moreover, incubation of the tissue in Matrigel prior to tumor implantation, significantly increases engraftment rates¹². We recommend delayed engraftment following definite pathological finding and immediate disposal of erroneously collected tissue specimens. Since the success rate of primary engraftment increases with immunodeficiency of the recipient mouse, we tend to use NSG mice for the very first PDX passage. After the first successful PDX engraftment, NMRI^{nu/nu} mice can and should be used for subsequent passages and tissue expansion. This strain is more robust, cheaper and easier to breed compared to NSG or similar immunodeficient strains, but still shows reasonable engraftment rates. Moreover, its nudeness facilitates implantation and tumor growth monitoring. To increase the engraftment rates in subsequent passages, we recommend direct transfer of freshly harvested PDX tissues to host mice whenever possible, especially for slow growing PDX and cases with a low primary engraftment success rate. Collins and Lang recently reviewed 14 studies of colorectal PDX establishment and reported engraftment rates varying from 14 to 100% with a median PDX establishment rate of 68%, the latter being consistent with our findings¹³. In

line with the literature, we observed lower establishment rates of pancreatic compared to colorectal cancer PDX¹⁴. Regardless of the host mouse strain and tumor entity, the outgrowth of human, Epstein-Barr Virus (EBV)-associated B-cell lymphomas and murine lymphomas at the implantation side poses an important pitfall^{15,16}. If unrecognized, such tumors can "contaminate" subsequent passages and thus confound consecutive results. Unusual fast PDX growth and swelling of cervical, axillar and inguinal lymph nodes are strong indicators of murine lymphoma growth, but regular histological examination of PDX is nevertheless advisable. Furthermore, genetic concordance between PDX and the corresponding donor patient should be tested regularly by STR-analysis. Ideally, the biobank should be linked to a clinical database comprising patients characteristics (general information, survival, relapse free survival, therapy, secondary neoplasia etc.). Due to legal regulations of privacy protection and lack of such an anonymized data base, our clinical data set is regularly administrated and updated manually by the cooperating physicians.

While conventional biobanks are limited to observatory research, a living biobank provides the opportunity for *in vitro* and *in vivo* interventions. Patient-derived cell lines are an important tool for fundamental research, high-throughput drug screenings and assessment of new pharmaceutical agents⁴. Corresponding PDX models, however, are of increasing importance, since they closely recapitulate the histology of the original tumor^{17,18} and show a high genetic stability over several passages^{19,20}. Our PDX biobank has proven itself as an excellent platform for preclinical and fundamental research^{6,21}. Moreover, since large PDX collections adequately reflect the inter-individual heterogeneity of the patient population, the PDX clinical trial (PCT) approach (one animal per model per treatment) has

gained importance for drug development since it allows the faithful prediction of clinical response to new drugs and combinatorial regimen⁸. We also are currently evaluating new experimental drugs in small PCT trials.

Despite these promising results, the median establishment duration of 12.2 month, impedes the clinical applicability of PDX models as "avatar mice" for testing anticancer treatment options, at least for those patients in need of immediate adjuvant or even neoadjuvant treatment²². An additional disadvantage of standard PDX models is the lack of usability for immunotherapy testing due to host mice's immunodeficiency. To overcome these limitations, several "humanized" mouse strains have been developed. These mice are heavily immunocompromised, but can be reconstituted with various types of human bone marrow-derived cells or CD34⁺ hematopoietic stem cells subsequent to PDX outgrowth²³, allowing the evaluation of lymphocyte-mediated cytotoxicity and of therapy response to immune checkpoint inhibitor treatment^{24,25}.

In recent years, patient-derived organoids (PDO) emerged as important cancer models competing with PDX. Derived from intact tumor pieces and cultured in an extracellular matrix scaffold, these three-dimensional structures closely reflect the histologic and genetic properties of the original tumor. The possibility of long-term expansion and cryopreservation renders PDO an ideal supplement of a living biobank^{26,27}. In addition to a relatively high establishment rate, reliable drug response prediction has been reported for PDO of several tumor entities²⁸. Moreover, PDOs have even been generated from circulating tumor cells and also the simultaneous establishment of organoids from corresponding healthy tissue is possible, allowing assessment of therapy-related toxicity on a patient-individual basis^{29,30}. However, compared to

conventional 2D cell cultures, organoid culture is time and resource consuming and artificial extracellular matrix compounds can interfere with certain analytic procedures³¹. Moreover, cancer organoids are susceptible to overgrowth by faster growing, non-malignant organoids derived from healthy epithelium³⁰. Due to a lack of stroma, blood vessels and immune cells, PDOs are mostly inapplicable for the testing of antiangiogenic immunotherapeutic agents. Yet, new culturing methods allow the modeling of tumor microenvironment *in vitro*, rendering PDOs a true contender for PDX models³². In the near future, patient-individual tumor models, combined with powerful genetic tools like next-generation sequencing, will hopefully pave the path to true precision medicine and tailored-treatment approaches.

Disclosures

None.

Acknowledgments

We kindly acknowledge Jenny Burmeister, our graphical assistant, for the recording and editing of the video. Furthermore, we thank our colleagues of the surgical and pathological department for the longstanding collaboration. We would also like to thank Marcus Müller, production manager of the IT and Media Centre, University of Rostock, for supplying the audio recording equipment and refining the sound quality.

FUNDING: The German Cancer Aid Foundation (DKH e.V.), grant number 108446, and grant number TBI-V-1-241-VBW-084 from the state Mecklenburg-Vorpommern partly funded this research.

References




1. Sartore-Bianchi, A. *et al.* PIK3CA mutations in colorectal cancer are associated with clinical resistance to EGFR-targeted monoclonal antibodies. *Cancer research*. **69** (5), 1851-1857, (2009).
2. Pauli, C. *et al.* Personalized In Vitro and In Vivo Cancer Models to Guide Precision Medicine. *Cancer discovery*. **7** (5), 462-477, (2017).
3. Lipson, D. *et al.* Identification of new ALK and RET gene fusions from colorectal and lung cancer biopsies. *Nature medicine*. **18** (3), 382-384, (2012).
4. Wilding, J.L., Bodmer, W.F. Cancer cell lines for drug discovery and development. *Cancer research*. **74** (9), 2377-2384, (2014).
5. Mouradov, D. *et al.* Colorectal cancer cell lines are representative models of the main molecular subtypes of primary cancer. *Cancer research*. **74** (12), 3238-3247, (2014).
6. Klier, U., Maletzki, C., Kreikemeyer, B., Klar, E., Linnebacher, M. Combining bacterial-immunotherapy with therapeutic antibodies: a novel therapeutic concept. *Vaccine*. **30** (17), 2786-2794, (2012).
7. DiMasi, J.A., Reichert, J.M., Feldman, L., Malins, A. Clinical approval success rates for investigational cancer drugs. *Clinical pharmacology and therapeutics*. **94** (3), 329-335, (2013).
8. Gao, H. *et al.* High-throughput screening using patient-derived tumor xenografts to predict clinical trial drug response. *Nature medicine*. **21** (11), 1318-1325, (2015).
9. Mullins, C.S. *et al.* Integrated Biobanking and Tumor Model Establishment of Human Colorectal Carcinoma Provides Excellent Tools for Preclinical Research. *Cancers*. **11** (10), (2019).

10. Kuehn, F. *et al.* Establishment and characterization of HROC69 - a Crohn's related colonic carcinoma cell line and its matched patient-derived xenograft. *Scientific reports*. **6**, 24671, (2016).
11. Dangles-Marie, V. *et al.* Establishment of human colon cancer cell lines from fresh tumors versus xenografts: comparison of success rate and cell line features. *Cancer research*. **67** (1), 398-407, (2007).
12. Gock, M. *et al.* Tumor Take Rate Optimization for Colorectal Carcinoma Patient-Derived Xenograft Models. *BioMed research international*. **2016**, 1715053, (2016).
13. Collins, A.T., Lang, S.H. A systematic review of the validity of patient derived xenograft (PDX) models: the implications for translational research and personalised medicine. *PeerJ*. **6**, e5981, (2018).
14. Brown, K.M. *et al.* Patient-derived xenograft models of colorectal cancer in pre-clinical research: a systematic review. *Oncotarget*. **7** (40), 66212-66225, (2016).
15. Zhang, L. *et al.* The extent of inflammatory infiltration in primary cancer tissues is associated with lymphomagenesis in immunodeficient mice. *Scientific reports*. **5**, (2015).
16. Moyer, A.M. *et al.* Spontaneous murine tumors in the development of patient-derived xenografts: a potential pitfall. *Oncotarget*. **10** (39), 3924-3930, (2019).
17. Prall, F., Maletzki, C., Hühns, M., Krohn, M., Linnebacher, M. Colorectal carcinoma tumour budding and podia formation in the xenograft microenvironment. *PloS one*. **12** (10), e0186271, (2017).
18. Guenot, D. *et al.* Primary tumour genetic alterations and intra-tumoral heterogeneity are maintained in xenografts of human colon cancers showing chromosome instability. *The Journal of pathology*. **208** (5), 643-652, (2006).
19. Mattie, M. *et al.* Molecular characterization of patient-derived human pancreatic tumor xenograft models for preclinical and translational development of cancer therapeutics. *Neoplasia (New York, N.Y.)*. **15** (10), 1138-1150, (2013).
20. Cho, Y.B. *et al.* Colorectal cancer patient-derived xenografted tumors maintain characteristic features of the original tumors. *The Journal of surgical research*. **187** (2), 502-509, (2014).
21. Maletzki, C. *et al.* Functional Characterization and Drug Response of Freshly Established Patient-Derived Tumor Models with CpG Island Methylator Phenotype. *PloS one*. **10** (11), e0143194, (2015).
22. Katsiampoura, A. *et al.* Modeling of Patient-Derived Xenografts in Colorectal Cancer. *Molecular cancer therapeutics*. **16** (7), 1435-1442, (2017).
23. Wege, A.K. *et al.* Humanized tumor mice--a new model to study and manipulate the immune response in advanced cancer therapy. *International journal of cancer*. **129** (9), 2194-2206, (2011).
24. Herndler-Brandstetter, D. *et al.* Humanized mouse model supports development, function, and tissue residency of human natural killer cells. *Proceedings of the National Academy of Sciences of the United States of America*. **114** (45), E9626-E9634, (2017).
25. Capasso, A. *et al.* Characterization of immune responses to anti-PD-1 mono and combination immunotherapy in hematopoietic humanized mice implanted with tumor xenografts. *Journal for immunotherapy of cancer*. **7** (1), 37, (2019).

26. Sato, T. *et al.* Long-term expansion of epithelial organoids from human colon, adenoma, adenocarcinoma, and Barrett's epithelium. *Gastroenterology*. **141** (5), 1762-1772, (2011).
27. Clevers, H. Modeling Development and Disease with Organoids. *Cell*. **165** (7), 1586-1597, (2016).
28. Vlachogiannis, G. *et al.* Patient-derived organoids model treatment response of metastatic gastrointestinal cancers. *Science (New York, N.Y.)*. **359** (6378), 920-926, (2018).
29. Gao, D. *et al.* Organoid cultures derived from patients with advanced prostate cancer. *Cell*. **159** (1), 176-187, (2014).
30. Drost, J., Clevers, H. Organoids in cancer research. *Nature reviews. Cancer*. **18** (7), 407-418, (2018).
31. Abe, Y. *et al.* Improved phosphoproteomic analysis for phosphosignaling and active-kinome profiling in Matrigel-embedded spheroids and patient-derived organoids. *Scientific reports*. **8** (1), 11401, (2018).
32. Neal, J.T. *et al.* Organoid Modeling of the Tumor Immune Microenvironment. *Cell*. **175** (7), 1972-1988.e16, (2018).

Article

The HROC-Xenobank—A High Quality Assured PDX Biobank of >100 Individual Colorectal Cancer Models

Stephanie Matschos ¹, Florian Bürtin ¹, Said Kdimati ¹, Mandy Radefeldt ², Susann Krake ², Friedrich Prall ³, Nadja Engel ⁴ , Mathias Krohn ¹, Bianca Micheel ¹, Michael Kreutzer ⁵, Christina Susanne Mullins ¹  and Michael Linnebacher ^{1,*} 

¹ Clinic of General Surgery, Molecular Oncology and Immunotherapy, University Medicine Rostock, Schillingallee 69, 18057 Rostock, Germany; stephanie.matschos@med.uni-rostock.de (S.M.); florian.buertin@med.uni-rostock.de (F.B.); said.kdimati@med.uni-rostock.de (S.K.); mathias.krohn@med.uni-rostock.de (M.K.); b.micheel@keh-berlin.de (B.M.); christina.mullins@med.uni-rostock.de (C.S.M.)

² CENTOGENE GmbH, 18055 Rostock, Germany; mandy.radefeldt@centogene.com (M.R.); susann.krake@centogene.com (S.K.)

³ Institute of Pathology, University Medicine Rostock, Strepelstraße 10, 18057 Rostock, Germany; friedrich.prall@med.uni-rostock.de

⁴ Department of Oral, Maxillofacial and Plastic Surgery, University Medicine Rostock, Schillingallee 69, 18057 Rostock, Germany; nadja.engel@med.uni-rostock.de

⁵ Medical Research Center, University Medicine Rostock, Schillingallee 69, 18057 Rostock, Germany; michael.kreutzer@med.uni-rostock.de

* Correspondence: michael.linnebacher@med.uni-rostock.de; Tel.: +49-381-494-6043



Citation: Matschos, S.; Bürtin, F.; Kdimati, S.; Radefeldt, M.; Krake, S.; Prall, F.; Engel, N.; Krohn, M.; Micheel, B.; Kreutzer, M.; et al. The HROC-Xenobank—A High Quality Assured PDX Biobank of >100 Individual Colorectal Cancer Models. *Cancers* **2021**, *13*, 5882. <https://doi.org/10.3390/cancers13235882>

Academic Editors: Marta Baiocchi and Ann Zeuner

Received: 28 October 2021

Accepted: 19 November 2021

Published: 23 November 2021

Publisher's Note: MDPI stays neutral with regard to jurisdictional claims in published maps and institutional affiliations.



Copyright: © 2021 by the authors. Licensee MDPI, Basel, Switzerland. This article is an open access article distributed under the terms and conditions of the Creative Commons Attribution (CC BY) license (<https://creativecommons.org/licenses/by/4.0/>).

Simple Summary: Considering recent research, it was established that the best experimental models to conserve biological features of human tumors and to predict individual clinical treatment success are patient-derived xenografts (PDX). Their recognized and growing importance for translational research, especially for late-stage preclinical testing of novel therapeutics, necessitates a high number of well-defined PDX models from individual patients' tumors. The starting platform for the Hanses-tadt Rostock colorectal cancer (HROC)-Xenobank was the assortment of colorectal tumor and normal tissue samples from patients stored in our university biobank.

Abstract: Based on our research group's large biobank of colorectal cancers (CRC), we here describe the ongoing activity of establishing a high quality assured PDX biobank for more than 100 individual CRC cases. This includes sufficient numbers of vitally frozen ($n > 30$ aliquots) and snap frozen ($n > 5$) backups, "ready to use". Additionally, PDX tumor pieces were paraffin embedded. At the current time, we have completed 125 cases. This resource allows histopathological examinations, molecular characterizations, and gene expression analysis. Due to its size, different issues of interest can be addressed. Most importantly, the application of low-passage, cryopreserved, and well-characterized PDX for in vivo studies guarantees the reliability of results due to the largely preserved tumor microenvironment. All cases described were molecularly subtyped and genetic identity, in comparison to the original tumor tissue, was confirmed by fingerprint analysis. The latter excludes ambiguity errors between the PDX and the original patient tumor. A cancer hot spot mutation analysis was performed for $n = 113$ of the 125 cases entities. All relevant CRC molecular subtypes identified so far are represented in the Hanses-tadt Rostock CRC (HROC)-Xenobank. Notably, all models are available for cooperative research approaches.

Keywords: PDX model; CRC; mutation analysis; histological examination

1. Introduction

Despite early diagnostic options and improved treatment, colorectal cancer (CRC) is still one of the leading causes of cancer-related deaths worldwide [1]. In particular,

the fact that some patients do not respond even to targeted therapies underlines the necessity of further patient-derived models to promote the development of personalized treatments [1,2].

Currently the best model to reflect the characteristics of the original tumor is the patient-derived xenograft (PDX) model because of its conservation of the original tumor's biological features, including microarchitecture, pathomorphology, and genetic alterations [2,3]. Tentler et al. have stated that CRC PDX tumors retain the intratumoral clonal heterogeneity, chromosomal instability, and histology of the parent tumor for up to 14 passages [2,4]. Furthermore, the possibility of precisely predicting individual clinical treatment success, especially for the late-stage preclinical testing of novel therapeutics, implies a clear exigency for more academically run PDX-biobanks, containing large numbers of individual tumors [2,3,5,6]. Inspired by this notion, we used our large collection of patient material, which included matching tumor and normal epithelial tissue, as a starting platform to establish a high number of individual PDX models. This resulted in a quality assured PDX biobank containing more than 100 individual CRC cases and encompassing all specific CRC molecular subtypes. Thus, this PDX biobank represents an ideal platform to study new agents for adjuvant therapy. As such, it is feasible to target specific molecular subtypes or alterations, in combination with investigations concerning different molecular pathways within the tumor cells as compared to the normal epithelial tissue. Such an approach has recently been described by Medico and colleagues. Here the authors identified tumor specific changes that consist of clinically actionable kinase targets for which approved drugs are already available [7]. Moreover, omics data from both the PDX model and the original patient tumor could, on the one hand, accelerate the entry of novel drugs into the clinic, and, on the other hand, such paired data sets would facilitate the identification and validation of predictive biomarkers [2].

Finally, as has been described by us and other groups, the PDX-derived tissue is an ideal source for repetitive cell line establishment [8,9] and also patient-derived organoid (PDO) generation attempts [9,10]. This can significantly boost the overall success rate, from 10–13% for primary patient material derived cell lines [8,11] to about 30% for secondary, i.e., PDX-derived, cell lines [8]. Our vision is an integrated biobank collection, consisting of deeply characterized primary patient material, 2D cell lines, PDX, and PDO. With this vision we would like to support orchestrated research strategies, from more basic mechanistic approaches to translational drug development and tests to end-stage preclinical studies. Besides dogmatic animal welfare policies, the establishment and proper long-term maintenance of platforms such as the integrated Hansestadt Rostock CRC (HROC) biobank are essential for minimizing the overall number of animals involved in oncological *in vivo* studies.

2. Materials and Methods

Surgically resected tissues were collected from consenting patients at the UMR from 2006 to 2019. The study was approved by the ethics committee of the UMR (II HV 43/2004, A45/2007, A2018-0054, and A2019-0187) [8,12].

2.1. PDX Generation

Tumor engraftment was performed according to the guidelines of the local animal use and care committee, Landesamt für Landwirtschaft, Lebensmittelsicherheit und Fischerei Mecklenburg-Vorpommern with the permit numbers: LALLF M-V/TSD/7221.3-1.1-071/10; 7221.3-1-015/14; and 7221.3-2-020/17. The mice strains used were bred in the animal facility of the Rostock University Medical Center and maintained in specified, pathogen-free conditions, exposed to 12 h light/12 h darkness cycles. The mice received standard pellet food and water *ad libitum*.

Prior cryopreserved matching patient-derived tumor and normal tissue samples in our biobank of CRC patients served as the starting platform for all established PDX models.

Detailed information on the patients' tumors, as well as clinico-pathological information, is given in Supplementary Table S1.

Pieces of the patients' tumors were implanted subcutaneously into the animals' left and right flanks, under anesthesia (ketamine/xylazine, 90/6 mg/kg bw). Due to the engraftment rate of up to 80%, the preferred mouse strain for this first passage is NOD.Cg-Prkdc^{scid} Il2rg^{tm1Wjl}/SzJ (NSG). Further passaging can be performed either with NSG or with NMRI-*Foxn1*^{nu} (NMRI nude mice). The PDX tumors were named with anonymized patient information followed by the abbreviation Tx, standing for the passage of the PDX tumor, and then followed by the abbreviation Mx, standing for consecutively numbered mice. All tumor engraftments were performed on 6–12 week-old mice, both male and female, weighing 18–30 g. Prior to xenografting, four vital tumor aliquots (3 × 3 × 3 mm) were soaked in 100 µL Matrigel (Corning, Kaiserslautern, Germany) for >10 min at 4 °C. After 30 days of antibiotic treatment (drinking water containing cotrimoxazole: dosage 8 mg trimethoprim and 40 mg sulfamethoxazole per kg BW), tumor growth was monitored weekly until tumor establishment and growth to a maximal diameter of 14.2 mm. When the maximum tumor volume of 1500 mm³ was reached or the mice became moribund, the tumors were explanted. The time of tumor growth until explantation was defined as tumor harvesting time.

After the explantation of the PDX tumors, the tumors were stored in Tissue Storage Solution (Miltenyi, Bergisch-Gladbach, Germany) until further processing. Snap frozen aliquots were made as soon as possible by immediately submerging tumor pieces in liquid nitrogen to ensure high quality, particularly for RNA molecules. Vital aliquots were made by transferring four tumor pieces of 3 × 3 × 3 mm in 1.5 mL freezer medium (fetal bovine serum with 10% DMSO) and cooling them down in CoolCell[®] LX—freezing containers (CryoShop, München, Germany) by −1 °C per minute to −80 °C [13].

While processing the PDX tumors, the degree of necrosis was assessed and documented, allowing a classification into not necrotic, barely necrotic, intermediately necrotic, and highly necrotic.

The process describing our PDX biobank establishment approach was recently published [14].

2.2. Histopathology

For each PDX model, one representative cross section of a subcutaneous PDX tumor or half of the PDX tumor was fixed immediately upon explantation in formalin and embedded in paraffin by routine procedures. H&E-stained sections (4–5 µm) were analyzed in light-microscopic studies to assess the morphologic features of each individual PDX model [15]. A comparison with the respective original patient tumor was performed by a board-certified pathologist (FP).

2.3. Quality Control via Short Tandem Repeat (STR) Analysis

The fluorescence-labeled, PCR-amplified DNA fragments of D5S818, D7S820, D16S539, D13S317, vWA, TPOX, THO1, CSF1PO, and Amelogenin were injected along with an appropriately sized standard GeneScan[™] LIZ500 (appliedbiosystems Thermo Fisher Scientific, Waltham, MA, USA) into the capillary for electrophoresis size separation, using ABI instrumentation. Size-separated PCR fragments were detected by reading their fluorescence intensity at different emission wavelengths and were recorded as FSA after their migration through the capillary from cathode to anode, in which smaller fragments migrate faster than larger fragments [16]. The application of primer pairs labeled with three different fluorescence dyes—FAM (blue), HEX (green), and TAMRA (red)—enabled the fragment size determination of all markers mentioned (primers listed in detail in Table 1) in a single analysis.

Table 1. Sequences of STR primers.

Primer	Sequence
D5S818 for	5'-HEX-GGT GAT TTT CCT CTT TGG TAT CC-3'
D5S818 rev	5'-AGC CAC AGT TTA CAA CAT TTG TAT CT-3'
D7S820 for	5'-HEX-ATG TTG GTC AGG CTG ACT ATG-3'
D7S820 rev	5'-GAT TCC ACA TTT ATC CTC ATT GAC-3'
D16S539 for	5'-HEX-GGG GGT CTA AGA GCT TGT AAA AAG-3'
D16S539 rev	5'-GTT TGT GTG TGC ATC TGT AAG CAT GTA TC-3'
D13S317 for	5'-HEX-ATT ACA GAA GTC TGG GAT GTG GAG GA-3'
D13S317 rev	5'-GGC AGC CCA AAA AGA CAG A-3'
vWA for	5'-6-FAM-GCC CTA GTG GAT GAT AAG AAT AAT CAG TAT GTG-3'
vWA rev	5'-GGA CAG ATG ATA AAT ACA TAG GAT GGA TGG-3'
TPOX for	5'-6-FAM-ACT GGC ACA GAA CAG GCA CTT AGG-3'
TPOX rev	5'-GGA GGA ACT GGG AAC CAC ACA GGT TA-3'
THO1 for	5'-6-FAM-ATT CAA AGG GTA TCT GGG CTC TGG-3'
THO1 rev	5'-GTG GGC TGA AAA GCT CCC GAT TAT-3'
CSF1PO for	5'-6-FAM-AAC CTG AGT CTG CCA AGG ACT AGC-3'
CSF1PO rev	5'-TTC CAC ACA CCA CTG GCC ATC TTC-3'
Amelogenin for	5'-ACC TCA TCC TGG GCA CCC TGG TT-3'
Amelogenin rev	5'-TAMRA-AGG CTT GAG GCC AAC CAT CAG-3'

2.4. Molecular Classification Analyses

The microsatellite instability (MSI) and methylation status of CpG islands [17–19] were determined for all cases included in this study. The classification was MSI-H if two or more microsatellite markers of either the Bethesda panel or the “six mononucleotide repeat” panel, consisting of BAT25, BAT26, CAT25, NR21, NR24, and NR27, showed band shifts [8,17]. Classification concerning the CpG island methylator phenotype (CIMP) was carried out as follows: if the analysis was performed according to Ogino et al., the subtype was divided into CIMP-H, non MSI, when ≥ 4 loci, and CIMP-L, non MSI, if 1–3 CIMP loci out of 5 loci analyzed were methylated [17,18]. When analyzed according to Weisenberger et al., ≥ 3 methylated CIMP Loci out of 5 loci analyzed defined CIMP-H, non MSI; no further distinction of CIMP-L, non MSI took place [19].

2.5. Next Generation Sequencing (NGS) Analyses

In total, 121 datasets were either generated by Centogene (Rostock, Germany) or extracted from a previous dataset [20]. This dataset consisted of Whole Exom Sequencing (WES) analyses of 20 PDX cases and 12 primary tumors. The remaining analyses were performed using a Solid Tumor Panel from Centogene consisting of 105 fully sequenced genes, plus mutational hot spots from an additional 146 genes. Library preparation was performed with the Twist Library Preparation Enzymatic Fragmentation Kit (Twist Bioscience, San Francisco, CA, USA). Exome enrichment was carried out, using either the TWIST Human Core Exome Plus probes (covering 36.5 Mb of the human coding exome) or custom designed probes, in the case of the Solid Tumor panel. Sequencing was performed using the NextSeq500 (Solid Tumor panel) or the HiSeq4000 and NovaSeq (WES) systems (Illumina, Inc., San Diego, CA, USA) to produce 2×150 bp reads. Raw sequencing reads were converted to standard fastq format using bcl2fastq software 2.17.1.14 (Illumina, Inc., San Diego, CA, USA). The short-reads were aligned to the GRCh37(hg19) build of the human reference genome using Bowtie version 2.4.2 [21]. The alignments were sorted (samtools v. 1.11) [22] and de-duplicated (PicardTools v. 2.23.8) [23]. Variant calling was performed with Strelka Somatic pipeline (v. 2.9.2) [24]. The variant table was filtered with vcftools v. 0.1.16 [25] and annotated with snpEff [26]. The filters applied were set to protein-coding mutations, filter “Pass”, allele frequency > 5%, quality > 50, and at least 20 reads for the tumor.

For one PDX case, tissues obtained from two different mice were analyzed, and for a second PDX case, tissues obtained from two different passages were analyzed.

Concerning the NGS data for this study we focused on mutations being pathogenic or likely pathogenic, but also included mutations of uncertain significance. Excluded were all benign mutations, as well as mutations classified as risk factor and influencing drug response. Moreover, only the mutations from the raw data which passed the following quality criteria, including the filter “Pass”, \neq coding synonym, a quality ≥ 30 , and a variant allele frequency of at least 15, were listed.

2.6. Statistical Analyses

Statistical analyses were performed using either the statistical program prism 8 or IBM SPSS Statistics. Heatmap and mutation frequency analyses were performed in Prism. In SPSS, a nonparametric bivariate correlation analysis according to Kendall-Tau and Spearman’s rank correlation coefficient and Fisher’s exact test were performed. The cluster analysis was performed with Origin Pro 2017G (parameters: cluster method = Furthest Neighbor; distance type = Euclidean).

3. Results

In order to achieve maximal quality and traceability, the data from the CRC PDX cases included in the end, were collected and were mostly presented according to the PDX-Minimal Information standard (PDX-MI) recommended by Meehan et al. [27]. The PDX-MI suggests four modules reflecting the process of generating and validating a PDX model: (1) clinical data, (2) model creation data, (3) model quality assurance data, and (4) model study and associated metadata. Detailed information on our analyzed PDX cases was arranged accordingly and listed in Supplementary Table S1.

3.1. Patient, Clinical and Molecular Tumor Data

In total, 261 CRC patients were included in this study in the time span of October 2006 to May 2019. From these cases, 167 individual PDX models could be generated (64.0%). The present study focuses on 125 of these cases, which have been selected according to the following criteria: (I) enduring growth in immunodeficient mice and (II) storing sufficient quantities of PDX tissues with (III) adequate quality. The latter criteria in particular, led to the exclusion of 20 cases (12.0%) due to very high proportions of necrotic areas reproducibly observed in the harvested PDX tissues. Analyses of 22 PDX are not yet finalized, and thus these were consequently excluded from the present study.

To anonymize the patient information, each case was assigned an alias consisting of: HRO for Hansesstadt Rostock, C for colon cancer, and a consecutive number. Metastases included were given the identifier Met as an abbreviation of metastasis. This was added directly after the HROC number. In case of multiple tumors, an additional tumor numeration was included.

All available patient information following surgical removal of the tumor, e.g., further treatments, disease recurrence, progression free and overall survival, were collected as described before [8] and updated in May 2020. These data are listed in Supplementary Table S1. The patient tumor samples consist of 100 primary adenocarcinomas, including one neuroendocrine tumor. Twenty-five samples are of metastatic origin, largely of the liver (80.0%). Metastases also manifested in the abdominal wall, brain, lung, peritoneum, and multivisceral ($n = 1$, each).

The gender distribution of the 125 patient cases included was 56.8% male and 43.2% female. The mean age was 69.7 years (ranging from 30 to 98). Tumor UICC staging was 11% stage I, 29% stage II, 27% stage III, and 33% stage IV. T stages were 30% T4, 59% T3, 10% T2, and 1% T1; M stages 1% M2 and 32% M1; 67% had no metastases identified (M0). Tumor grading (G) was 2% G1, 55% G2, and 43% G3.

Due to the fact that the integrated biobanking activities started in 2006 and are an ongoing process, the included cases cover the time period of 2006 to 2019. Thus, it was not possible to calculate the 5 year survival rate for all patients. Accordingly, setting a cutoff for the calculation of survival time was necessary. At the cutoff of May 2020, 54 patients were

still alive, and 71 patients were dead. Three patients died perioperative, within 30 days after surgery (congruent with Clavien-Dindo classification). For the remaining 68 deceased patients, progression free survival averaged 13.0 months (ranging from 0 to 119) and the mean overall survival was 32.6 months (ranging from 1 to 133).

Each patient's individual cancer history and therapy regiment was listed in detail if applicable, including type and duration of therapy, as well as applied chemotherapeutic agents (Supplementary Table S1). Because most of our in-house therapeutic studies with different agents compared to the standard of care are ongoing or will be published soon, the therapeutics which showed a reduction in the PDX tumor growth compared to the standard of care are simply listed in Supplementary Table S1.

Since an ideal CRC PDX collection should approximate the molecular heterogeneity of clinical cases, our 125 PDX were classified according to the following molecular subtypes [17]: chromosomal instable (CIN), sporadic microsatellite instable (spMSI), having the CpG island methylator phenotype (CIMP, sub classified into high level (CIMP-H) and low-level (CIMP-L)), and Lynch syndrome (LS) (Table 2).

Table 2. Molecular subclasses of the 125 investigated PDX, listed with total amount and percentage.

Molecular Subclass Determination (<i>n</i> = 125):		
CIN	65	52%
spMSI-H	29	23.2%
CIMP-H, non MSI	10	8%
CIMP-L, non MSI	10	8%
Lynch syndrome	10	8%
Neuroendocrine tumor	1	0.8%

The distribution of the molecular subtypes mostly corresponds to the general clinical distribution [28]. Only spMSI-H and LS are overrepresented, which is most likely attributable to the high engraftment rates of these molecular subtypes [29].

3.2. Biobanking of Established HROC PDX Models

Besides mirroring the clinical characteristics of patient cohorts, another major goal was to generate and biobank ample amounts of PDX tissue for subsequent analyses and future preclinical studies. In particular, $n \geq 30$ vital PDX tissue backups (consisting of four small cubes of approximately 3 mm side-length, to allow for a total of at least 120 implantations), plus a minimum of $n = 5$ snap frozen samples, ideally suited for molecular analyses, were generated and stored in the gas phase above liquid nitrogen for each case. It is notable that the backups of all 125 cases were generated within less than 10 passages, and usually in less than 5 passages. This ensured closest achievable proximity to the tissue of origin. Moreover, representative cross-sections and halves of the PDX tumors were fixed in formalin and paraffin-embedded (in the following, this is termed FFPE tissue) for histopathological assessment.

The HROC Xenobank contains eight sets of primary tumor and metastases derived tissues from the very same patients; namely: HROC72 and HROC72Met1; HROC147 and HROC147Met1; HROC277, HROC277Met1 (synchronous), and HROC277Met2 (metachronous); HROC278 and HROC278Met1; HROC300 and HROC300Met1; HROC348 and HROC348Met1; HROC362 and HROC362Met1; and HROC405 and HROC405Met1. Additionally, three sets of two metastases from the very same patient are included: HROC103Met1 and Met2, HROC230Met1 and Met2, as well as HROC313Met1 and Met2. Furthermore, two sets of different primary tumors from the very same patients are included as well: HROC252Tu1, Tu2, and Tu3, plus HROC386Tu1 and Tu2.

The mean duration from implantation to harvest for all the included PDX models and overall passages was 105 days (range 38 to 287). No significant differences in duration until harvest were observed for the initial passages with 120 days (range 36 to 329) compared to 106 days (range 35 to 324) for the last performed passages of the included PDX models. Mice

presenting health conditions leading to premature harvest were excluded from calculation of duration to harvest. These cases are indicated with >x days in Supplementary Table S1. Harvesting times were compared between the first and the last passage of each individual patient case, and increased or decreased growth is indicated with arrows in Supplementary Table S1 column AG and column AH. A trend for shorter duration until harvest for the last passage was observed in the majority of cases: 70/125 (56%). No correlations with molecular subtype or features of the PDX became apparent.

Moreover, a direct comparison of the utilization of fresh vs. vitally frozen tissues for subsequent passaging was possible for 28 cases (Supplementary Table S2). In 23 of those cases (82.1%), a shorter time to harvest was observed when PDX tissues were passaged fresh (unpaired *t*-test $p = 0.0003$).

A correlation analysis revealed, beside the expected positive correlations between the UICC stage and patient's progression free and overall survival, correlations between the PDX model features and the properties of the patient tumor (Supplementary Table S3). Further, 62.0% of the PDX established from male patients originated from patients in the age group 50–69 years old, whereas 53.7% of the tumors from female patients originated from patients > 70 years. Concerning only primary tumors, the distribution of models derived from male or female patients is balanced at 50.5% vs. 49.5%, but concerning metastases, more models derived from male patients are represented, with a division of 80.0% vs. 20.0%. Moreover, within the molecular subtypes, male patients' tumors dominated within the CIN cases (70.8%). Cases of the subtype spMSI-H were predominantly from female patients (79.3%).

Further, the molecular subtype and the time to harvest of PDX tumors were correlated (correlation $p < 0.001$, exact fisher test $p = 0.008$). Moreover, the number of mice necessary to generate sufficient backups correlated with the molecular subtype (correlation $p = 0.002$, exact fisher test $p = 0.048$). We observed again a correlation between the localization of the tumor and the duration until harvest (correlation $p = 0.002$, exact fisher test $p = 0.047$). Tumors of the right colon generally needed less than 90 days. For the other localizations, the duration was 90–180 days until outgrowth. Concerning the molecular subtype, it can be pointed out that MSI-H tumors, both sporadic as well as Lynch-associated, for the most part grew out in less than 90 days. The remaining molecular subtypes took 90–180 days to reach the designated size. Ample backups could, for most PDX cases of the spMSI-H type, be generated using fewer than 3 mice, whereas the highest numbers of mice, frequently > 4.5 mice, were necessary for CIMP-L, non MSI-type tumors. Furthermore, it is worth mentioning that there is a positive correlation between the time to harvest of the last passage performed and patients' overall survival (correlation $p = 0.033$, but not significant in exact fisher test).

3.3. Identity Testing

The genetic identity of all established PDX models in comparison to the original patient tissue was confirmed by fingerprint analysis as described before [30]. The PDX were found to be either genetically identical to or descended from the respective patient (data not shown) with two exceptions: no evaluable signals could be generated by fingerprint analysis for PDX HROC32 T3 M7 and HROC223 T2 M1. Allelic imbalances were regularly observed as well as small shifts in allele length for PDX of the MSI molecular subtype. These phenomena are both well-known. However, the possibility of comparing different patient tissues, as well as primary and secondary cell lines in many of the MSI-cases, still allowed valid identity verification.

3.4. Histological Examination

H&E-stained sections from FFPE blocks were used to assess morphologic features of each individual PDX model. Moreover, PDX tumors were compared to the respective original patient tumor by a board-certified pathologist (FP). Figure 1 depicts three selected cases: HROC172, HROC260, and HROC386Tu1. Details of the histological investigations are listed in Supplementary Table S4.

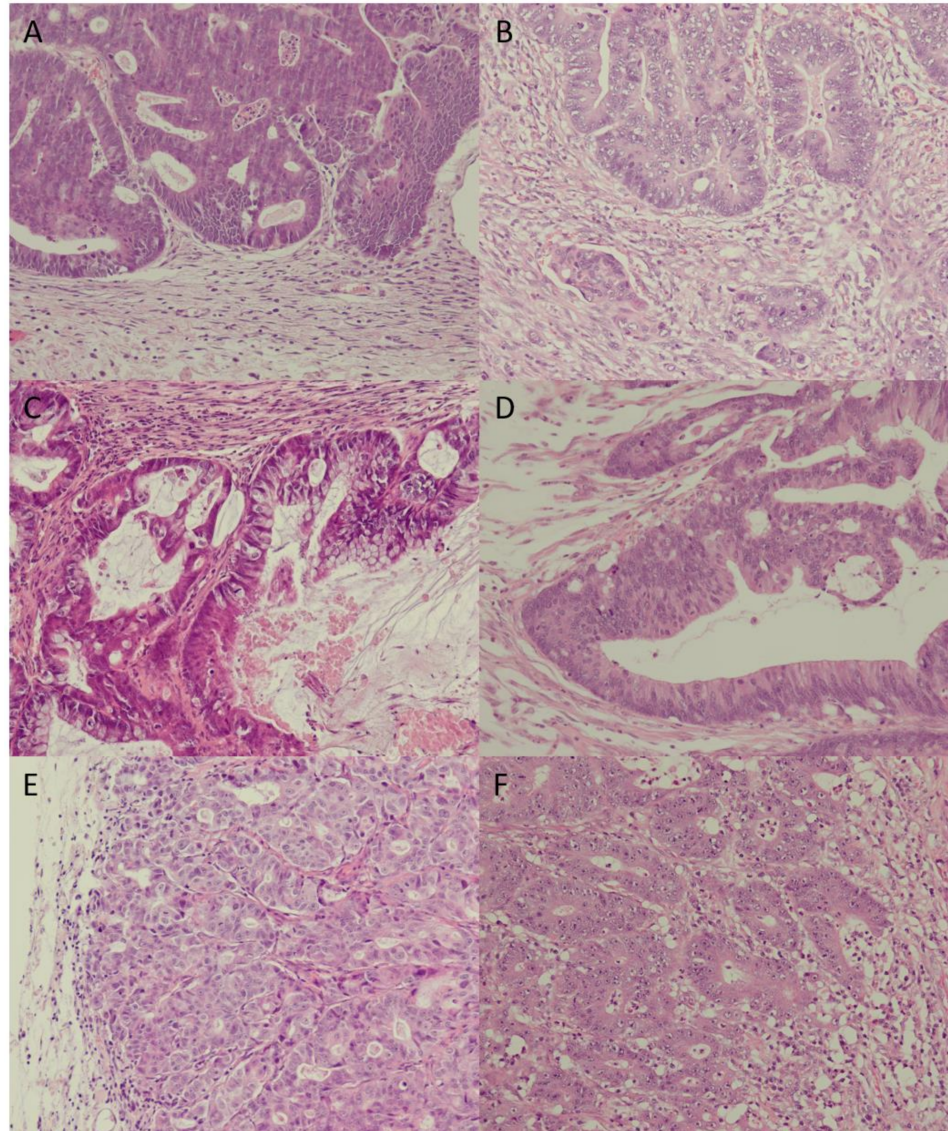


Figure 1. Comparison of primary tumor vs. PDX tumor in 20-fold magnification: (A) = HROC172 primary tumor, (B) = HROC172 T2 M2; (C) = HROC260 primary tumor, (D) = HROC260 T2 M5; (E) = HROC386Tu1 primary tumor, (F) = HROC386Tu1 T1 M1. In the case of HROC172, PDX cytomorphology and architecture match the primary tumor—stroma desmoplasia and tumor budding were markedly reduced; in the case of HROC260, PDX cytomorphology and architecture match the primary tumor—villous-mucinous structure was also reproduced; and, in the case of PDX HROC386Tu1, cytomorphology and architecture of the primary tumor was reproduced precisely.

A comparison was not possible for 17 out of the 125 cases due to a lack of patient tumor FFPE material, thus allowing a direct comparison for a total of 108 cases. Concordance of patient and PDX tumor structure was found in 92 cases (85.2%), minor differences were noticed 11 times (10.2%) and marked differences occurred in 5 cases (4.6%). Here, a fingerprint analysis performed with gDNA, isolated from sections of the very same FFPE tissue blocks

used for the histological examination, confirmed genetic identity with their respective patients of origin for three out of the five cases (HROC251, HROC370, and HROC447). For the cases HROC32 and HROC223, the pathologist suspected heavy contamination of the PDX tissues with murine or human lymphatic cells. Since the fingerprint analysis failed for these two PDX tissues, as mentioned above, species-specific PCR analyses were performed. The results allowed the conclusion that murine thymoma cells predominated in the PDX tissues. Of note, identity tests from HROC32 PDX tissue after the initial mouse passage, as well as from two PDX-derived cell lines generated from the same passage as the FFPE tissues, matched the patients' identities.

A side-by-side comparison of PDX tumors derived from the same passage, but different animals, for six cases with different molecular subtypes (HROC92, HROC111Met1, HROC131, HROC169, HROC324, and HROC430) delivered exactly matching pathomorphological results (Supplementary Table S4). Thus, we would conclude that the conservation of the original tumor's biological features such as microarchitecture and pathomorphology are an intrinsic feature of the individual model and we expect these to be stably maintained for several passages as shown before by Tentler et al. [2].

Finally, when PDX tumors were explanted, the degree of necrosis was assessed. Although this is not a very precise method, it allowed the classification of the PDX cases into four categories: not, barely, intermediately, and highly necrotic (Supplementary Table S1, column AJ). Here, we observed no significant correlations between the degree of necrosis and patient data. The MSI cases, both sporadic and LS, the PDX models which needed fewer mice for complete asservation, and the PDX cases with shorter duration until harvest were rarely highly necrotic: there were only 4/39 cases (10.3%) vs. 27/86 cases (31.4%) for the remaining molecular subtypes. Highly necrotic PDX tumors maintained this characteristic also in later passages. The paired PDX cases of primary and metastasis derived tumors from the very same patients ($n = 8$) always had very similar necrosis categories (Supplementary Table S1).

3.5. Mutation Analysis

Selected cases ($n = 113$) were analyzed using a Solid Tumor Panel NGS approach. The NGS data are presented in detail in Supplementary Table S5. For two cases (HROC277Met2 and HROC405), two individual PDX tumors were analyzed. Here, the same pathogenic or likely pathogenic mutations were observed. The PDX tumor with the lower passage for patient HROC405 presented additional mutations of uncertain significance. Furthermore, for four cases, NGS analyses were conducted with patient and PDX tumor tissue (HROC285, HROC404, HROC415Met1, and HROC419). Pathogenic or likely pathogenic mutations detected in the original patient tumors were also detected in the PDX tumors, with one exception: a mutation in *RHOA* was only found in the primary patient tumor of HROC419. However, the PDX tumors of HROC285, HROC404, and HROC415Met1 displayed additional pathogenic or likely pathogenic mutations. In case of HROC285, four additional mutations in the genes *ABCB4*, *KRAS*, *MSH2*, and *NF1* were observed, whereas HROC404 and HROC415Met1 displayed two additional mutations in *AXIN2* and *HRAS*, as well as in *KMT2D* and *KRAS*, respectively. Besides, the PDX tumors displayed more additional mutations of uncertain significance than the original tumors.

Next, an unsupervised cluster analysis including only the pathogenic or likely pathogenic mutations, was performed (Figure 2).

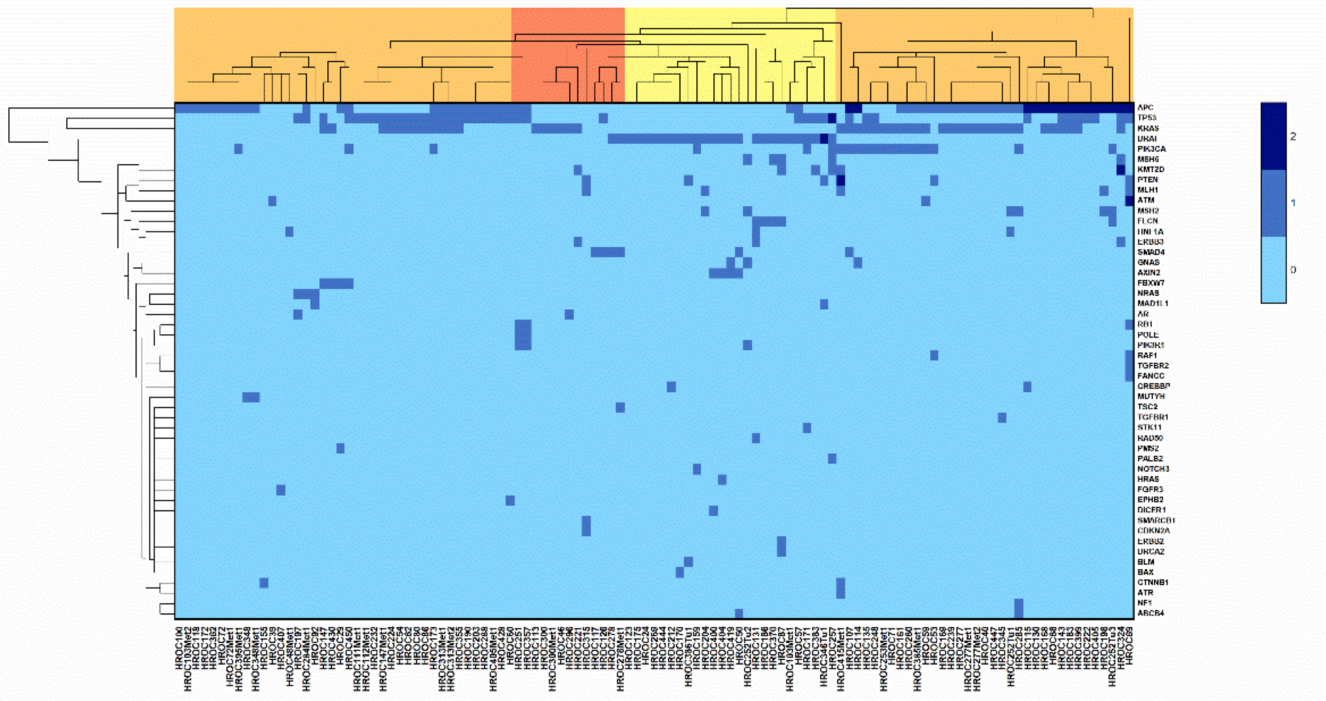
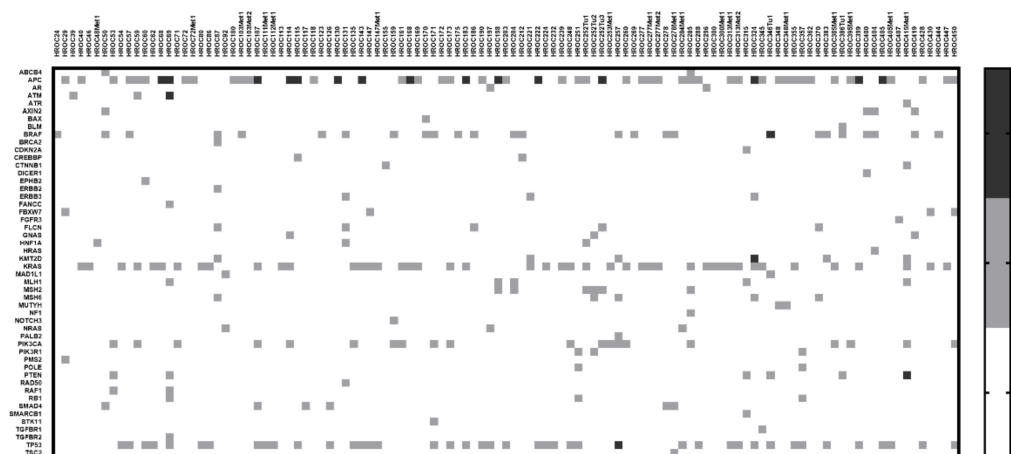


Figure 2. Unsupervised cluster analysis for all investigated tumors concerning the pathogenic or likely pathogenic mutations, with the following parameters: cluster method = Furthest Neighbor; distance type = Euclidean.

The clusters highlighted in orange contain mostly CIN cases (70.0 and 65.7%), whereas the cluster highlighted in yellow consists almost exclusively of sporadic MSI tumors (88%). However, the cluster highlighted in red could not be linked to a specific molecular subtype.

Furthermore, the number of pathogenic and likely pathogenic mutations detected per gene and case are illustrated in a heatmap (Figure 3A). The mutation frequency of each gene can be found in Figure 3B. The most frequently mutated genes in the HROC-Xenobank are *APC* (50.4%), *KRAS* (39.8%), *TP53* (37.2%), *BRAF* (23.0%) and *PIK3CA* (17.7%).



(A)

Figure 3. Cont.

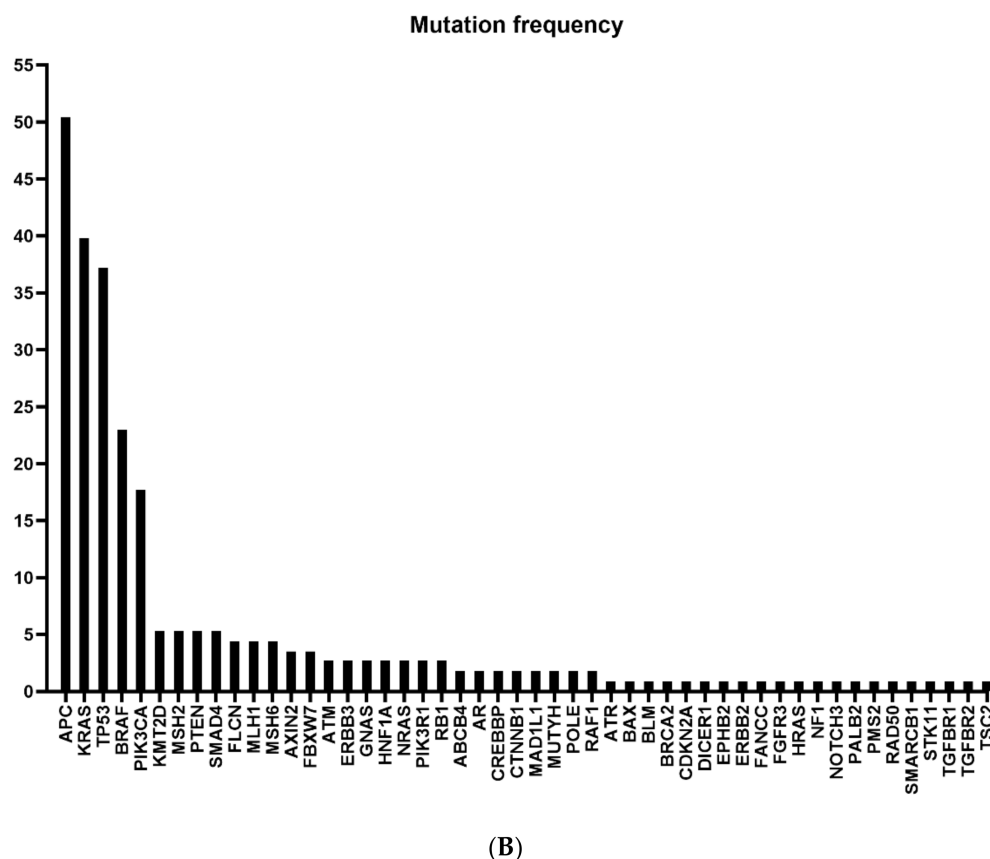


Figure 3. (A) = heat map. (B) = mutation frequency; (A) illustrates the number of pathogenic and likely pathogenic mutations per gene and case in a heat map, and the mutation frequency for each gene calculated out of this data is illustrated in (B).

4. Discussion

In summary, in this study we succeeded in establishing a CRC xenobank containing 125 individual PDX models with sufficient numbers of vital backups, snap frozen aliquots for molecular analysis, and FFPE material.

Mattar et al. described the challenges of creating a PDX biobank and proposed requirements for sample characterization and validation [31]. These included the collection of the above-mentioned sample types, namely, vital tissue, snap frozen samples, and FFPE specimens. In addition, they urged for genomic profiling and comparative histological reviewing. All of these recommendations were followed in our study. Comparative pathomorphological analysis and genetic identity testing confirmed the close proximity of the HROC-Xenobank models to the original patient tumors. Moreover, we could confirm previous findings that PDX models, in the majority of cases, maintain the original tumor's biological features [2,3,32]. For each individual HROC PDX model we described in detail, the pathomorphological structures were reproduced from the original patient tumor. A side-by-side comparison of PDX tumors derived from the same passage but different animals selected randomly revealed exactly matching pathomorphological results. Thus, we concluded that the original tumor's biological features, such as microarchitecture and pathomorphology, are intrinsic features of the individual tumor; thus, they are also conserved in the derived models and are most likely stable for several passages. It has been shown before that CRC PDX retain the histology as well as other features of the parental tumor, including intratumoral clonal heterogeneity and chromosomal instability, for up to 14 passages [2].

A surprising observation of the present study was the comparable duration until harvest for PDX tumors of the first and the last performed passage, at least with regard to

mean values. Others have described a significantly accelerated growth rate with increasing passages [33]. One possible explanation for this discrepancy might come from the fact that we used different mouse strains. Because the engraftment efficacy for CRC ranges between ~60 and 70% in NMRI nude mice and up to ~80–90% in NSG mice [34], the preferred mouse strain for the first passage was NSG. Subsequent passaging was performed either with NSG or NMRI nude mice. The latter strain was preferred, since the risk of murine and/or human lymphoma development is reduced [35–37]. When considering this, we cannot formally exclude the possibility that this may have biased our results and this might explain why similar harvesting times between different passages were observed. Another factor affecting the time to harvest is the tissue condition at the time of engraftment, i.e., fresh vs. vitally frozen samples. For 23/28 (82.1%) cases, passaging with fresh material resulted in a significantly diminished duration until harvest.

Abdirahman et al. reported an engraftment success of 22/33 (67%) cases for their CRC PDX series, but because four cases turned out to be human lymphomas, their rate dropped to 18/33 (55%) [32]. Their lymphoma rate was surprisingly high (4/22; 18.2%). When comparing this with the 1.6% (2/125) rate of murine lymphoma in our study, and considering that Abdirahman and colleagues performed all passaging in NSG mice, it becomes clear why switching from NSG for initial engraftment to passaging in NMRI nude mice is preferable.

Further, the HROC PDX models precisely recapitulated the mutation profiles of the original patient tumors, thereby confirming previous data [32,38,39]. In particular, our study pointed out that pathogenic or likely pathogenic mutations detected in the original tumors were maintained in the PDX tumors. The current gold standard of NGS data analysis to compare are the data contained in the Cancer Genome Atlas Network (TCGA). In comparison to the TCGA results, the HROC-Xenobank mutational landscape differed in parts. The frequency for the most commonly mutated gene, *APC*, was 72.5% in the TCGA data set, compared to our frequency of only 50.4%. The *PIK3CA* gene had a frequency of 27.5% in TCGA and of 17.7% in the HROC-Xenobank. Frequencies for *BRAF* mutations were 11.6% (TCGA) and 23% (HROC-Xenobank). The most striking difference was noticed for *TP53* mutation frequency. Here 58.8% were reported for TCGA, and we observed merely 37.2% in our cohort. However, similar frequencies were observed for *KRAS* with 40.8% (compared to 39.8%) [40]. Compared to mutation frequencies reported by Lee et al. for *APC* (60%) and *KRAS* (49%), no apparent differences to our results were seen [41]. Similarly, the mutation frequency published by Burgenske et al. for *PIK3CA*, 15–25%, did not differ from our observation (17.7% in the HROC-Xenobank) [42].

When focusing on hypermutated tumors, the mutation frequency in TCGA increased to 57.5% for *BRAF*. The overrepresentation of hypermutated tumors in our cohort most likely explains the higher frequency of *BRAF* mutations observed in our cohort.

Mutation patterns of CRC from adolescent and young adults are also different. Tricoli et al. stated that in tumors of younger patients, genes were mutated significantly more frequently, particularly genes associated with DNA repair pathways *BRCA2* (39% vs. 3%) and *RAD9B* (22% vs. 0%), as well as the cell-cycle checkpoint kinases *ATM* (35% vs. 7%) and *ATR* (48% vs. 13%). Despite the limited number of mutations associated with DNA repair pathway genes in our cohort, some of the HROC-Xenobank models might yet be interesting for functional analyses in that particular area of research.

In addition, many of our PDX models carry a higher number of mutations with uncertain significance than the original tumors, whereas Abdirahman et al. did not observe such additional mutations in their serially transplanted tumors [32]. Brown et al. suggested that mutations detected in PDX but not in original patient tumor samples could reflect hard to detect low-frequency clones in the original tumors [43].

The data from the German cancer registry ZfKD (Zentrum für Krebsregisterdaten) pointed out that 56% of patients with advanced CRC were male. The mean age among male patients ranged from 67.6 to 68.3 years and among female patients from 70.6 to 71.0 years [44]. The mean age of our study population is 69.7 (range 30 to 98) and thus lies

precisely within the ZfKD ranges. Moreover, the male percentage of our study population is, with 56.8% of patients being male, the same as reported by the ZfKD. Tumor UICC staging was 11% (stage I), 29% (stage II), 27% (stage III), and 33% (stage IV) in our study, compared to 19.5% (stage I), 29% (stage II), 30% (stage III), and 21.5% (stage IV) in the general German CRC population [45]. Thus, the proportion of CRC stage II exactly matches, and the percentage of stage III nearly matches, the general German CRC population. However, CRC stage IV was considerably overrepresented and stage I considerably underrepresented in our study, as compared to the normal distribution of CRC stages in Germany. Partly, this is simply attributable to the fact, that our biobank collection is restricted to cases with sufficient tumor material available upon diagnosis in the pathology; therefore smaller, lower-staged cases frequently must be excluded. Additionally, all cases were collected at a university center, which is typically also biased towards more advanced, higher staged cases by the referring doctors.

The molecular subtype analyses revealed that our HROC-Xenobank cohort represents the common CRC subtypes [28]. However, spMSI-H and LS cases are overrepresented. This can best be explained by the fact that MSI tumors engraft significantly better than MSS tumors. Such a discrepancy in engraftment rates linked to the MS status was also reported for gastric cancer with 55.93% vs. 23.64%; $p < 0.0001$ [29]. This improved biological fitness in the xenograft environment was also highlighted by the fact that these PDX grew out faster, and fewer mice were necessary to generate ample amounts of backups. Our group previously described the molecular subtype ($p = 0.003$), especially the MS status ($p = 0.001$), as a potent parameter likely to influence the success rate of PDX establishment from CRC resection specimens [8]. It is also of relevance, albeit to a lesser extent, that MSI-H PDX tumors were not often highly necrotic and were, thus, rarely excluded from our final cohort due to this undesirable characteristic.

We want to emphasize the fact that the HROC-Xenobank has, already in its establishment phase, supported “standard” in vivo studies [46,47], detailed molecular pathway investigations [48], biomarker studies, and more basic studies which took advantage of snap-frozen samples [49]. A first pre-clinical PDX trial has been started in-house, preceded by a dose finding study [34]. Due to the fact that all samples have been collected exclusively after informed consent of all patients and the irrevocable anonymization of any personal or clinical data, the use of the HROC-Xenobank models is not restricted by the General Data Protection Regulation in the EU.

5. Conclusions

In summary, this study succeeded in generating 125 individual PDX models with sufficient numbers of vital and snap frozen aliquots as well as FFPE material. The preservation of the original tumor’s biological features such as microarchitecture and pathomorphology as intrinsic features of the individual models remain stable for several passages. Moreover, we were able to confirm the high concordance of pathomorphological as well as mutation patterns of the HROC-Xenobank to the underlying clinical case series. This enables the selection of individual models according to desired features and allows future investigations, such as pre-clinical PDX trials and detailed molecular pathway investigations, with well-characterized samples. Notably, the models of the HROC-Xenobank are available upon reasonable request.

Supplementary Materials: The following are available online at <https://www.mdpi.com/article/10.3390/cancers13235882/s1>, Table S1: Patient data and PDX detail, The patient clinical data, including patient information, tumor information, patient treatment information, and PDX model information as well as PDX model validation and sharing and contact, Table S2: Comparison of fresh vs. vitally frozen transfer, Data for the direct comparison of fresh vs. vitally frozen tissues for subsequent passaging, presented for 28 cases listed with the individual time to harvest of each individual case and the calculated mean values, Table S3: Correlation analysis, Data for nonparametric bivariate correlation analysis according to Kendall-Tau and Spearman’s rank correlation coefficient, as well as data of the consequential Fisher exact tests, Table S4: FFPE tissue Comparison PDX vs. primary

tumor, Data of PDX tumors concerning detailed histological investigation and comparison to original patient tumor Table S5: NGS data, The included datasets are derived according to the quality criteria described in materials and methods. Three further datasets of WES data (HROC405Tu, HROC405Met1, and HROC425Tu) failed these quality criteria and are, therefore, not listed. The NGS data include mutations classified as pathogenic or likely pathogenic as well as mutations of uncertain significance. Excluded are all benign mutations as well as mutations classified as risk factor and drug response.

Author Contributions: Conceptualization, S.M. and M.L.; methodology, S.M., F.B. and M.K. (Mathias Krohn); investigation, S.M., F.B., S.K. (Said Kdimati), F.P., N.E. and M.K. (Mathias Krohn); data curation, S.M., B.M., M.R., S.K. (Susann Krake) and M.K. (Michael Kreutzer); writing—original draft preparation, S.M.; writing—review and editing, C.S.M.; writing—review and editing supervision, M.L.; visualization, S.M. and M.K. (Michael Kreutzer); project administration, S.M. and M.L. All authors have read and agreed to the published version of the manuscript.

Funding: This research was, in part, funded by grant number TBI-V-1-241-VBW-084 from the state of Mecklenburg-Vorpommern for the project “Peptide-Based Immunization for Colon- and Pancreas-Carcinoma (PiCoP)”.

Institutional Review Board Statement: The study was conducted according to the guidelines of the Declaration of Helsinki. All procedures were approved by the Ethics Committee of the University of Rostock University Medical Centre (Reference numbers: II HV 43/2004, A 45/2007, A 2018-0054, and A 2019-0187) in accordance with generally accepted guidelines for the use of human material. All animal experiments were performed according to the guidelines of the local animal use and care committee (Landesamt für Landwirtschaft, Lebensmittelsicherheit und Fischerei Mecklenburg-Vorpommern, permit numbers: LALLF M-V/TSD/7221.3-1.1-071/10; 7221.3-1-015/14; and 7221.3-2-020/17).

Informed Consent Statement: Informed consent was obtained from all subjects involved in the study.

Data Availability Statement: The data and materials are available from the corresponding author upon reasonable request.

Acknowledgments: We thank Daniel Wolter and Mohamed Elhensheri (University Medicine Rostock, Department of oral and maxillofacial surgery, Rostock University Medical Center) for their excellent technical assistance.

Conflicts of Interest: The authors declare no conflict of interest.

References

- Oh, B.Y.; Lee, W.Y.; Jung, S.; Hong, H.K.; Nam, D.H.; Park, Y.A.; Huh, J.W.; Yun, S.H.; Kim, H.C.; Chun, H.K.; et al. Correlation between tumor engraftment in patient-derived xenograft models and clinical outcomes in colorectal cancer patients. *Oncotarget* **2015**, *6*, 16059–16068. [[CrossRef](#)] [[PubMed](#)]
- Tentler, J.J.; Tan, A.C.; Weekes, C.D.; Jimeno, A.; Leong, S.; Pitts, T.M.; Arcaroli, J.J.; Messersmith, W.A.; Eckhardt, S.G. Patient-derived tumour xenografts as models for oncology drug development. *Nat. Rev. Clin. Oncol.* **2012**, *9*, 338–350. [[CrossRef](#)]
- Hidalgo, M.; Amant, F.; Biankin, A.V.; Budinská, E.; Byrne, A.T.; Caldas, C.; Clarke, R.B.; De Jong, S.; Jonkers, J.; Mari, G. Europe PMC Funders Group Patient Derived Xenograft Models: An Emerging Platform for Translational Cancer Research. *Cancer Discov.* **2015**, *4*, 998–1013. [[CrossRef](#)]
- Bleijns, M.; Van De Wetering, M.; Clevers, H.; Drost, J. Xenograft and organoid model systems in cancer research. *EMBO J.* **2019**, *38*, e101654. [[CrossRef](#)]
- Yoshida, G.J. Applications of patient-derived tumor xenograft models and tumor organoids. *J. Hematol. Oncol.* **2020**, *13*, 4. [[CrossRef](#)]
- Inoue, A.; Deem, A.K.; Kopetz, S.; Heffernan, T.P.; Draetta, G.F.; Carugo, A. Deem Current and Future Horizons of Patient-Derived Xenograft Models in Colorectal Cancer Translational Research. *Cancers* **2019**, *11*, 1321. [[CrossRef](#)] [[PubMed](#)]
- Medico, E.; Russo, M.; Picco, G.; Cancelliere, C.; Valtorta, E.; Corti, G.; Buscarino, M.; Isella, C.; Lamba, S.E.; Martinoglio, B.; et al. The molecular landscape of colorectal cancer cell lines unveils clinically actionable kinase targets. *Nat. Commun.* **2015**, *6*, 7002. [[CrossRef](#)]
- Mullins, C.S.; Micheel, B.; Matschos, S.; Leuchter, M.; Bürtin, F.; Krohn, M.; Hühns, M.; Klar, E.; Prall, F.; Linnebacher, M. Integrated biobanking and tumor model establishment of human colorectal carcinoma provides excellent tools for preclinical research. *Cancers* **2019**, *11*, 1520. [[CrossRef](#)] [[PubMed](#)]

9. Namekawa, T.; Ikeda, K.; Horie-Inoue, K.; Inoue, S. Application of Prostate Cancer Models for Preclinical Study: Advantages and Limitations of Cell Lines, Patient-Derived Xenografts, and Three-Dimensional Culture of Patient-Derived Cells. *Cells* **2019**, *8*, 74. [[CrossRef](#)] [[PubMed](#)]
10. Nelson, S.; Zhang, C.; Roche, S.; O'Neill, F.; Swan, N.; Luo, Y.; Larkin, A.; Crown, J.; Walsh, N. Modelling of pancreatic cancer biology: Transcriptomic signature for 3D PDX-derived organoids and primary cell line organoid development. *Sci. Rep.* **2020**, *10*, 2778. [[CrossRef](#)] [[PubMed](#)]
11. Dangles-Marie, V.; Pocard, M.; Richon, S.; Weiswald, L.-B.; Assayag, F.; Saulnier, P.; Judde, J.-G.; Janneau, J.-L.; Auger, N.; Validire, P.; et al. Establishment of Human Colon Cancer Cell Lines from Fresh Tumors versus Xenografts: Comparison of Success Rate and Cell Line Features. *Cancer Res.* **2007**, *67*, 398–407. [[CrossRef](#)] [[PubMed](#)]
12. Oberländer, M.; Linnebacher, M.; König, A.; Bogoevska, V.; Brodersen, C.; Kaatz, R.; Krohn, M.; Hackmann, M.; Ingenerf, J.; et al.; On behalf of the ColoNet consortium. The “North German Tumor Bank of Colorectal Cancer”: Status report after the first 2 years of support by the German Cancer Aid Foundation. *Lagenbeck's Arch. Surg.* **2013**, *398*, 251–258. [[CrossRef](#)] [[PubMed](#)]
13. Linnebacher, M.; Maletzki, C.; Ostwald, C.; Klier, U.; Krohn, M.; Klar, E.; Prall, F. Cryopreservation of human colorectal carcinomas prior to xenografting. *BMC Cancer* **2010**, *10*, 362. [[CrossRef](#)] [[PubMed](#)]
14. Bürtin, F.; Matschos, S.; Prall, F.; Mullins, C.S.; Krohn, M.; Linnebacher, M. Creation and maintenance of a living bi-obank-how we do it. *J. Vis. Exp.* **2021**, *2021*, 62065.
15. Prall, F.; Maletzki, C.; Hühns, M.; Krohn, M.; Linnebacher, M. Colorectal carcinoma tumour budding and podia formation in the xenograft microenvironment. *PLoS ONE* **2017**, *12*, e0186271. [[CrossRef](#)]
16. Covarrubias-Pazarán, G.; Diaz-Garcia, L.; Schlautman, B.; Salazar, W.; Zalapa, J. Fragman: An R package for fragment analysis. *BMC Genet.* **2016**, *17*, 62. [[CrossRef](#)] [[PubMed](#)]
17. Prall, F.; Ostwald, C.; Linnebacher, M.; Weirich, V. Chromosomally and microsatellite stable colorectal carcinomas without the CpG island methylator phenotype in a molecular classification. *Int. J. Oncol.* **2009**, *35*, 321–327. [[CrossRef](#)]
18. Ogino, S.; Cantor, M.; Kawasaki, T.; Brahmandam, M.; Kirkner, G.J.; Weisenberger, D.J.; Campan, M.; Laird, P.W.; Loda, M.; Fuchs, C.S. CpG island methylator phenotype (CIMP) of colorectal cancer is best characterised by quantitative DNA methylation analysis and prospective cohort studies. *Gut* **2006**, *55*, 1000–1006. [[CrossRef](#)]
19. Weisenberger, D.J.; Siegmund, K.D.; Campan, M.; Young, J.; Long, T.I.; Faasse, M.A.; Kang, G.H.; Widschwendter, M.; Weener, D.; Buchanan, D.; et al. CpG island methylator phenotype underlies sporadic microsatellite instability and is tightly associated with BRAF mutation in colorectal cancer. *Nat. Genet.* **2006**, *38*, 787–793. [[CrossRef](#)]
20. Lazzari, L.; Corti, G.; Picco, G.; Isella, C.; Montone, M.; Arcella, P.; Durinikova, E.; Zanella, E.R.; Novara, L.; Barbosa, F.; et al. Patient-Derived Xenografts and Matched Cell Lines Identify Pharmacogenomic Vulnerabilities in Colorectal Cancer. *Clin. Cancer Res.* **2019**, *25*, 6243–6259. [[CrossRef](#)]
21. Langmead, B.; Salzberg, S.L. Fast gapped-read alignment with Bowtie 2. *Nat. Methods* **2012**, *9*, 357–359. [[CrossRef](#)] [[PubMed](#)]
22. Li, H.; Handsaker, B.; Wysoker, A.; Fennell, T.; Ruan, J.; Homer, N.; Marth, G.; Abecasis, G.; Durbin, R. Subgroup, 1000 Genome Project Data Processing The Sequence Alignment/Map format and SAMtools. *Bioinformatics* **2009**, *25*, 2078.
23. Broad Institute. Picard Toolkit. Available online: <http://broadinstitute.github.io/picard/> (accessed on 1 September 2020).
24. Kim, S.; Scheffler, K.; Halpern, A.L.; Bekritsky, M.A.; Noh, E.; Källberg, M.; Chen, X.; Kim, Y.; Beyter, D.; Krusche, P.; et al. Strelka2: Fast and accurate calling of germline and somatic variants. *Nat. Methods* **2018**, *15*, 591–594. [[CrossRef](#)] [[PubMed](#)]
25. Danecek, P.; Auton, A.; Abecasis, G.; Albers, C.A.; Banks, E.; DePristo, M.A.; Handsaker, R.E.; Lunter, G.; Marth, G.T.; Sherry, S.T.; et al. The variant call format and VCFtools. *Bioinformatics* **2011**, *27*, 2156–2158. [[CrossRef](#)]
26. Cingolani, P.; Platts, A.; Wang, L.L.; Coon, M.; Nguyen, T.; Wang, L.; Land, S.J.; Lu, X.; Ruden, D.M. A program for annotating and predicting the effects of single nucleotide polymorphisms, SnpEff: SNPs in the genome of *Drosophila melanogaster* strain w1118; iso-2; iso-3. *Fly* **2012**, *6*, 80–92. [[CrossRef](#)]
27. Meehan, T.F.; Conte, N.; Goldstein, T.C.; Inghirami, G.; Murakami, M.A.; Brabetz, S.; Gu, Z.; Wisner, J.A.; Dunn, P.; Begley, D.A.; et al. PDX-MI: Minimal Information for Patient-Derived Tumor Xenograft Models. *Cancer Res.* **2017**, *77*, e62–e66. [[CrossRef](#)] [[PubMed](#)]
28. Wang, W.; Kandimalla, R.; Huang, H.; Zhu, L.; Li, Y.; Gao, F.; Goel, A.; Wang, X. Molecular subtyping of colorectal cancer: Recent progress, new challenges and emerging opportunities. *Semin. Cancer Biol.* **2018**, *55*, 37–52. [[CrossRef](#)]
29. Corso, S.; Isella, C.; Bellomo, S.E.; Apicella, M.; Durando, S.; Migliore, C.; Ughetto, S.; D'Errico, L.; Menegon, S.; Rull, D.M.; et al. A Comprehensive PDX Gastric Cancer Collection Captures Cancer Cell-Intrinsic Transcriptional MSI Traits. *Cancer Res.* **2019**, *79*, 5884–5896. [[CrossRef](#)]
30. Maletzki, C.; Gock, M.; Randow, M.; Klar, E.; Huehns, M.; Prall, F.; Linnebacher, M. Establishment and characterization of cell lines from chromosomal instable colorectal cancer. *World J. Gastroenterol.* **2015**, *21*, 164–176. [[CrossRef](#)]
31. Mattar, M.; McCarthy, C.; Kulick, A.R.; Qeriqi, B.; Guzman, S.; De Stanchina, E. Establishing and Maintaining an Extensive Library of Patient-Derived Xenograft Models. *Front. Oncol.* **2018**, *8*, 19. [[CrossRef](#)]
32. Abdirahman, S.M.; Christie, M.; Preaudet, A.; Burstroem, M.C.U.; Mouradov, D.; Lee, B.; Sieber, O.M.; Putoczki, T.L. A biobank of colorectal cancer patient-derived xenografts. *Cancers* **2020**, *12*, 2340. [[CrossRef](#)]
33. Houghton, J.A.; Taylor, D.M. Growth characteristics of human colorectal tumours during serial passage in immune-deprived mice. *Br. J. Cancer* **1978**, *37*, 213.

34. Maletzki, C.; Bock, S.; Fruh, P.; Macius, K.; Witt, A.; Prall, F.; Linnebacher, M. NSG mice as hosts for oncological precision medicine. *Lab. Investig.* **2019**, *100*, 27–37. [CrossRef]
35. Tillman, H.; Janke, L.J.; Funk, A.; Vogel, P.; Rehg, J.E. Morphologic and Immunohistochemical Characterization of Spontaneous Lymphoma/Leukemia in NSG Mice. *Veter. Pathol.* **2019**, *57*, 160–171. [CrossRef]
36. Bondarenko, G.; Ugolkov, A.; Rohan, S.; Kulesza, P.; Dubrovskiy, O.; Gursel, D.; Mathews, J.; O'Halloran, T.V.; Wei, J.J.; Mazar, A.P. Patient-Derived Tumor Xenografts Are Susceptible to Formation of Human Lymphocytic Tumors. *Neoplasia* **2015**, *17*, 735–741. [CrossRef]
37. Chateau-Joubert, S.; Hopfe, M.; Richon, S.; Decaudin, D.; Roman-Roman, S.; Reyes-Gomez, E.; Bieche, I.; Nemati, F.; Dangles-Marie, V. Spontaneous mouse lymphoma in patient-derived tumor xenografts: The importance of systematic analysis of xenografted human tumor tissues in preclinical efficacy trials. *Transl. Oncol.* **2021**, *14*, 101133. [CrossRef] [PubMed]
38. Woo, X.Y.; Giordano, J.; Srivastava, A.; Zhao, Z.-M.; Lloyd, M.W.; de Bruijn, R.; Suh, Y.-S.; Patidar, R.; Chen, L.; Scherer, S.; et al. Conservation of copy number profiles during engraftment and passaging of patient-derived cancer xenografts. *Nat. Genet.* **2021**, *53*, 86.
39. Rizzo, G.; Bertotti, A.; Leto, S.M.; Vetrano, S. Patient-derived tumor models: A more suitable tool for pre-clinical studies in colorectal cancer. *J. Exp. Clin. Cancer Res.* **2021**, *40*, 178. [CrossRef] [PubMed]
40. cBioPortal for Cancer Genomics. Available online: http://www.cbioportal.org/study/summary?id=coadread_tcga_pan_can_atlas_2018 (accessed on 7 October 2021).
41. Lee, C.S.; Song, I.H.; Lee, A.; Kang, J.; Lee, Y.S.; Lee, I.K.; Song, Y.S.; Lee, S.H. Enhancing the landscape of colorectal cancer using targeted deep sequencing. *Sci. Rep.* **2021**, *11*, 8154. [CrossRef] [PubMed]
42. Burgenske, D.M.; Monsma, D.J.; Dylewski, D.; Scott, S.B.; Sayfie, A.D.; Kim, D.G.; Luchtefeld, M.; Martin, K.; Stephenson, P.; Hostetter, G.; et al. Establishment of genetically diverse patient-derived xenografts of colorectal cancer. *Am. J. Cancer Res.* **2014**, *4*, 824–837. [PubMed]
43. Brown, K.M.; Xue, A.; Mittal, A.; Samra, J.S.; Smith, R.; Hugh, T.J. Patient-derived xenograft models of colorectal cancer in pre-clinical research: A systematic review. *Oncotarget* **2016**, *7*, 66212–66225. [CrossRef]
44. Oppelt, K.A.; Luttmann, S.; Kraywinkel, K.; Haug, U. Incidence of advanced colorectal cancer in Germany: Comparing claims data and cancer registry data. *BMC Med Res. Methodol.* **2019**, *19*, 142. [CrossRef] [PubMed]
45. Robert Koch Institut. Krebs in Deutschland 2015/2016. 2015. Available online: https://www.krebsdaten.de/Krebs/DE/Content/Publikationen/Krebs_in_Deutschland/kid_2019/krebs_in_deutschland_2019.pdf?__blob=publicationFile (accessed on 5 October 2021).
46. Shang, Y.; Zhang, X.; Lu, L.; Jiang, K.; Krohn, M.; Matschos, S.; Mullins, C.S.; Vollmar, B.; Zechner, D.; Gong, P.; et al. Pharmaceutical immunoglobulin G impairs anti-carcinoma activity of oxaliplatin in colon cancer cells. *Br. J. Cancer* **2021**, *124*, 1411–1420. [CrossRef] [PubMed]
47. Nörz, D.; Mullins, C.S.; Smit, D.J.; Linnebacher, M.; Hagel, G.; Mirdogan, A.; Siekiera, J.; Ehm, P.; Izbicki, J.R.; Block, A.; et al. Combined Targeting of AKT and mTOR Synergistically Inhibits Formation of Primary Colorectal Carcinoma Tumouroids In Vitro: A 3D Tumour Model for Pre-therapeutic Drug Screening. *Anticancer. Res.* **2021**, *41*, 2257–2275. [CrossRef]
48. Marx, C.; Sonnemann, J.; Beyer, M.; Maddocks, O.D.K.; Lilla, S.; Hauzenberger, I.; Pié-Staffa, A.; Siniuk, K.; Nunna, S.; Marx-Blümel, L.; et al. Mechanistic insights into p53-regulated cytotoxicity of combined entinostat and irinotecan against colorectal cancer cells. *Mol. Oncol.* **2021**. [CrossRef] [PubMed]
49. Bock, S.; Mullins, C.S.; Klar, E.; Pérot, P.; Maletzki, C.; Linnebacher, M. Murine Endogenous Retroviruses Are Detectable in Patient-Derived Xenografts but Not in Patient-Individual Cell Lines of Human Colorectal Cancer. *Front. Microbiol.* **2018**, *9*, 789. [CrossRef]



NSG mice as hosts for oncological precision medicine

Claudia Maletzki¹ · Stephanie Bock² · Philipp Fruh² · Karolis Macius² · Anika Witt² · Friedrich Prall³ · Michael Linnebacher²

Received: 4 February 2019 / Revised: 14 June 2019 / Accepted: 14 June 2019 / Published online: 13 August 2019
© United States & Canadian Academy of Pathology 2019

Abstract

Patient-derived xenograft (PDX) models have been rediscovered as meaningful research tool. By using severely immunodeficient mice, high-engraftment rates can be theoretically achieved, permitting clinical stratification strategies. Apart from engraftment efficacy, tolerability towards certain cytostatic drugs varies among individual mouse strains thus impeding large-scale screenings. Here, we aimed at optimizing an in vivo treatment schedule using the widely applied cytostatic drug 5-fluoruracil (5-FU) for exemplary response prediction in colorectal cancer (CRC) PDX models. Four different individual CRC PDX models were engrafted into NOD.Cg-Prkdc^{scid}I2rg^{tm1Wjl} (NSG) mice. Mice with established PDX were allocated to different treatment groups, receiving 5-FU, the oral prodrug Capecitabine, or 5-FU/leucovorin (LV) at different doses. Body weight, tumor size, and general behavior were assessed during therapy. Ex vivo analyses were done from blood samples, liver, as well as tumor resection specimen. Engraftment efficacy was high as expected in NSG mice, yielding stable PDX growth for therapy stratification. However, overall tolerability towards 5-FU was unexpectedly low, whereas the prodrug Capecitabine as well as the combination of 5-FU/LV at low doses were well tolerated. Accompanying plasma level determination of DYPD, the rate-limiting enzyme for 5-FU-mediated toxicity, revealed reduced activity in NSG mice compared with other common laboratory mouse strains, offering a likely explanation for the drug incompatibility. Also, the *De Ritis quotient* was highly elevated in treated mice, reflecting overall organ injury even at low doses. Summarizing these findings, NSG mice are ideal hosts for in vivo engraftment studies. However, the complex immunodeficiency reduces tolerance to certain drugs, thus making those mice especially sensitive. Consequently, such dose finding and tolerance tests constitute a necessity for similar cancer precision medicine approaches.

Introduction

Patient-derived xenograft (PDX) models have significantly improved basic and translational research. Direct xenografting of human cancerous tissue allows faithful resemblance of the patients' tumors with regard to histopathology, tumor microenvironment, gene expression, mutational status, and inflammation [1]. Also, high-throughput screening can be done to assess bioavailability, pharmacokinetic, and

toxicity profile of clinically approved drugs/combinations and—even more important—novel drugs [2, 3].

Prior to performing in vivo drug response studies, selection of an appropriate immunodeficient mouse strain is recommended [4]. Several strains are available, with competing advantages and limitations when considering the rational design of therapy [1]. Athymic Foxn1^{nu} mice constitute the “classical” hosts enabling simple injection or implantation of foreign tumor material due to acoma and ease of handling. T cell deficiency enables engraftment with varying efficacy. In addition to the type and quality of the tumor used for xenografting, remnant immune function provides an obstacle, often resulting in poor engraftment efficiency. SCID (severe combined immunodeficiency), NOD-SCID (Nonobese diabetic-SCID), and recombination-activating gene 2 (Rag2)-knockout mice are other commonly used strains; albeit still primarily used to create xenografts using human cancer cell lines.

Primary patient-derived tumors require higher immunodeficiency levels for good engraftment rates, avoiding

✉ Michael Linnebacher
michael.linnebacher@med.uni-rostock.de

¹ Department of Medicine, Clinic III-Hematology/Oncology/
Palliative Care Rostock, Rostock, Germany

² Molecular Oncology and Immunotherapy; Department of General
Surgery, Rostock, Germany

³ Institute of Pathology, University Medical Centre, 18057
Rostock, Germany

xenograft rejection as well as enabling sufficient PDX growth kinetics for subsequent therapy trials. NOD.Cg-Prkdc^{scid}Il2rg^{tm1}Wjl (NSG) mice lack T, B, functional NK cells as well as both alleles of the IL2 receptor common gamma chain, thus lacking cytokine signaling through multiple receptors. NSG mice were described to be lymphoma-resistant, providing a major advantage compared with other immunodeficient mouse strains, in which spontaneous lymphomagenesis is frequent [5, 6]. The severe immunodeficiency of NSG mice additionally allows successful humanization using human CD34⁺ hematopoietic stem cells, peripheral blood mononuclear cells or adult stem cells; and tumor tissues engraft to high frequencies [7, 8]. Hence, NSG is currently the only available mouse strain in which reconstitution of the human immune system, including functional T cell responses has been described. While creating an environment that guarantees full compatibility between the graft and the host, clinical responses to novel (immuno-) therapeutic interventions can be monitored. This is likely to be realized when malignant and immune cells are used from the same donor [9].

NSG mice principally meet all requirements for research addressing immune function, infectious disease, diabetes, stem cell biology, and oncology. The latter is an increasingly growing research field inspired by deeper knowledge of tumor biology and molecular pathology. PDX may guide the way to precision medicine shortly, i.e., “the right drug, for the right patient, at the right time” [6].

The first-line cytostatic agent for adjuvant treatment of colorectal cancer (CRC) patients is the antimetabolite 5-fluoruracil (5-FU), applied as single substance, its inactive prodrug Capecitabine or in combination with other cytostatics, such as oxaliplatin and irinotecan [10]. Upon application, 5-FU is metabolized intracellularly to several active metabolites (fluorodeoxyuridine monophosphate, fluorodeoxyuridine triphosphate, and fluorouridine triphosphate). These exert anticancer effects via two main mechanisms: (I) inhibition of thymidylate synthase (TYMS) and (II) incorporation into RNA and DNA. However, 5-FU response rates vary owing to the tumors’ molecular heterogeneity and (still) poorly defined mechanisms of drug efficacy and resistance [11, 12].

Given these facts, a comprehensive in vivo study to accurately predict 5-FU response is indicated. This challenging question may be best answered in a PDX clinical trial (PCT), with a “one animal per model per treatment” experimental design [13]. The predictive value of such a trial is reliant on high-engraftment efficacy and tumor outgrowth within an appropriate time. NSG mice are thus the favored host. Prior to performing such a PCT, determining the best dose and treatment schedule with tolerable side effects and an optimal response is desirable. Hence, we here aimed to optimize in vivo doses of 5-FU in NSG mice

harboring CRC PDX of different molecular subtypes to reflect the clinical situation at best.

Methods

Human cell lines and treatment schedule

The patient-derived CRC cell lines HROC24, HROC370 (both microsatellite instable; MSI), HROC40, HROC43 (both CpG island methylation phenotype; CIMP), HROC46 T0 M1, and HROC222 T1 M2 (both chromosomal instable; CIN) were established in our lab directly from patient material or after in vivo xenografting (nomenclature: HRO—Hansestadt Rostock; C—Colon; T—transfer; M—mouse; Table 1). Analyses were done on passages <40. Cells were maintained in complete medium: DMEM/F12 supplemented with 10% fetal calf serum, glutamine (2 mmol/l), and antibiotics (PAN-Biotech GmbH, Aidenbach, Germany). Cells were seeded in 96-well plates at a density of 1×10^4 cells/well and allowed to adhere overnight. Thereafter, cells were treated with increasing 5-FU doses for two 72 h cycles. IC₅₀ values were calculated upon crystal violet staining from at least three independent experiments in comparison to untreated controls.

Mice and tumor xenografting

Experiments were performed on female and male 6–8-week-old NSG mice ($n = 40$) weighting 16–25 g. Mice were bred in the animal facility of the Rostock University Medical Center and maintained in specified pathogen-free conditions. Animals were exposed to 12 h light/12 h darkness cycles and standard pellet food and water ad libitum. All experiments were performed according to the guidelines of the local animal use and care committee, also approving this study (Landesamt für Landwirtschaft, Lebensmittelsicherheit und Fischerei Mecklenburg-Vorpommern, permit number: LALLF M-V/TSD/7221.3-1-005/17). Tumor pieces were obtained from previously xenografted patients’ tumors and subsequent cryopreservation as described [14]. Detailed information on the patients’ tumors as well as clinicopathological information is given in Table 1. PDX in passage <5 were used to retain tumor microenvironment and thus warrant reliability of results. PDX were implanted subcutaneously into the animals’ right flank under anesthesia (ketamine/xylazine, 90/6 mg/kg bw). Tumor specimens (3 × 3 × 3 mm) were soaked in 100 μL Matrigel (Corning, Kaiserslautern, Germany) for >10 min at 4 °C prior to xenografting. Tumor growth was regularly monitored and therapy was initiated upon tumor establishment (~6 mm diameter).

Table 1 Clinicopathological characteristics as well as patients' follow-up information

Lab ID	Sex/age	Tumor type	Localization	TNM classification								UICC	Molecular subtype	Adjuvant therapy	Outcome	
				T	N	Lk (n)		M	G	R	L					V
				+ Σ												
29	M/59	Adenocarcinoma	Hepatic (right) flexure	T3	N2	8	30	M1	G3	R0	L0	V1	IVa	Lynch syndrome	None	59 years [†]
40	M/69	Adenocarcinoma	Descending	T3	N1	2	18	M0	G3	R0	L1	V1	IIIb	CIMP-H	5-FU	Alive
46	M/65	Adenocarcinoma	Ascending	T3	N0	0	34	M1	G3	R2	L0	V1	IVa	spCIN	Capecitabine	67 years [†]
222	M/79	Adenocarcinoma	Transverse	T3	N0	0	13	M0	G2	R0	L0	V0	Ila	spCIN	None	Alive

CIMP-H CpG island methylator phenotype high, *spCIN* sporadic chromosomal instable, † indicated dead

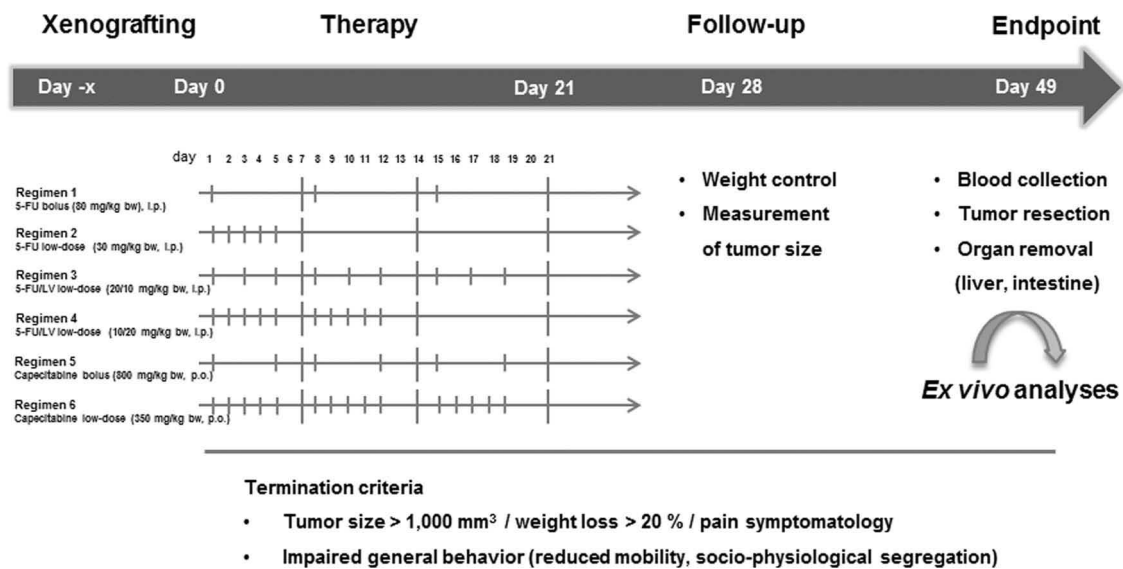


Fig. 1 Schedule of the experimental treatment protocol for dose optimization in vivo. NSG mice were implanted tumor tissue from individual CRC xenografts (size: 3 × 3 × 3 mm, soaked in matrigel). Upon tumor establishment (~6mm), mice were divided into six treatment arms as shown (injection intervals are indicated by short vertical lines, long lines indicate weeks). Each group consisted of two mice.

Follow-up was done by weekly weight control as well as tumor growth monitoring. The experimental endpoint was defined by excessive tumor growth (>1000 mm³) or impaired general behavior as stated in the figure. Ex vivo analyses were done as stated in material and methods

Treatment groups

Upon tumor establishment, mice were randomized into the following therapy groups with two animals/group (Fig. 1): (1) 5-FU bolus (80 mg/kg bw, intraperitoneal (i.p.), weekly, three times in total); (2) 5-FU low-dose (30 mg/kg bw, i.p. daily, five times in total); (3) 5-FU/leucovorin (LV) low-dose (20/10 mg/kg bw, i.p. thrice weekly, nine times in total); (4) 5-FU/LV low-dose (10/20 mg/kg bw, i.p. five times weekly, ten times in total); (5) Capecitabine bolus (800 mg/kg bw, peroral (p.o.), biweekly, six times in total); and (6) Capecitabine low-dose (350 mg/kg bw, p.o., five times weekly, 15 times in total). All mice received daily prepared soaked food during the experiments. Tumor growth and body weight were determined thrice weekly, to

monitor any treatment-related toxicity. Mice were sacrificed after therapy completion, when they became moribund (weight loss >20% vs. start of therapy), when they exhibit impaired socio-physiological behavior, or when tumor sizes reached >1000 mm³. Blood samples as well as tumor tissues, liver, kidney, small, and large intestine were resected for further studies.

Dihydropyrimidine dehydrogenase (DYPD) ELISA

DYPD plasma levels were examined in untreated NSG mice ($n = 9$) and after therapy ($n = 2$). For comparison, plasma samples from wildtype C57Bl/6 J and Foxn1^{nu} mice ($n = 3$ and 2, respectively) were also included into this analysis. DYPD levels were determined using a classical sandwich

Table 2 In vitro drug response analysis on selected patient-derived cell lines and comparison with in vivo growth pattern

Molecular subtype	Cell line	IC ₅₀ 5-FU [μM]	Tumorigenic potential in vivo	Time of tumor outgrowth [d]	In vivo response
spMSI	HROC24	8	✓	23.0	Moderate ^a
	HROC370	4	✓	42.5	N.a.
spCIN	HROC46 T0 M1	8	✓	40.7	Moderate
	HROC222 T1 M2	18	✓	45.0	None
CIMP-H	HROC40	22	✓	50.6	Moderate
	HROC43	7	N.a.	N.a.	N.a.

5-FU sensitivity: high (italics)—low (bold)

spMSI sporadic microsatellite instable, *spCIN* sporadic chromosomal instable, *CIMP-H* CpG island methylator phenotype high

^a[16]

ELISA according to the manufacturers' instructions (Abbexa, Cambridge, UK).

Serum parameters

Blood samples were taken for spectrophotometric determination of plasma alanine aminotransferase (ALAT) and aspartate aminotransferase (ASAT) activities. Then, the *De Ritis quotient* was calculated by using the following formula: $\frac{ASAT}{ALAT}$ [15].

Histopathology

Immediately upon explantation, one half of the subcutaneous PDX tumor nodules was fixed in formalin and embedded in paraffin by routine procedures. H&E-stained sections (4 μm) were taken for light-microscopic study. Sections were assessed for morphologic features of therapy-induced tumor regression, namely necrosis, stromal fibrosis, and dystrophic calcifications.

Statistics

Statistical evaluation was performed using GraphPad PRISM software, version 5.02. Values are reported as the mean ± SD. After proving the assumption of normality (*D'Agostino & Pearson omnibus normality test*), multiple comparisons were done by using one way ANOVA on ranks (Bonferroni's Multiple Comparison Test). The criterion for significance was taken to be $p < 0.05$.

Results

In vitro drug response analysis

5-FU responsiveness was first determined in vitro on a panel of patient-derived low-passage CRC cell lines. They

were exposed to increasing drug concentrations (range: 0.49 μM–7.69 mM). Read out was done after two 72 h treatment rounds using crystal violet staining and IC₅₀ value determination.

The response profile was quite individual among cells (Table 2), nicely reflecting the heterogeneous clinical response towards 5-FU. Still, in vivo analysis is advisable for validation.

To prove 5-FU sensitivity in preclinical PDX models, four individual CRC cases were used which cover the percentual distribution of the CRC molecular subtypes, i.e., two cases from CIN tumors (HROC46 and HROC222), and one each with CIMP (HROC40) and MSI (HROC29) phenotype. Additional selection criteria were tumorigenic potential in vivo and tumor outgrowth within a reasonable time (Table 2).

In vivo dose-finding study

NSG mice carrying PDX from different CRC cases were initially treated with 30 mg/kg bw 5-FU (i.p. thrice weekly, nine times in total; $n = 4$ cases). Though tumor growth inhibition up to shrinkage was evident and thus largely confirmed in vitro findings, this dose was toxic to mice with unexpected death occurring in 4/4 PDX cases. Reducing 5-FU dose to 20 mg/kg bw, as described recently in another in vivo trial on 5-FU response towards HROC-PDX in NMRI Foxn1^{nu} mice (namely HROC24), prevented toxicity [16]. However, dose-reduction abrogated therapeutic effects of 5-FU, with tumor growth curves similar to control mice (*data not shown*). Consequently, we decided to systematically determine and thus optimize the 5-FU regimen to be used for subsequent studies in the NSG strain. More precisely, the best tolerated regimen(s) out of six different 5-FU applications with optimal therapeutic effects had to be identified. Mice with established PDX ($n = 4$ individual PDX models, namely HROC29, HROC40, HROC46, and HROC222, $n = 2$

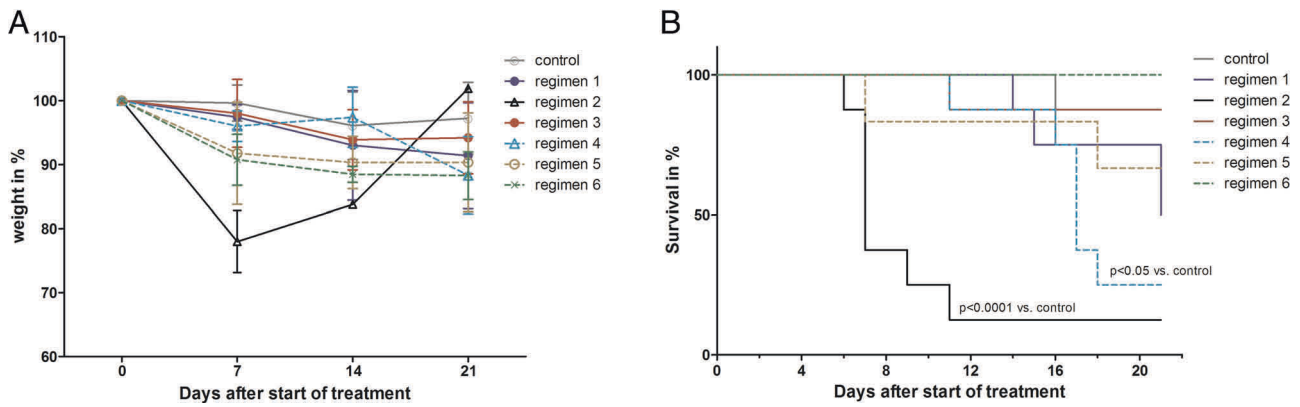


Fig. 2 Weight curve and survival analysis. **a** Body weight was checked thrice weekly and identified weight loss predominantly in the early phase of treatment, with recovery in most cases. Values are given as % weight vs. day 0 ± SD; *n* = 8 mice per regimen, *n* = 1 control mouse/individual PDX case. **b** Kaplan–Meier survival curve analysis revealed changes between individual treatments, with highest treatment-related

toxicity in regimen 2 independent of PDX case. *n* = 8 mice per regimen, *n* = 1 control mouse/individual PDX case. Significant differences between treatment and control mice are as follows: *p* < 0.05 regimen 4 vs. control; *p* < 0.0001 regimen 2 vs. control. One way ANOVA on ranks (Bonferroni’s Multiple Comparison Test)

Table 3 Therapy-related and unexpected death in dose-optimization trial

Regimen	Deceased %		Median time of death [d]
	Treatment-related	Unexpected	
1	25.0	0.0	14
2	75	0.0	7
3	12.5	0	11
4	0.0	0.0	–
5	12.5	25	3
6	0.0	12.5	1.0

mice/group) were randomized into the six treatment groups (see Fig. 1 for details).

All treatment regimens were accompanied by transient weight loss (Fig. 2a), ruffling of fur and differing degree of diarrhea. Regimen 1 (5-FU bolus injection) exhibited low toxicity with 75% of mice surviving this therapy (Table 3 and Fig. 2b). Weight loss predominantly occurred 3–4 days after injection, with mice recovering afterwards (Fig. 2a). Regimen 2 (low-dose 5-FU) severely impaired state of health contributing to massive weight loss of affected mice (day 7: –23% vs. day 0). As a result, most mice died because of 5-FU-mediated toxicity within 1 week of treatment (Table 3 and Fig. 2b). The overall survival was only 25%. By contrast, the mice’ general condition was not considerably impaired after treatment with 5-FU/LV (regimens 3 and 4) or Capecitabine (regimens 5 and 6), which was found to be favorable with regard to their side effects profile. In this latter regimen, weight changes were mainly seen at later time points (days 11–16), but persisted until the end of therapy (~10% vs. day 0) (Fig. 2a). 5-FU/LV

affected weight pattern only marginally, especially when given in low dose (regimen 4).

In vivo drug response

The in vivo drug response is shown in Fig. 3. Tumor sizes are standardized and given in percent of the respective control of each individual PDX case. The different toxicity profiles of the regimens were accompanied by individual treatment responses. Drug responses varied between regimens and PDX models from different molecular classes.

In detail, regimen 1 decelerated tumor growth the entire observation period in 3/4 cases (HROC29, HROC40, and HROC46) compared with the respective control groups (*p* < 0.05 vs. HROC222; Fig. 3). Due to differences in treatment response in the PDX model HROC40, tumor growth curves of this particular PDX are illustrated separately (Fig. 4a, tumor size as determined with a caliper).

In case of HROC222, no treatment response was observed at all; nicely confirming in vitro data (see Table 2). Regimen 2 impaired tumor growth in the two PDX models HROC40 and HROC46, but was accompanied by massive toxicity (*p* < 0.05 vs. HROC222; Fig. 2b). Tumor growth of all individual PDX models was marginally affected by regimen 3 and no treatment response was seen in regimen 4 (Fig. 3). We even observed a tendency towards an accelerated tumor growth (HROC40 at the beginning, HROC222 at later time points) in this particular treatment group. Regimens 5 and 6 slightly delayed tumor growth, with, however, individual differences.

By histological study, an effect of the various chemotherapeutic treatments was not seen in any of the PDX. Representative pictures taken from a control and 5-FU

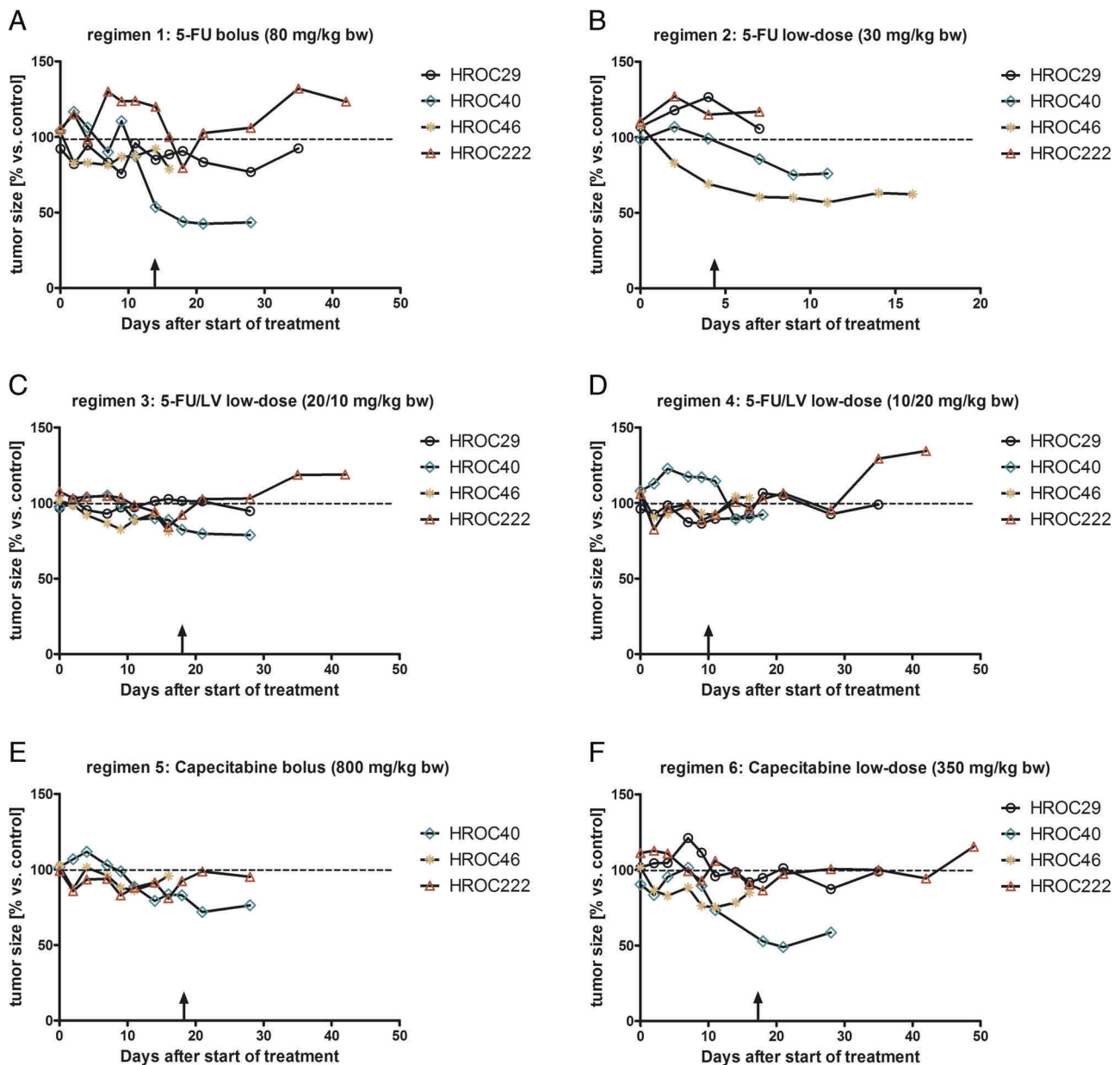


Fig. 3 Tumor growth curve. NSG mice with established PDX were treated as described in “Material and methods” section. Tumor size was measured thrice weekly using a caliper. Growth curves for each PDX case (namely HROC29, HROC40, HROC46, and HROC222) and treatment regimen is shown. Arrows indicate end of treatment. Values are given as % tumor size vs. tumor size of the corresponding control mouse (=untreated, set to be 100%); $n = 8$ mice per regimen,

$n = 1$ control mouse/individual PDX case. Significant differences between individual PDX cases of each regimen include: regimen 1: $p < 0.05$ HROC222 vs. HROC29, HROC40, and HROC46; regimen 2/3: $p < 0.05$ HROC222 vs. HROC40 and HROC46; regimen 6: $p < 0.05$ HROC222 vs. HROC40 and HROC46; $p < 0.05$ HROC29 vs. HROC40 and HROC46; One way ANOVA on ranks (Bonferroni’s Multiple Comparison Test)

treated PDX (case HROC40, regimen 6) are shown in Fig. 4b.

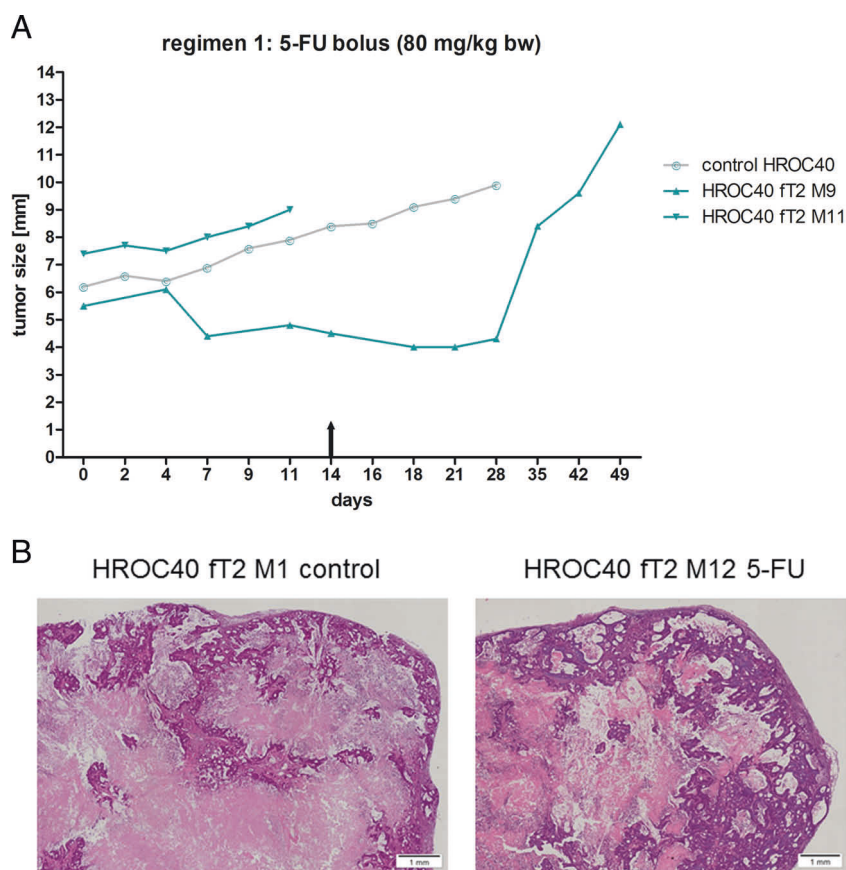
DYPD level and hematological changes upon therapy

Myelosuppression is a common side effect of 5-FU treatment, characterized by leukopenia and thrombocytopenia.

In this study, blood counts revealed only marginal hematological changes upon therapy. This was independent from the applied treatment regimen (*data not shown*) and most likely due to the complex immunodeficiency of NSG mice.

DYPD is the rate-limiting enzyme for pyrimidine base degradation and plays a pivotal role in 5-FU metabolism. Reduced DYPD activity due to gene polymorphism leads to severe toxicity following 5-FU injection in patients and

Fig. 4 a HROC40 PDX showing heterogeneous growth kinetic (slow vs. fast) within two mice and also different drug response. **b** Microscopic image of PDX HROC40. (Left) Control and (right) after 5-FU treatment. Note: Neoplastic gland invading the subcutaneous fat. However, just as in all other PDX, treatment effects were not observed



obliges individualized administration schemes [17]. Hence, we examined whether DYPD deficiency or low-expression level could explain the observed *in vivo* toxicity of high-dose 5-FU applications in NSG mice. By examining DYPD plasma levels using a classical ELISA assay in different standard laboratory mouse strains (NSG, C57Bl/6J, and NMRI Foxn1^{nu}), variances became obvious (Fig. 5a). DYPD levels were significantly lower in NSG mice than in NMRI Foxn1^{nu} mice ($p < 0.01$). Of note, we even identified additional reduction of the DYPD levels upon treatment, providing a likely explanation for the observed toxicity in NSG mice (Fig. 5a).

Analysis of plasma ALAT activities demonstrated no considerable differences between individual treatment groups as well as normal control values (Fig. 5b). However, ASAT activities were elevated in all treatment arms, with highest values observed in regimens 5 and 6 (Fig. 5c). Accordingly, the *De Ritis quotient* was highest in these two groups, reflecting overall organ injury upon treatment (Fig. 5d).

Discussion

Viability and sterility of tumor tissue are principal determinants for successful *in vivo* engraftment. Depending on

the tumor origin (solid vs. hematological; primary vs. metastasis) and the mouse model used for engraftment, tumor take rates differ. Engraftment efficacy for CRC ranges between ~70% in NMRI Foxn1^{nu} mice and ~80% in NSG mice [14] (*and own unpublished data*), providing a rationale for preferential use of NSG mice as hosts. Our lab possesses a huge collection of low-passage patient-derived CRC models to generate PDX from all currently known molecular subtypes [14, 16, 18–21]. Besides, this unique collection paves the way for a PCT to test candidate agents, helping to select effective treatments in a minimized number of animals [13]. The predictive value of preclinical trials in terms of clinical response is well-documented in literature [6, 22]. Different mouse strains were either engrafted with established cell lines (such as HCT116 or HT-29 for CRC) or with PDX for response prediction. Though not systematically addressed in literature, there is evidence of differential tolerability among individual mouse strains towards certain cytostatic drugs [23–25].

Thus, we here aimed to establish an effective treatment schedule with acceptable toxicity in NSG mice. 5-FU was chosen for drug response analysis on a basis of: (I) the broad clinical use for adjuvant and palliative therapy of different tumor entities, among them CRC; (II) the low level of side effects in clinical application, especially when given

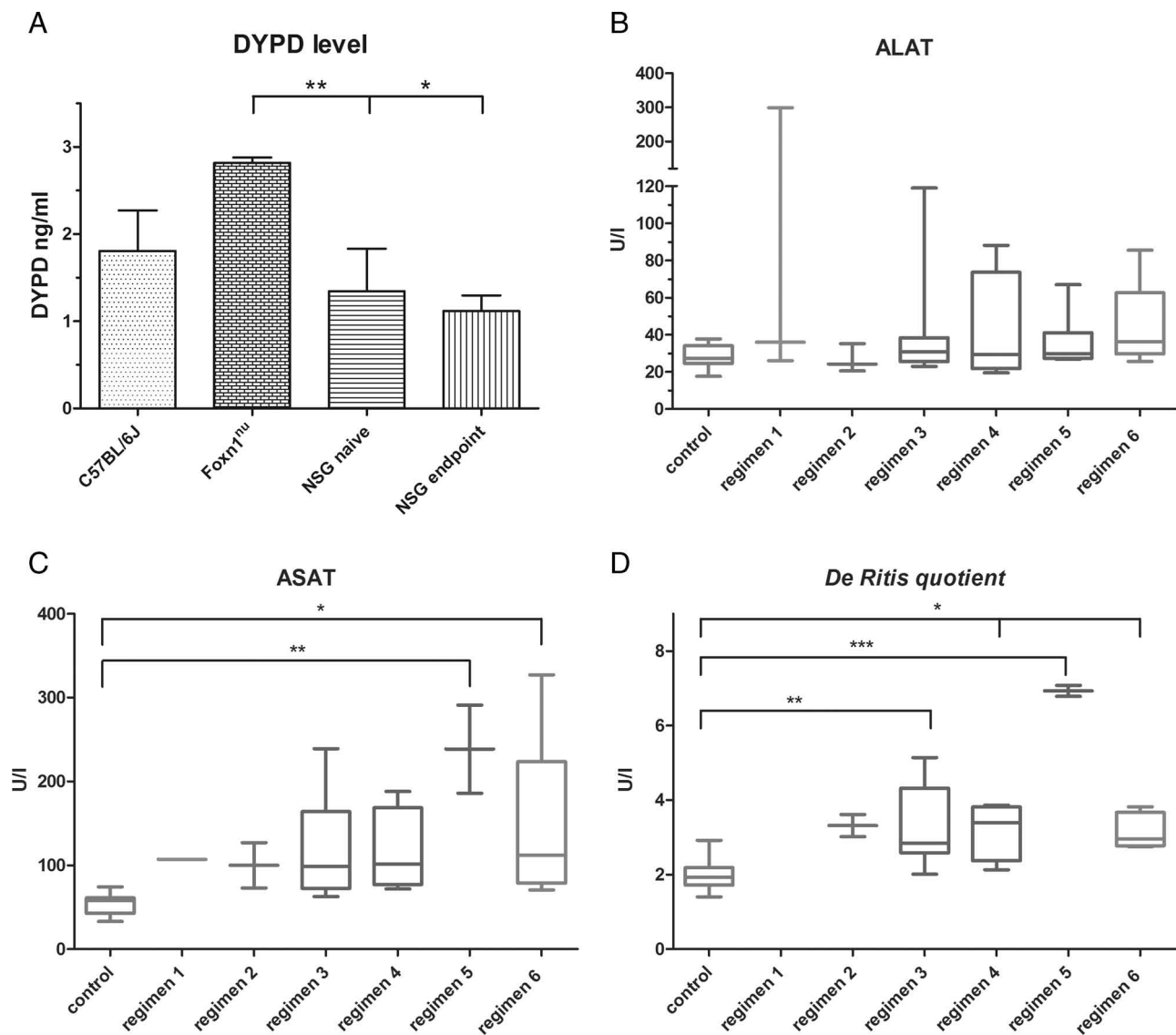


Fig. 5 In vivo and ex vivo analyses. **a** Basal plasma DYPD level revealed different between individual standard laboratory mouse strains. Values are given as mean \pm SD. * p < 0.05 Foxn1^{nu} vs. NSG endpoint; ** p < 0.01 Foxn1^{nu} vs. NSG naive; one way ANOVA on ranks. NSG mice (n = 9) and after therapy (n = 2). Plasma samples from wildtype C57BL/6J and Foxn1^{nu} mice result from n = 3 and 2 mice, respectively. **b–d** Plasma activity of liver enzymes **b** ASAT and **c** ALAT as well as the resulting **d** *De Ritis quotient* showing liver

injury upon therapy. Single measurement was done with plasma of n = 1–7 mice/regimen. n = 12 control mice. Values of are given as mean \pm SD. Significant differences between individual regimens in comparison to controls are displayed in the graph. **b** * p < 0.05 regimen 6 vs. control and regimen 4 vs. control; ** p < 0.01 regimen 3 vs. control; **d** *** p < 0.0001 regimen 5 vs. control. One way ANOVA on ranks (Bonferroni's Multiple Comparison Test)

as oral prodrug (=Capecitabine); and (III) synergism with other drugs (e.g., Irinotecan or Oxaliplatin) in combination regimens. 5-FU dose adjustment was done in compliance with guidelines for phase I clinical trials. Six different treatment regimens were applied.

Previous studies with NMRI Foxn1^{nu} mice already described gradual weight loss as well as slight myelosuppression and gastrointestinal toxicity as most commonly seen 5-FU side effects [23–26]. Still, the heterogeneity in terms of (I) used mouse strains (NMRI Foxn1^{nu} mice vs.

NSG mice); (II) tumor models (ectopic vs. orthotopic and syngeneic vs. xenograft); (III) the choice of treatment; and (IV) the chosen therapeutic regimen (weekly vs. daily, local vs. systemic application) hampers comparability of these previous studies. In our study, drug response and toxicity were quite heterogeneous, with an unexpectedly low tolerability towards half of the applied regimens.

Germline polymorphisms and resulting differences in terms of pharmacology between individual mouse strains may at least partly explain 5-FU-related toxicity. In men,

polymorphisms in the 5-FU converting enzyme DYPD are associated with reduced enzymatic activity or complete deficiency, present in ~3–5% of the general population [27]. It even constitutes a contraindication for 5-FU-based therapy due to the risk of potentially life-threatening toxicity, such as bone marrow suppression and neurotoxicity [27–30]. In mice, basal DYPD plasma levels significantly differed between the NMRI Foxn1^{nu} and NSG strains, with additional slight reductions of plasma DYPD upon 5-FU treatment in the latter. Of note, basal DYPD plasma level of NMRI Foxn1^{nu} mice exceeded those of another commonly used laboratory mouse strain (C57Bl/6J), providing a possible explanation for the in vivo toxicity present in NSG, but not in NMRI Foxn1^{nu} mice. Moreover, it is very likely that the complex immunodeficiency not only makes NSG mice particularly susceptible to 5-FU-based regimens, but it might also impact overall tolerability and response to other drugs. In a parallel unpublished study, the anthracycline topoisomerase inhibitor Doxorubicin was given at very low dose to leukemic NSG mice (PDX of different acute lymphoblastic leukemia [31]). However, all mice deceased within seven days of therapy (single or double i.p. application of 8 and 4 mg/kg bw, respectively, *own unpublished data*). With these results we back up the hypothesis that metabolisms are quite individual among laboratory animals. Though several studies hint towards gender-specific effects, we here provide, to the best of our knowledge, for the first time experimental evidence of mouse strain specific drug sensitivities. Keeping that in mind, the results of our systematic study lay ground for upcoming cancer precision medicine approaches aiming at validation of novel (potentially toxic) substances. In addition to the necessity of complex immunodeficiency, variations in pharmacogenetics among mice strains should be taken into consideration. We therefore strongly recommend performing a similar dose-finding prestudy to prevent unnecessary, expensive, and animal-consuming repetitive PCT with different drug regimens.

With regard to treatment efficacy, regimens 2, 5, and 6 tended to be best in the present study. Since regimen 2 was associated with severe toxicity, we cannot recommend this dosing schedule for future trials. Mice receiving regimens 5 and 6 were given Capecitabine orally. In support of clinical observations, this prodrug had antitumoral efficacy with low to moderate side effects in NSG mice. The observed increase in liver enzymes ASAT and ALAT in these two groups may be due to the higher local drug concentration, of note, without affecting mice' general condition.

By contrast, the addition of LV to 5-FU (therapy regimens 3 and 4) did not potentiate drug-mediated activity in vivo. In the clinic, LV is usually given after 5-FU infusion to reduce gastrointestinal toxicity and increase its efficacy. Here, we followed suggestions from a recent study

showing that simultaneous application of both substances is superior to sequential injection [32]. Functionally, effects were due to inhibited *TYMS* gene expression—the major target of 5-FU. Though not analyzed in detail, upregulation of *TYMS* instead of suppression might provide an explanation for treatment failure in our approach. This assumption is supported by in vitro findings, showing high upregulation of *TYMS* after single 5-FU exposure of CRC cells. Besides, *TYMS* is considered as another potential factor for drug-related toxicity [33]. But that has to be addressed prospectively.

Another challenge for PCT studies is the individual growth pattern of different PDX. Here, we selected PDX cases with stable engraftment efficacy (100%) and comparable growth kinetics. Still, in one case, an intrinsically decelerated growth pattern was seen, thus potentially biasing results. The different tumor development in case of HROC40 yielded conflicting outcomes with good response in one case showing slow tumor growth vs. no response in the other fast-growing tumor. This has to be considered while planning a PCT as well as analyzing obtained data afterwards.

Finally, we would like to emphasize that all treatment regimens were given after establishment of solid and clearly palpable tumors (~6–7 mm longitudinally). Virtually all PDX were allowed to grow for more than 40 days. In most studies documented in literature, therapy is started at earlier time with—in some cases—hardly visible tumors and resulting impressive growth inhibition. Still, the setting applied here better reflects the clinical situation of an advanced CRC and may explain our findings of only partial growth inhibition at best.

When comparing the clinical outcome of patients from which PDX were established with our in vitro findings, mixed results were obtained. All PDX models were generated from primary CRC cases representative for hereditary CRC (i.e., Lynch syndrome; HROC29), chromosomal instable CRC (HROC46 and HROC222), and CpG island methylator phenotype CRC (HROC40) [34]. Two patients presented with synchronous liver metastases at time of resection; one of them died immediately after surgery (HROC29; UICC IV). The second patient received palliative chemotherapy with Capecitabine, but deceased soon after (HROC46; UICC IV). The remaining two cases were staged lower according to the UICC system. One patient received 5-FU-based treatment (HROC40; UICC IIIa) and the other one no adjuvant therapy (HROC222; UICC IIa) in line with clinical recommendations for these UICC stages. Both patients are still alive (follow-up of 142 and 81 months, respectively). Although definitely not a primary endpoint of the current study, we want to emphasize the fact that the PDX treatment results of HROC40 and HROC46 very well correspond with the clinical course.

Data availability

The datasets used and/or analyzed during the current study are available from the corresponding author on reasonable request.

Acknowledgements The authors kindly thank Mrs Ilona Klammuss for breeding mice and providing blood samples from different mouse strains. We additionally thank Dr H. Zettl and Mrs S. Klöcking from the Rostock Cancer Registry for providing us information about patient's follow-up.

Funding This work was supported by a grant from the German research foundation to CM [grant number MA5799/2–1].

Compliance with ethical standards

Conflict of interest The authors declare that they have no conflict of interest.

Ethical approval and consent to participate Specimen collection was conducted in accordance with the ethics guidelines for the use of human material, approved by the Ethics Committee of the University of Rostock (Reference numbers: II HV 43/2004 and A 45/2007) and with informed written consent from all patients prior to surgery.

Publisher's note: Springer Nature remains neutral with regard to jurisdictional claims in published maps and institutional affiliations.

References

- Lai Y, Wei X, Lin S, Qin L, Cheng L, Li P. Current status and perspectives of patient-derived xenograft models in cancer research. *J Hematol Oncol.* 2017;10:106.
- Meehan TF, Conte N, Goldstein T, Inghirami G, Murakami MA, Brabetz S, et al. PDX-MI: minimal information for patient-derived tumor xenograft models. *Cancer Res.* 2017;77:e62–6.
- Byrne AT, Alferez DG, Amant F, Annibaldi D, Arribas J, Biankin AV, et al. Interrogating open issues in cancer precision medicine with patient-derived xenografts. *Nat Rev Cancer.* 2017;17:254–68.
- Xu C, Li X, Liu P, Li M, Luo F. Patient-derived xenograft mouse models: a high fidelity tool for individualized medicine. *Oncol Lett.* 2019;17:3–10.
- Mullins CS, Bock S, Krohn M, Linnebacher M. Generation of xenotransplants from human cancer biopsies to assess anti-cancer activities of HDACi. *Methods Mol Biol.* 2017;1510:217–29.
- Jung J, Seol HS, Chang S. The generation and application of patient derived xenograft (PDX) model for cancer research. *Cancer Res Treat.* 2017;50:1–10.
- Shultz LD, Brehm MA, Bavari S, Greiner DL. Humanized mice as a preclinical tool for infectious disease and biomedical research. *Ann N Y Acad Sci.* 2011;1245:50–4.
- Zhou Q, Facciponte J, Jin M, Shen Q, Lin Q. Humanized NOD-SCID IL2rg $-/-$ mice as a preclinical model for cancer research and its potential use for individualized cancer therapies. *Cancer Lett.* 2014;344:13–9.
- Zitvogel L, Pitt JM, Daillère R, Smyth MJ, Kroemer G. Mouse models in oncoimmunology. *Nat Rev Cancer.* 2016;16:759–73.
- Gustavsson B, Carlsson G, Machover D, Petrelli N, Roth A, Schmoll H-J, et al. A review of the evolution of systemic chemotherapy in the management of colorectal cancer. *Clin Colorectal Cancer.* 2015;14:1–10.
- Rodrigues D, Longatto-Filho A, Martins SF. Predictive biomarkers in colorectal cancer: from the single therapeutic target to a plethora of options. *Biomed Res Int.* 2016;2016:6896024.
- Devaud N, Gallinger S. Chemotherapy of MMR-deficient colorectal cancer. *Fam Cancer.* 2013;12:301–6.
- Gao H, Korn JM, Ferretti S, Monahan JE, Wang Y, Singh M, et al. High-throughput screening using patient-derived tumor xenografts to predict clinical trial drug response. *Nat Med.* 2015;21:1318–25.
- Linnebacher M, Maletzki C, Ostwald C, Klier U, Krohn M, Klar E, et al. Cryopreservation of human colorectal carcinomas prior to xenografting. *BMC Cancer.* 2010;10:362.
- Peltenburg HG, Hermens WT, Willems GM, Flendrig JG, Schmidt E. Estimation of the fractional catabolic rate constants for the elimination of cytosolic liver enzymes from plasma. *Hepatology.* 1989;10:833–9.
- Rohde S, Lindner T, Polei S, Stenzel J, Borufka L, Achilles S, et al. Application of in vivo imaging techniques to monitor therapeutic efficiency of PLX4720 in an experimental model of microsatellite instable colorectal cancer. *Oncotarget.* 2017;8:69756–67.
- Sun W, Yan C, Jia S, Hu J. Correlation analysis of peripheral DPYD gene polymorphism with 5-fluorouracil susceptibility and side effects in colon cancer patients. *Int J Clin Exp Med.* 2014;7:5857–61.
- Maletzki C, Huehns M, Knapp P, Waukosin N, Klar E, Prall F, et al. Functional characterization and drug response of freshly established patient-derived tumor models with cpG island methylator phenotype. *PLoS ONE.* 2015;10:e0143194.
- Maletzki C, Stier S, Gruenert U, Gock M, Ostwald C, Prall F, et al. Establishment, characterization and chemosensitivity of three mismatch repair deficient cell lines from sporadic and inherited colorectal carcinomas. *PLoS ONE.* 2012;7:e52485.
- Muller MF, Ibrahim AEK, Arends MJ. Molecular pathological classification of colorectal cancer. *Virchows Arch.* 2016;469:125–34.
- Kuehn F, Mullins CS, Krohn M, Harnack C, Ramer R, Kramer OH, et al. Establishment and characterization of HROC69—a Crohn's related colonic carcinoma cell line and its matched patient-derived xenograft. *Sci Rep.* 2016;6:24671.
- Hidalgo M, Amant F, Biankin AV, Budinská E, Byrne AT, Caldas C, et al. Patient derived xenograft models: an emerging platform for translational cancer research. *Cancer Discov.* 2014;4:998–1013.
- El-Salhy M, Hilding L, Royson H, Tjomsland V. Comparison between triple therapy with octreotide, galanin and serotonin vs. irinotecan or oxaliplatin in combination with 5-fluorouracil/leucovorin in human colon cancer. *Int J Oncol.* 2005;27:687–91.
- Dorsey JF, Mintz A, Tian X, Dowling ML, Plastaras JP, Dicker DT, et al. Tumor necrosis factor-related apoptosis-inducing ligand (TRAIL) and paclitaxel have cooperative in vivo effects against glioblastoma multiforme cells. *Mol Cancer Ther.* 2009;8:3285–95.
- Kang HJ, Lee SH, Price JE, Kim LS. Curcumin suppresses the paclitaxel-induced nuclear factor-kappaB in breast cancer cells and potentiates the growth inhibitory effect of paclitaxel in a breast cancer nude mice model. *Breast J.* 2009;15:223–9.
- Chang C-W, Liu C-Y, Lee H-C, Huang Y-H, Li L-H, Chiau J-SC, et al. *Lactobacillus casei* Variety *rhamnosus* probiotic preventively attenuates 5-fluorouracil/oxaliplatin-induced intestinal injury in a syngeneic colorectal cancer model. *Front Microbiol.* 2018;9:983.
- Papanastopoulos P, Stebbing J. Molecular basis of 5-fluorouracil-related toxicity: lessons from clinical practice. *Anticancer Res.* 2014;34:1531–5.

28. Gross E, Ullrich T, Seck K, Mueller V, de Wit M, von Schilling C, et al. Detailed analysis of five mutations in dihydropyrimidine dehydrogenase detected in cancer patients with 5-fluorouracil-related side effects. *Hum Mutat.* 2003;22:498.
29. Kleibl Z, Fidlerova J, Kleiblova P, Kormunda S, Bilek M, Bouskova K, et al. Influence of dihydropyrimidine dehydrogenase gene (DPYD) coding sequence variants on the development of fluoropyrimidine-related toxicity in patients with high-grade toxicity and patients with excellent tolerance of fluoropyrimidine-based chemotherapy. *Neoplasma.* 2009;56:303–16.
30. Dean L. Medical Genetics Summaries [Internet]. In: Pratt V, McLeod H, Rubinstein W, Dean L, Malheiro A, editors. *Fluorouracil therapy and DPYD genotype*. Bethesda, MD: National Center for Biotechnology Information; 2012. p. 2012–2016.
31. Roof C, Richter A, Konkolefski C, Knuebel G, Sekora A, Krohn S, et al. Decitabine demonstrates antileukemic activity in B cell precursor acute lymphoblastic leukemia with MLL rearrangements. *J Hematol Oncol.* 2018;11:62.
32. Di Paolo A, Orlandi P, Di Desidero T, Danesi R, Bocci G. Simultaneous, but not consecutive, combination with folinate salts potentiates 5-fluorouracil antitumor activity in vitro and in vivo. *Oncol Res.* 2017;25:1129–40.
33. Lecomte T, Ferraz J-M, Zinzindohoue F, Lorient M-A, Tregouet D-A, Landi B, et al. Thymidylate synthase gene polymorphism predicts toxicity in colorectal cancer patients receiving 5-fluorouracil-based chemotherapy. *Clin Cancer Res.* 2004;10:5880–8.
34. Ostwald C, Linnebacher M, Weirich V, Prall F. Chromosomally and microsatellite stable colorectal carcinomas without the CpG island methylator phenotype in a molecular classification. *Int J Oncol.* 2009;35:321–7.